THE REACTIVITY AND CATALYTIC ACTIVITY OF COPPER CHLORIDES

by

NG CHING FAI

B.E. (Chemical), The University of Melbourne, 1963
M.Sc., The University of Melbourne, 1965

A THESIS SUBMITTED IN PARTIAL FULFILMENT OF THE REQUIREMENTS FOR THE DEGREE OF DOCTOR OF PHILOSOPHY in the Department of CHEMISTRY

We accept this thesis as conforming to the required standard

THE UNIVERSITY OF BRITISH COLUMBIA

AUGUST, 1969

In presenting this thesis in partial fulfilment of the requirements for an advanced degree at the University of British Columbia, I agree that the Library shall make it freely available for reference and study. I further agree tha permission for extensive copying of this thesis for scholarly purposes may be granted by the Head of my Department or by his representatives. It is understood that copying or publication of this thesis for financial gain shall not be allowed without my written permission.

Department of Chemistry

The University of British Columbia
Vancouver 8, Canada

Date 19-9-69

ABSTRACT

The reactivity of copper chloride ($CuCl_x$, $1 < x < 2$) towards chlorine and its catalytic activity in the chlorination of propane have been studied. The oxidation of copper (I) chloride by chlorine was found to be diffusion controlled after the first 25% of reaction.

For the chlorination of propane, CuCl was catalytically inactive, $CuCl_2$ was active, but the maximum activity was found in the range $CuCl_{1.5}$ to $CuCl_{1.8}$ with two peaks at roughly $CuCl_{1.57}$ and $CuCl_{1.78}$.

Both reactions appear to have an active centre in common — a Cu^+ ion which is capable of accepting a proton. The phase of maximum catalytic activity is a highly defective $CuCl_2$ phase containing such centres. The mechanism for the catalytic chlorination involves the homolytic splitting of C_3H_8 and stabilization of surface radicals through proton transfer into the bulk.

No compound other than CuCl and $CuCl_2$ was found in the $CuCl_x$ system by X-ray powder studies. However, the results of X-ray powder, electrical conductivity and magnetic susceptibility studies provide convincing evidence for the existence of a defective $CuCl_2$ phase with interstitial cations as well as a cation-deficient CuCl phase in $CuCl_x$. Furthermore, these results are consistent with a structural change at $x \sim 1.63$ as suggested also by the kinetic studies.

While the present work shows many interesting features of the $CuCl_x$ system, there is plenty of room for further exploration in this hitherto virtually unknown field. Suggestions for future work related to the present findings are outlined in this thesis.

Now through a glass darkly,

But when face to face?

Now we see in part,

But do we ever see as we are seen?

A thought after four years on Catalysis

TABLE OF CONTENTS

LIST OF TABLES

LIST OF FIGURES

ACKNOWLEDGMENTS

The author wishes to express his sincere thanks to Prof. L. G. Harrison for his interest, encouragement and illuminating guidance in this work.

He is grateful to the following for their generosity in making apparatus available:

Dr. R. C. Thompson for magnetic susceptibility apparatus, (and for much useful discussion of the magnetic results);

Dr. J. Trotter for X-ray diffraction equipment;

Prof. C. A. McDowell for low-temperature ESR apparatus; and

Dr. F. Aubke for the use of his high quality dry box.

He is indebted to Dr. S. Whitlow for the use of a computer programme for calculating lattice parameters from powder photographs, and to Mr. M. Prasad for advance information on his preliminary results on conductivity of pure CuCl.

Finally, the author would like to thank U.B.C. for a research fellowship for the year 1966-67, and the National Research Council of Canada for a postgraduate scholarship for the years 1967-69.

CHAPTER I

INTRODUCTION

In the field of heterogeneous catalysis involving ionic compounds, metal oxide catalysts have received great attention. A vast amount of work has been carried out to elucidate the nature of defects and non-stoichiometry in the metal oxide systems. The application of the oxides as catalysts in many reaction systems has also been extensively tested.

By contrast, transition metal halides are relatively unknown in respect of both their non-stoichiometry and their catalytic activity. It appears therefore profitable to intrude upon this hitherto barren field.

The reasons for the study of the copper chloride/Cl_2/C_3H_8 system are threefold.

Firstly, in this laboratory, reaction intermediates involving electronic defects associated with anion vacancies were found in Group I and Group II halides [1,2,3]. Therefore, it appeared reasonable to expect similar defects to be present in copper chloride during the reaction between C_3H_8 and Cl_2, and the possibility arose that copper chloride containing such defects might be catalytically active for reactions involving chlorine gas.

Secondly, copper (I) chloride is readily oxidised and hence the chance for obtaining a variety of non-stoichiometric phases was expected to be reasonably good.

Thirdly, Halpern et al[4] carried out extensive studies of catalytic hydrogenation by Cu^{2+} ions (transition metal ions in general) in homogeneous systems and it appeared interesting to see how Cu^{2+} ion in the solid state behaves for a system involving the splitting of a hydrogen atom from a hydrocarbon.

While the present work shows many interesting features of the copper chloride system as a catalyst, not all the expectations set forth were realized. Contrary to expectation, the copper chloride system involves cationic defects. Also, no non-stoichiometric phase of significantly different structure (i.e. with a different X-ray diffraction pattern) from those of CuCl and $CuCl_2$ was found.

In 1934, Yuster and Reyerson [5] studied catalytic chlorination of propane using $CuCl_2$ on silica gel supports as catalyst. Their approach to the problem, however, belongs to the "know-how" school rather than the "know-why" school. Consequently they were contented with observing a higher rate for the reaction due to catalysis and a rather generalized mechanism for the catalytic reaction in terms of decomposition of $CuCl_2$ to CuCl and Cl atom, and regeneration of $CuCl_2$ by reaction with Cl_2, with no serious attempt to identify active centres.

In this work, an attempt is made to elucidate the mechanism of the catalytic chlorination of propane in relation to the reactivity of

the catalyst towards chlorine and to various physico-chemical properties of the catalyst revealed by the studies using X-ray diffraction, electrical conductivity, magnetic susceptibility, ESR and microscopic techniques.

The copper chloride/Cl_2/C_3H_8 system is a complicated one for study because of the continuously-changing composition of the "catalyst" due to the oxidation of CuCl by chlorine. In the conventional sense, there is no true catalysis since none of the materials in the system remains unchanged after the reaction. However, since the findings show that the presence of the solid phase accelerates the chlorination of propane and the presence of propane accelerates the oxidation of CuCl, effects which may reasonably be called "catalytic" occur in the reaction system.

Since the catalyst powder sample contained particles of different sizes, the method of analysis of kinetic data for the chlorination of copper chloride is somewhat involved in details of computation although straightforward in principle. Harrison [6] has reviewed the applicability of various existing equations for diffusion-controlled reactions in a spherical shell of reaction product. He also developed the modified form of the Ginstling-Brounshtein equation for the case of a volume change during a reaction, the derivation of which is given in the Appendix I to this thesis. The results were analysed with the aid of this equation and with allowance for the particle size distribution.

It is noteworthy that the particle size effect in diffusion-controlled kinetics in a powder sample was also considered by Gallagher [7]. The diffusion mechanism involved in his studies is interdiffusion mechanism with no sharp interface, for which the Dünwald-Wagner equation is the appropriate rate law, whereas in the copper chloride case, the system is assumed to have a sharp reaction interface. While there is no essential difference in principle between these two cases, the mathematical labour involved in the present case is considerably less and hence no computation programming was required in the present work.

In passing, mention should perhaps be made that in 1961, Cini et al studied the kinetics of oxidation of CuCl (uniformly-sized) by Cl_2 using gravimetric [8] and magnetic method [9]. While their results are also consistent with diffusion-controlled kinetics, their quantitative data are quite different from the present ones. It appears, however, that there is inconsistency in their results.

The change in crystal lattice in going from CuCl to $CuCl_2$ is an interesting one. CuCl has the zinc blende structure, with each ion in the FCC arrangement, ions of one sign occupying tetrahedral interstices of the sublattice of opposite sign.

The structure of $CuCl_2$ was determined by A. F. Wells [10]. He described it as consisting of chains of Cu atoms with bridging Cl, and also drew attention to the distorted octahedral environment of Cu^{2+} at a time when the Jahn-Teller distortion was not widely known. It

has not usually been pointed out that the $CuCl_2$ lattice can also be regarded as a severely distorted version of the $MgCl_2$ lattice. The latter is equivalent to an NaCl lattice with alternate (111) planes of cation sites completely vacant. The presence of similar vacant planes of octahedral sites (albeit distorted octahedra, and not exactly the same size as the occupied octahedral sites) in $CuCl_2$ should be borne in mind in all discussions of defective $CuCl_2$ structures in this thesis.

The anion lattice of $CuCl_2$ is thus not altogether different from that of CuCl. Though distorted, it still fairly closely resembles FCC. It is somewhat contracted; one mole of Cl in $CuCl_2$ occupies 0.83 times the volume of 1 mole of Cl in CuCl.

Comparatively little work has been done on the physical properties of $CuCl_2$. Wells' work appears to be the only X-ray diffraction study, and no search has been made for non-stoichiometric phases. The electrical conductivity of $CuCl_2$ does not appear to have been studied. The present author, under the supervision of Dr. C. G. Barraclough, has previously studied the magnetic properties of $CuCl_2$ & $CuBr_2$ and has established that they behave according to a model of antiferromagnetic ordering in linear chains of Cu^{2+} (the one-dimensional Ising model) [11].

CHAPTER II

EXPERIMENTAL DETAILS

The experimental techniques employed in this thesis may be classified into two main categories.

(a) Kinetic Studies

(i) In the case of catalytic activity of copper chloride on the chlorination of propane, a high vacuum system was built to carry out reactions, with gas-liquid chromatography as the tool to follow reactions.

(ii) In the case of chlorine uptake of CuCl, the above high vacuum system was used with a spiral gauge to follow the reactions manometrically. Also, a separate high vacuum system was built to study the reactions by a gravimetric method.

(b) Characterisation of the Catalyst

D. C. conductivity, X-ray powder, E.S.R., magnetic susceptibility and microscopic techniques were used to study the structure of catalysts.

In addition, chemical compositions of catalysts were determined by weighing and conventional quantitative analysis.

II.(1) KINETIC STUDIES OF CATALYTIC ACTIVITY OF COPPER CHLORIDE FOR THE CHLORINATION OF PROPANE

(A) Apparatus

The reactions were carried out in a static reactor at a controlled temperature.

A schematic diagram of the apparatus is shown in Figure II.1.

(i) Reactor

The reactor is of a static type. As shown in Figure II.1, it consists of a main bulb A (the cylindrical part) and a side arm B which can be heated to a temperature higher than the rest of the system and thereby facilitates mixing of gases by convection. The part C is anchored to A & B by two greaseless viton ball and socket joints S_1 and S_2 (Westglass, W-1551, 18/7). Two thermocouple wells (T/C) are provided in Part C and part A as shown. The calibrated volume of the reactor area is 475 ml. Through SC 11, gases are admitted to the reactor and through a capillary Q and SC 12, samples are withdrawn from the reactor for gas analysis. When SC 14 is open, the reactor is connected (through capillary P) to one side of a spiral gauge for pressure measurement. The whole reactor is immersed in an oven (Labline Forced Draft 'Thermocirculator' Oven, Cat. #3500M) which provides a uniform temperature inside the oven to within $\pm$ 1.5°C. It should be noted

FIGURE II.1

MAIN FEATURES OF APPARATUS FOR KINETIC STUDIES

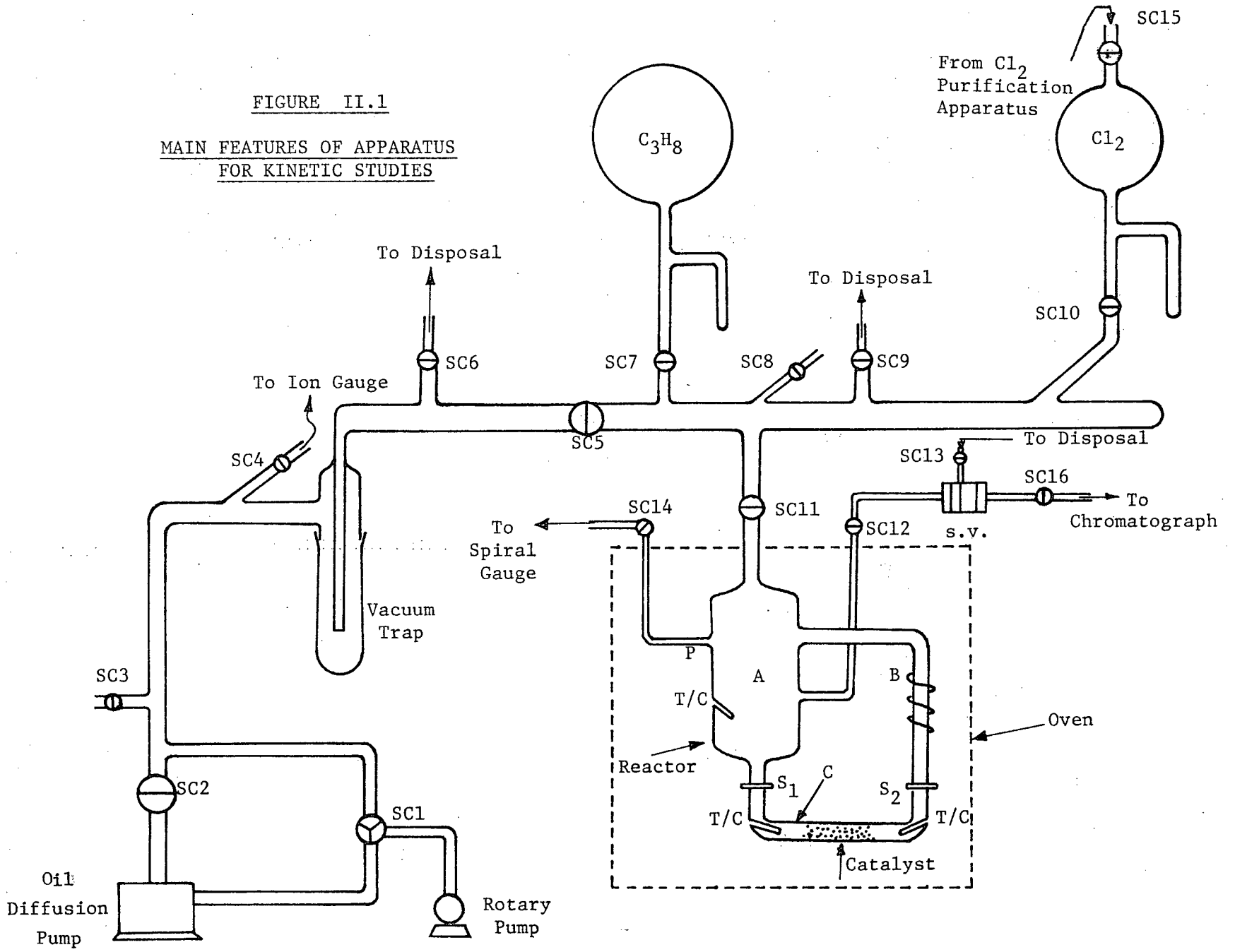

that all the reacting area is protected from light to avoid photocatalytic effect which is well-known for chlorination of propane in the gaseous phase.

(ii) Pumping System

High vacuum is catered for by a silicone diffusion pump (Balzers Dif. 170) coupled with an ordinary rotary pump (Welch Duo-Seal #1392).

(iii) Disposal

The waste gas can be evacuated by a separate disposal pump through stopcocks 11 & 9 with 5, 7, 8, & 10 closed. An absorption column packed with 2 ft. of soda-lime and a liquid nitrogen trap are installed between 9 and the pump. Therefore, the waste gases if not absorbed by the column are trapped in the liquid nitrogen trap as solids which can be transferred to a fume hood at the end of the experiment.

(iv) Stopcocks (Abbreviated SC)

Owing to different requirements, stopcocks used are of three types.

(a) Teflon stopcocks made by Fisher & Porter or Westglass. They were used to keep the gas in storage bulbs and when constant contact with corrosive gas was required (e.g. 7, 10, 11, 12, 14). While Westglass stopcocks provided a higher vacuum, Fisher & Porter stopcocks enabled easier manipulation without too much loss in vacuum and in fact for a vacuum of the

order of 10^{-6} mm Hg, Fisher & Porter stopcocks did not pose any difficulty.

(b) Stopcocks greased with Kel-F. These were used when constant contact with corrosive gas as well as a large bore were required. Thus 5, 8 (for high vacuum), 9 (disposal) are of this type.

(c) Stopcocks with Apiezon-N grease. All other stopcocks which were at no time in contact with corrosive gas(es) are of this type.

(v) Measurement of Pressure & Vacuum

(a) Pressure Measurement - Spiral Gauge

The pressure of gas in the reactor was measured by a Pyrex spiral gauge which is schematically shown in Figure II. 2.

The mirror position depends on the pressure difference between the two sides of the spiral and consequently light coming from a lamp would be reflected at different positions on the scale. The outside jacket of the spiral was filled with CO_2 whose pressure was always higher than the reactor pressure and was measured by an ordinary mercury manometer. CO_2 was chosen because its pressure could be conveniently regulated in most of the pressure range without resort to a pump (simply by condensing in trap T using liquid N_2). It is thus in principle possible to use the spiral only as a

null detector; but in practice the sensitivity and linearity of calibration are satisfactory for use of the spiral, with a calibration curve, as a manometer with fixed outside frame. One cm. on the scale corresponds to a pressure difference of 0.185 cm Hg. A typical calibration chart of the spiral gauge is shown in Figure II.3. The gauge was calibrated from time to time because minor change in sensitivity could occur due to change of lamp position, etc.

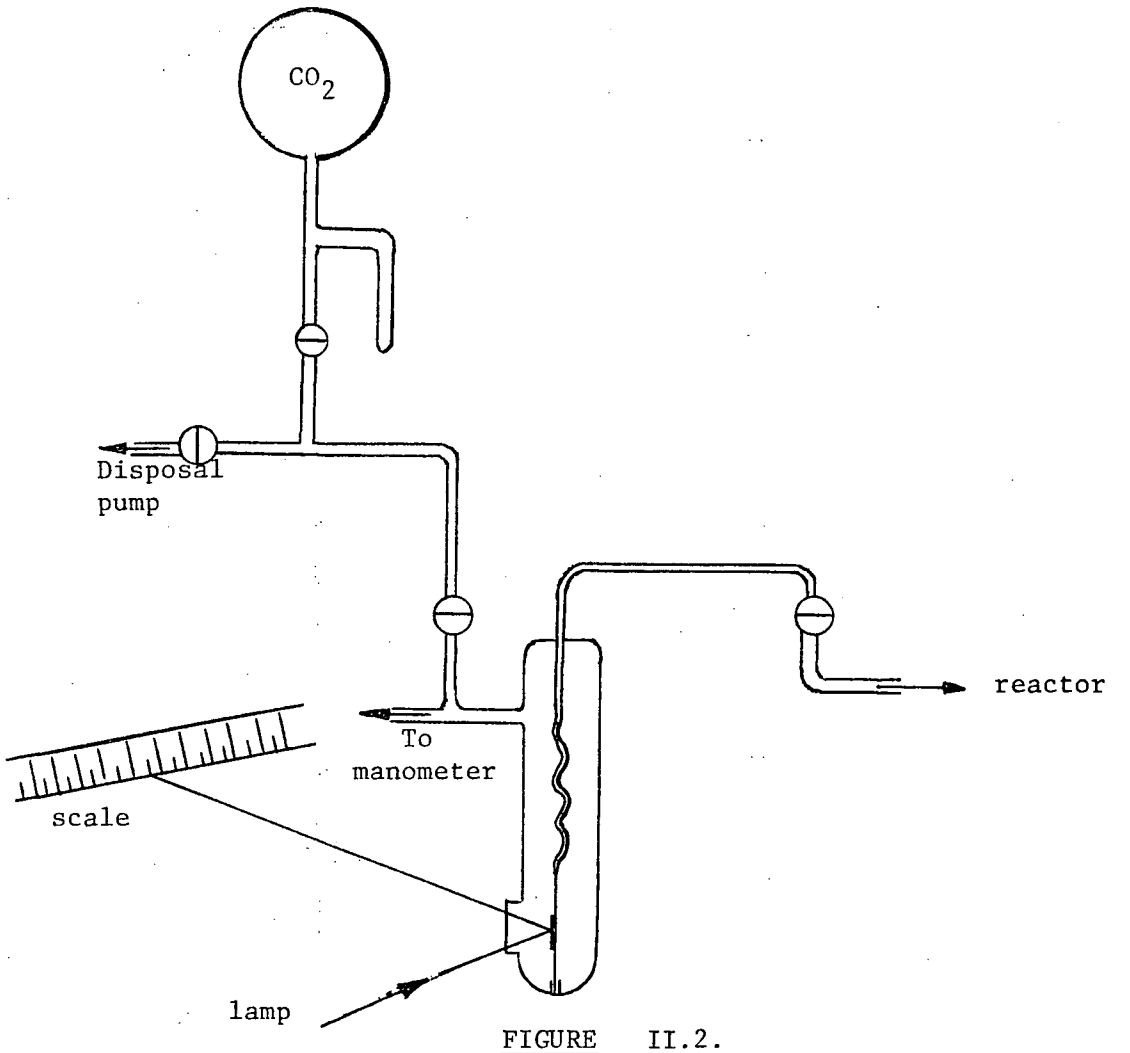

FIGURE II.2.

ASSEMBLY OF SPIRAL GAUGE FOR MANOMETRIC MEASUREMENT

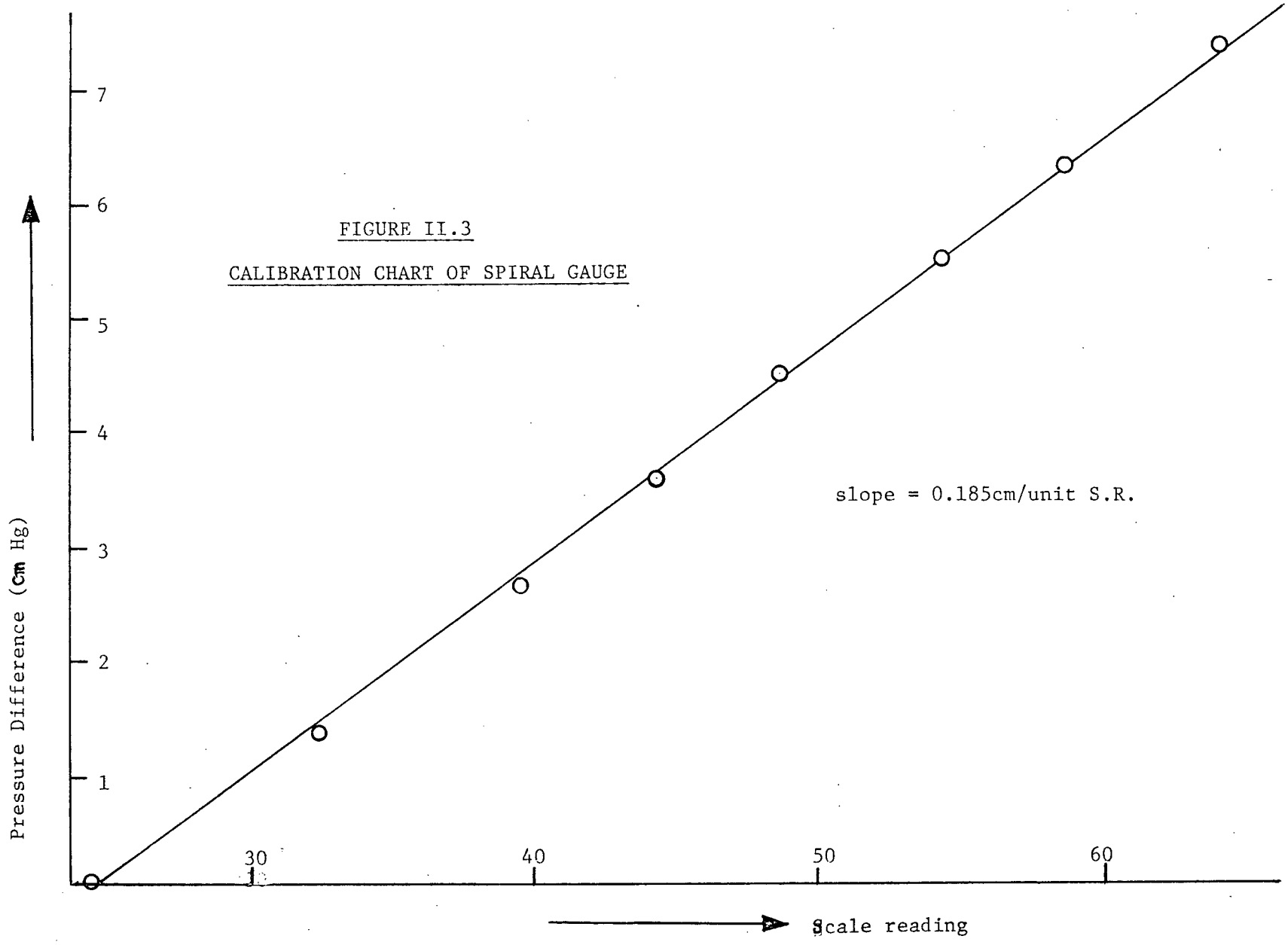

FIGURE II.3

CALIBRATION CHART OF SPIRAL GAUGE

(b) The vacuum of the system was measured by a Veeco R G 75 P ionization gauge. There are two points in the system for measurement viz. from SC 6 & 8. The arrangement is shown below. The gauge plus the U-tube which acts as a liquid nitrogen trap are removable so that measurement at SC 6 or SC 8 position could be conveniently carried out.

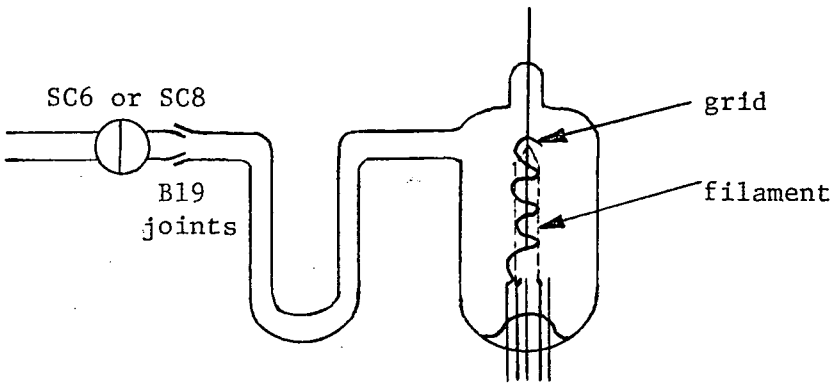

FIGURE II.4

IONIZATION GAUGE

(vi) Chlorine Purification System

The chlorine obtained from Matheson Company was quoted as 99.5% pure. Water vapor would be the major component of impurity. Figure II.5 shows the apparatus which was used to remove water vapor and also uncondensable gases (if any) from the supplied chlorine.

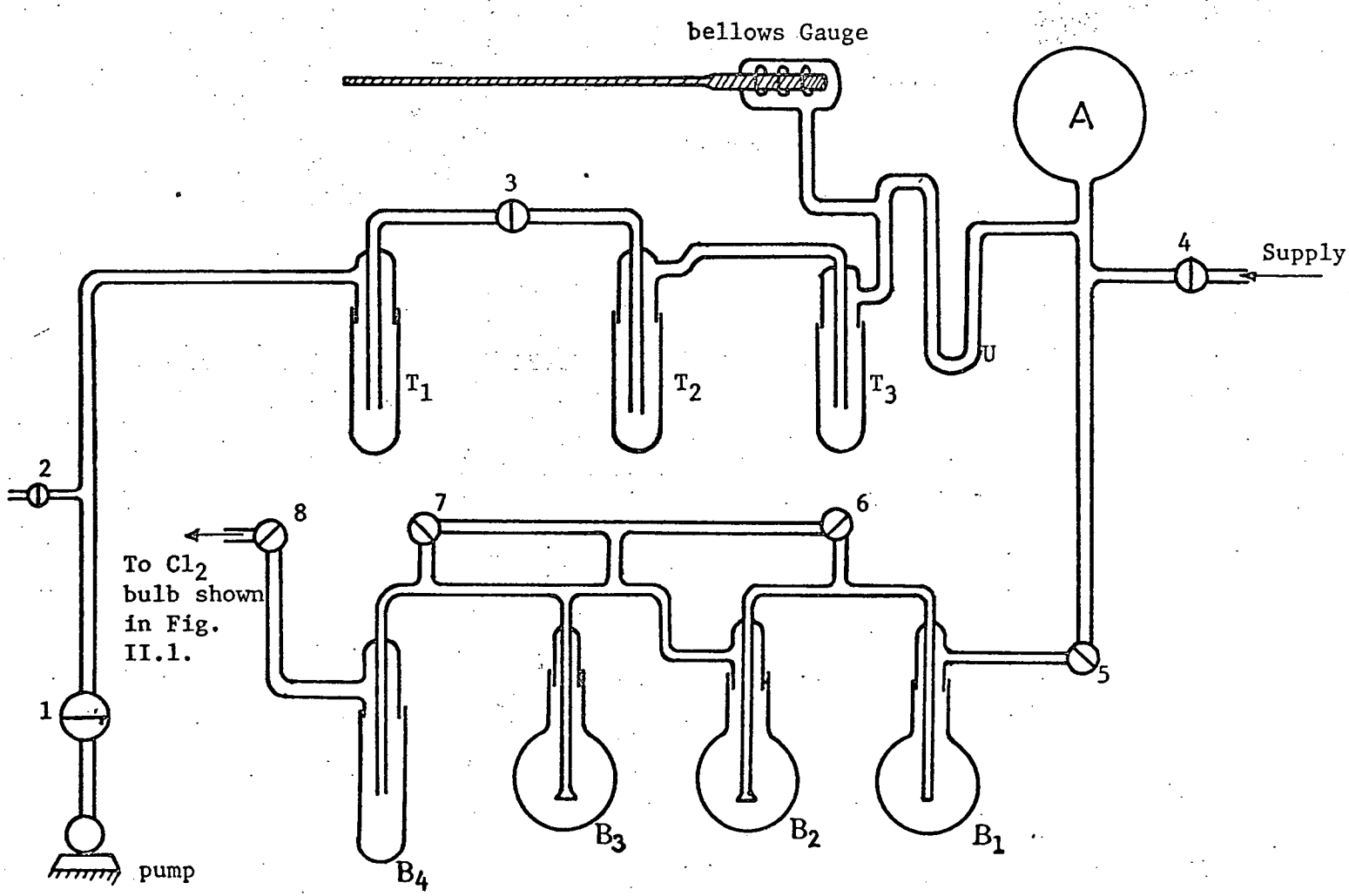

FIG. II.5 Cl_2 - PURIFICATION SYSTEM

The procedure for purification of chlorine is as follows:-

The whole system was first evacuated by a rotary pump. Cl_2 was admitted through stopcock 4 to the area enclosed by 3 and 5. The pressure is indicated by a bellows gauge previously calibrated (approx. 1 atmosphere pressure of Cl_2 was normally admitted.) The gas was then condensed in the U-tube U and the two traps T_2 and T_3 using liquid nitrogen. Stopcock 3 was then opened; with T_1 also in liquid nitrogen, the system was connected to the pump. Uncondensable gases should then be pumped away. Thereafter, with 3 closed and liquid nitrogen removed, the gas was allowed to pass through 5 and B_1, B_2, B_3, B_4. B_2 & B_4 were half filled with A.R. Conc. H_2SO_4 . The water-free chlorine was then admitted through stopcock 8 to the chlorine bulb in the main reactor system as shown in Figure II.1 which was in a neighbouring rack to the purification system. The water-free chlorine then collected was condensed in the side arm of the Cl_2 bulb and further pumped on by the high vacuum system to get rid of any residual uncondensable gases. The presence of B_1 & B_4 was to avoid suckback of conc. H_2SO_4. For the same reason, SC 6 & 7 were installed. When Cl_2 was not passing through B_1, B_2, B_3, B_4, 6 & 7 were opened and the pressures in all the four bulbs were equalised. Hence no suckbacks were possible.

(vii) Gas Chromatography System

Gas samples can be withdrawn from the reactor through a 6 way valve (described in detail below)(S.V. in Figure II.1) and allowed to pass through copper tubing to a 25' long ¼" ϕ column (in the oven

of a chromatograph) with 10% Kel-F grease on 40/60 chromosorb T (polytetrafluoroethylene) support as the packing materials. The chormatograph used is Model A-90-P3 made by Aerograph, with thermal conductivity detectors. The detecting elements are teflon coated tungsten. Helium was used as carrier gas. Recording is by a Leeds-Northrup speedomax H recorder equipped with a Model 207-4 disc chart integrator.

The 6-way sampling value is also made by Aerograph. With such a device, dead volume in the sampling process can be kept very small and the total volume withdrawn in each sampling amounts only to 2% of the reactor volume. A schematic diagram for the sampling system is shown in Figure II.6.

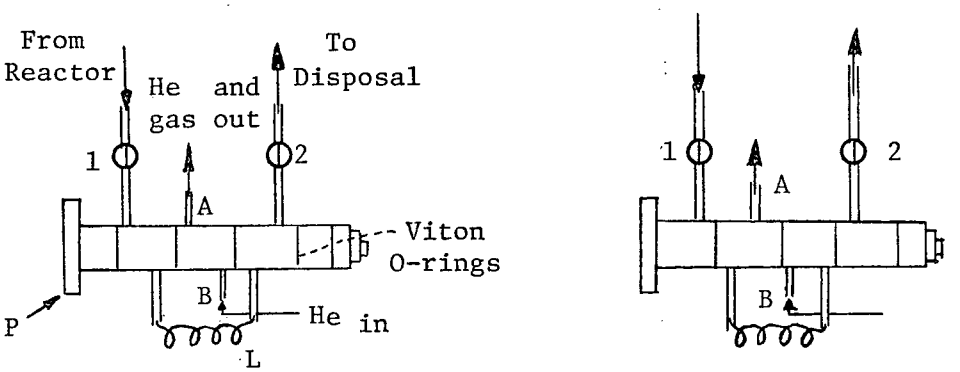

(a) (b)

FIGURE II.6

GAS SAMPLING SYSTEM

(a) Sampling Position
(b) Injecting position

The 6-way valve consists of a hollow cylinder (not shown) enclosing a piston P, both made of stainless steel. There are six ports of entry in the cylinder. SC 1 is identical with SC 12 in Figure II.1 whereas SC 2 (13 in Figure II.1) is connected to the disposal system as described earlier. The sampling loop L is made of stainless steel 363K having a volume of 2 ml. the on and off position of the 6-way valve is controlled by adjusting the piston P. When a sample is to be taken out, P is held in the position shown in (a) and stopcock SC 2 is closed. It can be seen that the He inlet and outlet B & A are cut off and the gas would fill the area from SC 1 to SC 2, sampling loop L included. When the sample is being injected, P is pushed to the far right. Then as shown in (b), the loop and A & B are connected so that the He can sweep all the gas in the loop, and carry it to the column.

After injection, P is returned to the original position (with SC 1 closed) and the residual gas in the dead volume can be pumped off through SC 2. In actual practice, gas was first taken out with P in a position like that in (b). This volume was immediately pumped off by closing SC 1, returning P to (a) position and thereafter opening SC 2. Following half a minute of pumping, SC 2 was closed and the gas was withdrawn to fill the whole area from SC 1 to SC 2 (time allowed for equilibrium was 0.6 min.). Thence injection followed. Such practice ensured that the samples analysed came from the bulk of the reactor and not the residue left in the capillary Q (see Figure II.1) in the reactor system from previous sampling.

The column was found to have reasonably satisfactory resolving power. In Figure II.7, a typical chromatogram together with the

optimum operating conditions are shown.

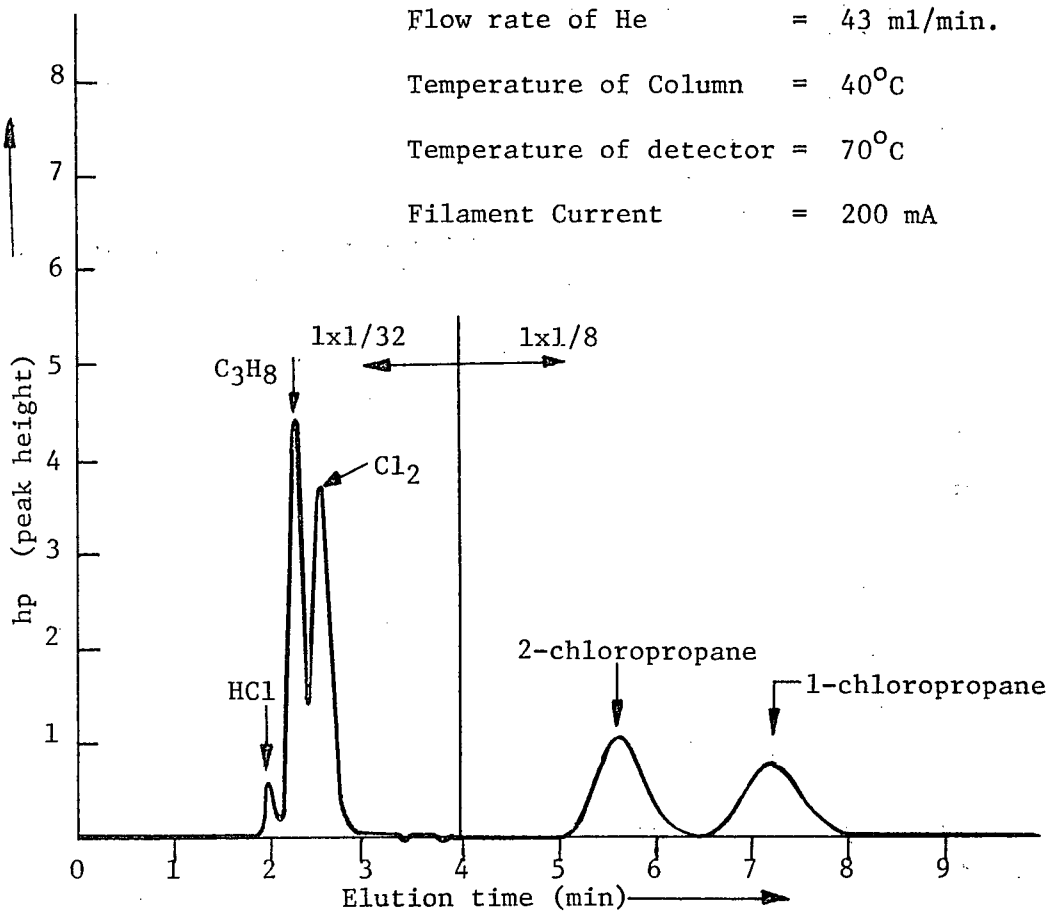

FIGURE II.7

A TYPICAL CHROMATOGRAM

By calibration using known amounts of gases, the peak heights were found to vary directly with pressures (or partial pressures if a mixture) of gases. The resolution of HCl, C_3H_8 & Cl_2 peaks was

fortunately good enough to introduce no complication. However, it was found that the sensitivity of the column changed with time, especially for HCl and Cl_2. Also, after prolonged use of the column, resolution of peaks was found less efficient. The efficiency could be recovered to a certain degree by heating the column to $\sim 100^{o}C$ overnight with slow passage of He. Consequently calibration was carried out fairly frequently to ensure correct reading of the pressure of gases. Typical calibration charts for each component are shown in Figure II.8. All the plots appearing in Figure II.8 are linear except that of HCl in the low pressure region. Since the elution time of the HCl peak was close to those of C_3H_8 and Cl_2, it was not convenient to scan the HCl peak at a higher sensitivity range. Consequently, detection of small amount of HCl was difficult. This introduced uncertainty in the application of material balance to check the amounts of various substances present. Nevertheless, the use of C_3H_8 peak for analysis of C_3H_8 was well justified as witnessed by the good resolution and the linearity of the hp v.s. pressure plot shown in Figures 7 and 8 respectively.

(B) Experimental Procedure

(i) Calibration of volumes

A glass vessel of known volume was attached to the point next to SC 8 in Figure II.1. The reactor volume (including the part connected to the spiral gauge) was found to be 480 ± 3 c.c. and the volume of the sampling area was found to be 6 ± 0.5 c.c.

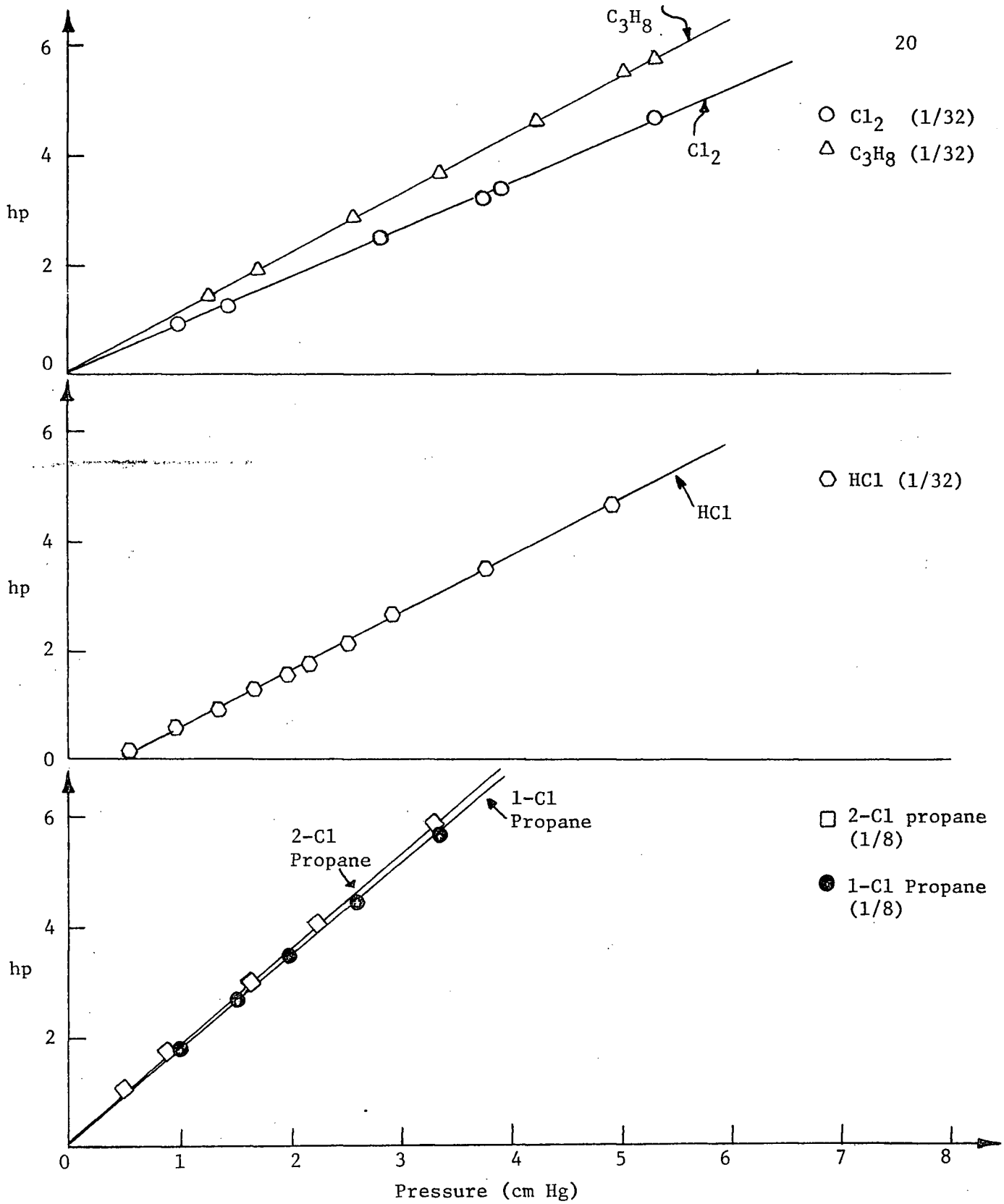

FIGURE II.8

CALIBRATION CHARTS FOR CHROMATOGRAPHIC ANALYSIS

(Peak Height v s. Pressure)

(ii) Filling of storage bulbs of Propane and Chlorine

(a) When the whole system was evacuated (including reactor area), with stopcocks 1, 2, 4, 6, 8, 9, 10, 12 closed, C_3H_8 was then admitted through 3. When the pressure measured by the spiral gauge indicated ~ 60 cm Hg, 3 was closed and propane was allowed to condense in the side arm of the propane bulb. Those gases not condensable in this way were pumped off through the disposal line. 1 & 2 were then opened and the system was evacuated to high vacuum ($\sim 10^{-6}$ mm Hg) before 7 was closed and the propane was allowed to vaporise.

(b) Cl_2 was stored as described in the Cl_2 purification system.

(iii) Kinetic Runs

(a) Charging of catalyst

The lower part C of the reactor was removed from the system and about 4.5 - 4.9 gm of CuCl powder was weighed and charged into it. The total weight, and the weight of the lower part of reactor were recorded. It was then returned to the system which was evacuated to $\sim 10^{-3}$ torr by the fore pump. The reactor was heated to 130°C (side arm was heated to ~ 145°C) while high vacuum pumping was applied. High vacuum was found to be achievable only when the reactor was heated; apparently the viton o-rings connecting the two parts of the reactor provided a better sealing action when they were thermally expanded.

(b) Admission of gases

After heating and pumping overnight, the pressure of the system was normally $\sim 1 \times 10^{-5}$ to 1×10^{-6} mm Hg. SC 5 and 11 were then closed and 7 was opened; then 11 was opened slowly until the pressure of propane in the reactor was 5 cm Hg. 7 & 4 were then closed and the residual propane was pumped away through 9. 5 was then opened and after the pressure was again as low as 10 to 1×10^{-6} mm Hg, it was closed again. By the same procedure, 5 cm Hg of chlorine was admitted (total pressure 10 cm Hg.)

(c) Following of Reaction

As soon as Cl_2 was admitted, SC 11 was closed and a timer was turned on. After two and half minutes, a little gas was released through SC 12 (presumably mainly propane in the capillary) as described under 'gas chromatography'. Then at 3.2 min., a sample was taken out as described earlier. The time allowed for sampling was 0.6 min. Injection then followed. At 22.5 minutes, a second sample was taken out. The reason why 2.5 minutes was allowed to elapse before the first sampling is that it was found by many trial runs that this is the minimum time required for thorough mixing of the two gases. If only two readings were required, the gas mixture was immediately pumped away through the disposal line as soon as the second sampling was accomplished (after the system was pumped to high vacuum, the reactor was ready for another run.) During each sampling period and at the end of each run, the

pressure of the reacting mixture was noted. By analysis of chromatograms and the pressure readings, the amount of Cl_2 reacted with propane and that taken up by the catalyst (irreversibly) could be worked out, and hence the content of chlorine in the catalyst for each run.

(d) Discharge of Catalyst

At the end of each series of runs (this applied in the case of adsorption studies as well), the oven was turned off and the reactor was allowed to cool. SC 1 & 2, 4, 12, 14 were closed, and air was admitted gently through a drying tube filled with Silica Gel. The part C of the reactor was then removed and stoppered immediately before it was taken to the dry box where the catalyst was weighed, broken into smaller lumps and stored in a dry bottle which was subsequently placed in a desicator.

(C) Materials

For Kinetics:

Chlorine	- Matheson high quality Cl_2 (99.5% pure)
Propane	- Philips 66, Research Grade (99.99% pure)
CuCl	- Baker & Adams A.C.S. Powder (> 95% CuCl)
$CuCl_2$ (Anhydrous)	- Fisher Scientific (Certified) (Found by author - 99.8% $CuCl_2$)

For Calibration Purpose:

Hydrogen Chloride	- Matheson (Reagent Grade)
2-Chloropropane	- Matheson Coleman & Bell (Chromatography Reagent)
1-Chloropropane	- Matheson Coleman & Bell (Chromatography Reagent)

II.(2) KINETIC STUDIES OF CHLORINE UPTAKE BY CuCl

In order to obtain information about the growth of the $CuCl_2$ phase from CuCl, uptake of chlorine by CuCl was carried out using the apparatus shown in Figure I.1 in a similar manner to that for the reaction between C_3H_8 and Cl_2 except that C_3H_8 was absent and the starting pressure was not necessarily fixed at 5 cm. The reaction, however, was followed manometrically using a pyrex spiral gauge, not by gas chromatography.

In addition, some reactions of Cl_2 with CuCl were followed gravimetrically using the apparatus shown in Figure II.9.

In this method, approximately 1 g. CuCl powder is placed in a quartz pan (P) which is situated in the middle of a 2 litre flask. The quartz balance onto which the pan is hooked was calibrated with a sensitivity of 10.02 cm; the change of the position of the hair H for a difference of 1 g. in weight. Thus the rate of reaction could be determined by the weight change of the sample. The rest of the diagram is self-explanatory.

Since the conditions of access of gas to the solid were quite different in this apparatus, the results were not very informative for comparison with those obtained in the regular reaction vessel.

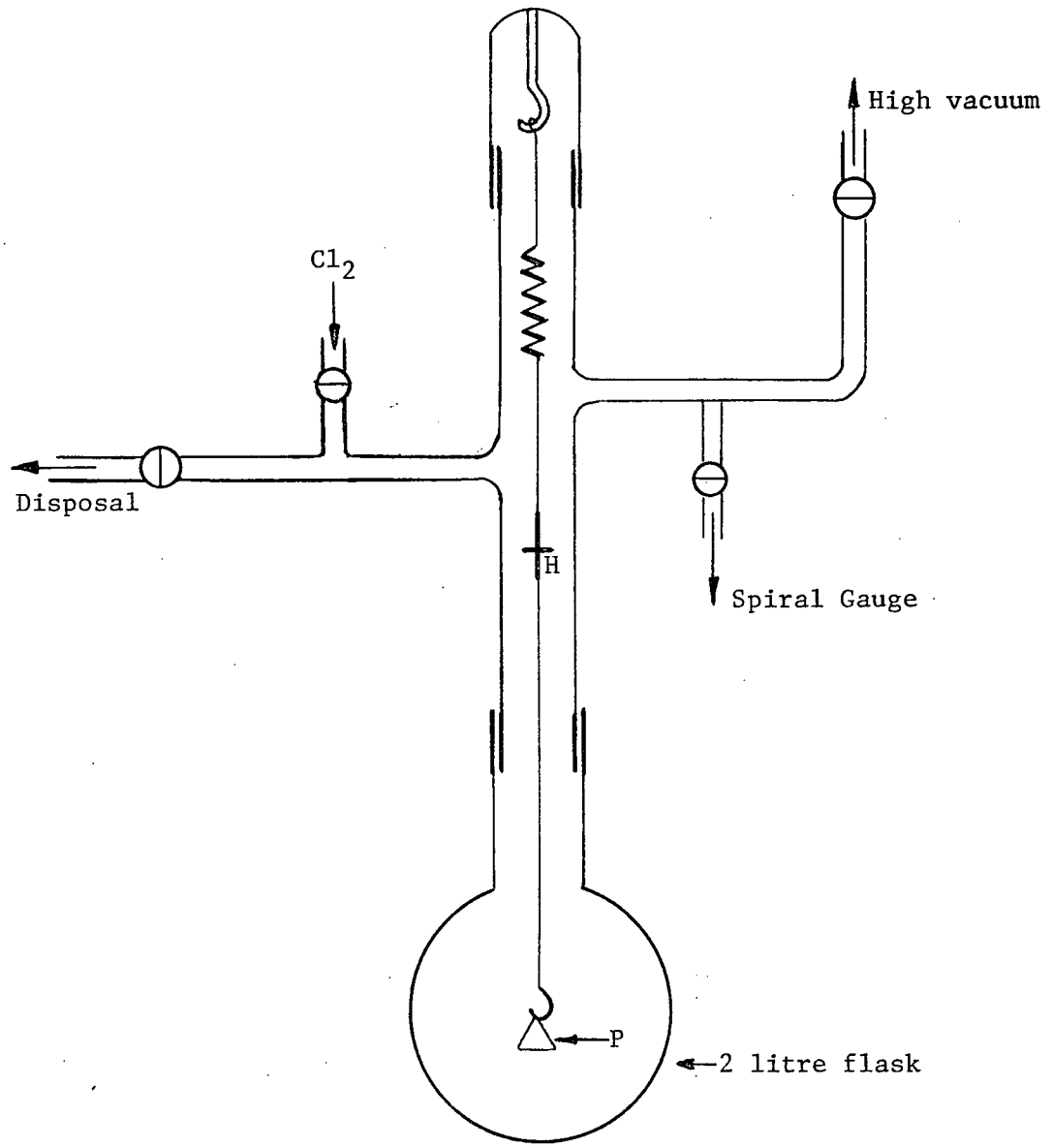

FIGURE II.9

APPARATUS FOR THE CHLORINE UPTAKE STUDIES OF CuCl USING GRAVIMETRIC METHOD

II.(3) D. C. CONDUCTIVITY MEASUREMENT

(A) Apparatus

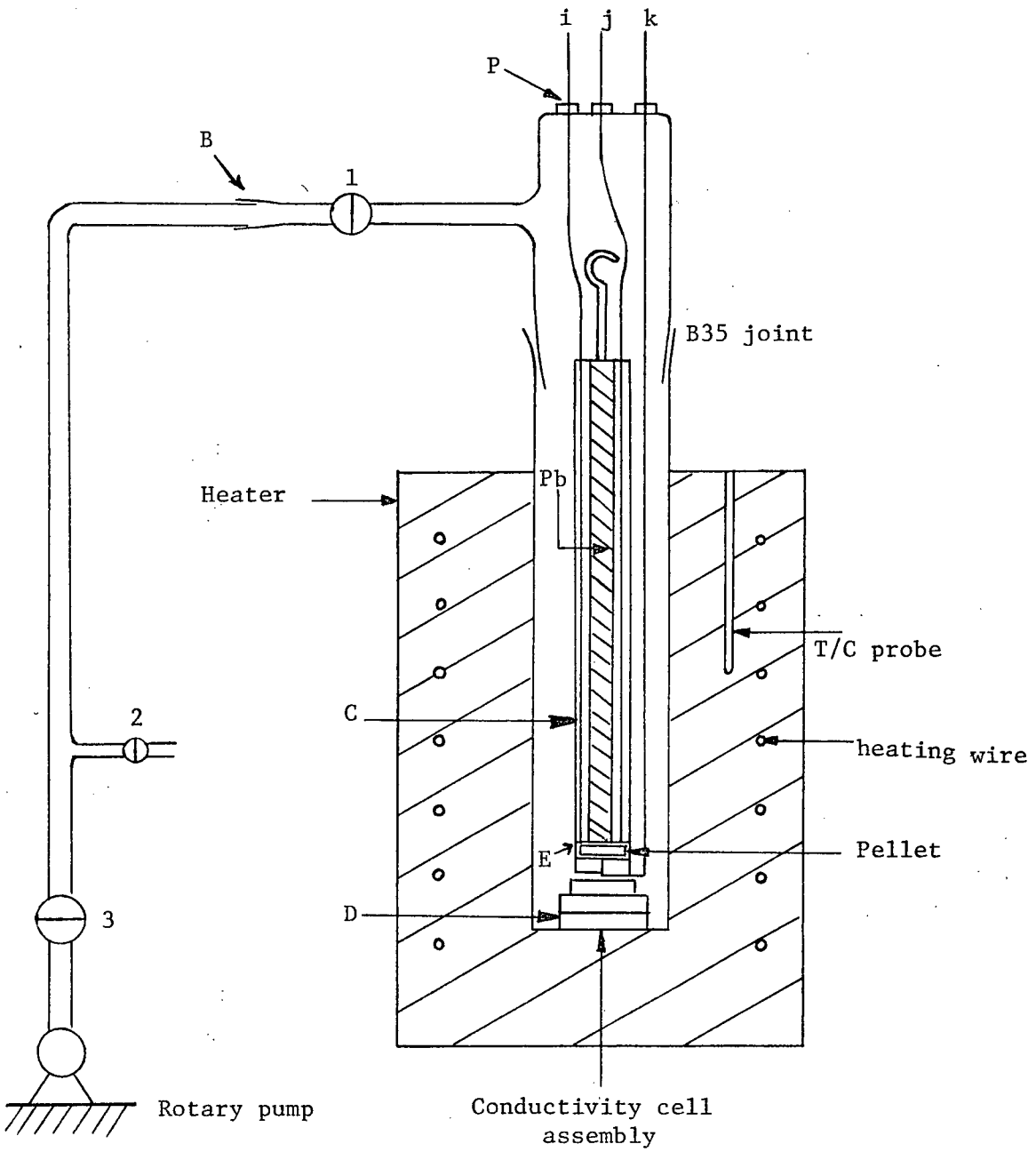

FIGURE II.10

D. C. CONDUCTIVITY MEASUREMENT APPARATUS

(i) Conductivity Cell Assembly

As shown in Figure II.10, the assembly consists of a jacket (pyrex) containing a teflon cylinder C weighted with lead to ensure contact between electrodes and pellet, and hooked onto a glass bar H. The assembly can be placed in a heater equipped with a thermocouple probe. The whole assembly can be evacuated and can be removed from the evacuating system at a ball and socket joint B. The pellet sample is placed between two platinum discs E (the electrodes.) The wires i, j, k, are spotwelded to the electrodes and sealed at P by a highly resistant wax, de Khotinsky cement (specific resistance $\sim 10^{15}$ ohm cm). j & k are made with Pt whereas i is made of Pt/10% Rh. When conductivity is to be measured, j and k can be connected to the conductivity measurement circuit. On the other hand, i and j can be used as part of a thermocouple circuit for accurate temperature measurement of the sample.

(ii) Temperature Control Unit

The temperature of the sample could be maintained to $\pm$ 1°C by a heater control unit shown in the following block diagram.

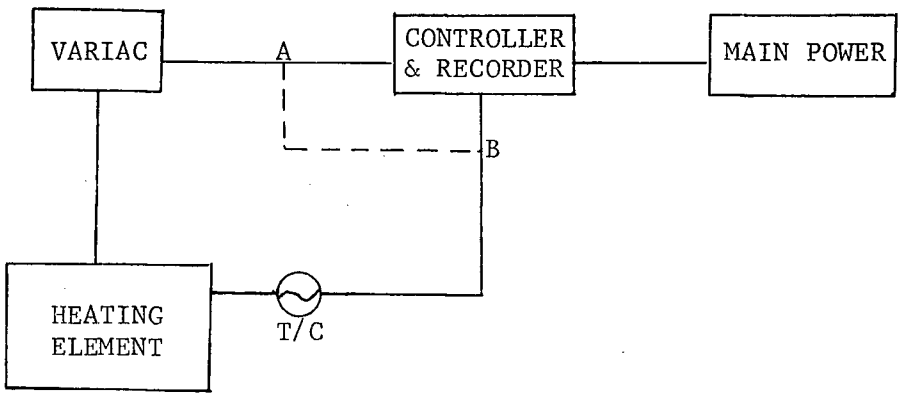

FIGURE II.11

HEATER CONTROL UNIT

The recorder used is of Honeywell Model Y156C 18-V(s) H-61 type with a range of 1-21 mv and control is performed by a micro-switch. A copper constantan thermocouple placed in a probe shown in Figure II.10 is the sensing element. The recorder is first set at a certain voltage corresponding to a required temperature. When the temperature detected is higher than the preset value, the variac will be shut off at A until the temperature drops to the preset value again. The temperature in the probe position would of course be somewhat higher than that of the sample. However, since the exact temperature is recorded by the Pt - Pt/Rh thermo-couple as mentioned earlier, only a rough correlation between the sample temperature and the probe temperature is required; this can easily be obtained by a rough calibration.

(iii) Electronic Euqipment and Circuit

The electrical circuit used to measure conductivity is shown in Figure II.12. The cell is wired in series with a Keithley decade shunt having resistances from 10^3 ohm to 10^{12} ohm, and a P.D. of about 22.5 volt is applied across the whole arrangement by means of dry cells. The P.D. across the shunt is measured with a Keithley model 200B battery-operated electrometer (d.c. VTVM) having an input resistance of 10^{14} amp., and ranges down to 0.8 mv. full scale deflection. A simple high impedance switch gear is used to permit polarity reversal and measurement of applied EMF(E_1), to check its constancy over a period of time.

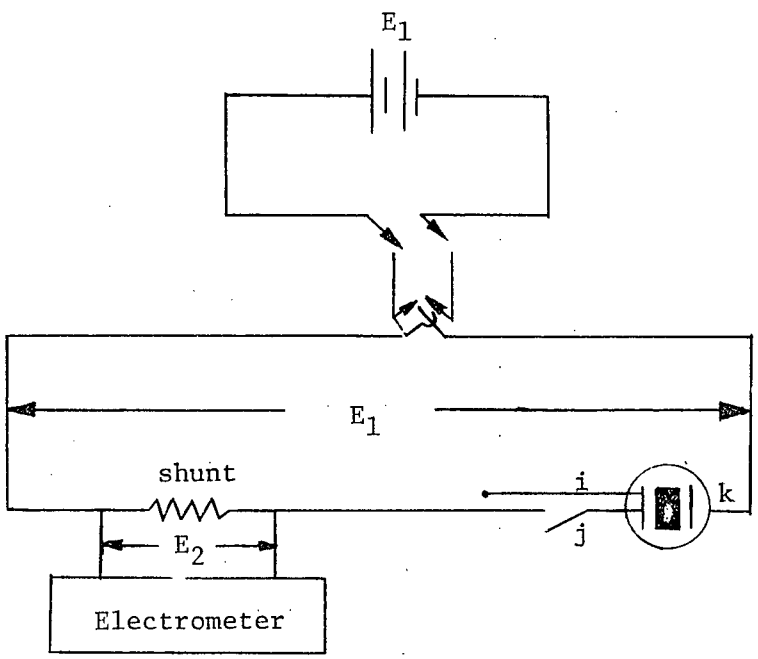

FIGURE II.12

CIRCUIT DIAGRAM FOR CONDUCTIVITY MEASUREMENT

From the simple circuit diagram, it can be easily seen that the conductance of the pellet is given by

$$\sigma = \frac{I}{E_1 - E_2}$$

where I is current, E_1 is the supplied voltage and E_2 is P.D. across the shunt.

The electrometer measures E_2 and the current range (i.e. reciprocal of resistance of shunt) R, thus

$$\sigma = \frac{E_2 R}{E_1 - E_2} \text{ ohm}^{-1} \quad \ldots\ldots \quad (1)$$

and specific conductance σ_{sp} is given by

$$\sigma_{sp} = \sigma . \frac{1}{A} \text{ ohm}^{-1} \text{ cm}^{-1} \quad \ldots\ldots \quad (2)$$

where A is the cross-sectional area of the pellet.

(B) Procedure

(i) Preparation and Charging of Pellets

The pellet-making die assembly (Perkin-Elmer KBr Die, 186-0002) is shown in Figure II.13. It consists of a casing C, a hollow cylinder B in which powder can be charged and pressure can be applied through a piston P and a die D, a lid L which provides air-tightness by its O-ring and finally an evacuation device.

The catalyst samples used were the products of the chlorination of CuCl [from the procedure described under III.(1)(B)(iv)]. To avoid the possible presence of a trace of water adhered to the solid surface, the samples of CuCl and $CuCl_2$ were first evacuated to $\sim 10^{-5}$ mm Hg for $\sim$ 5 hours before they were used.

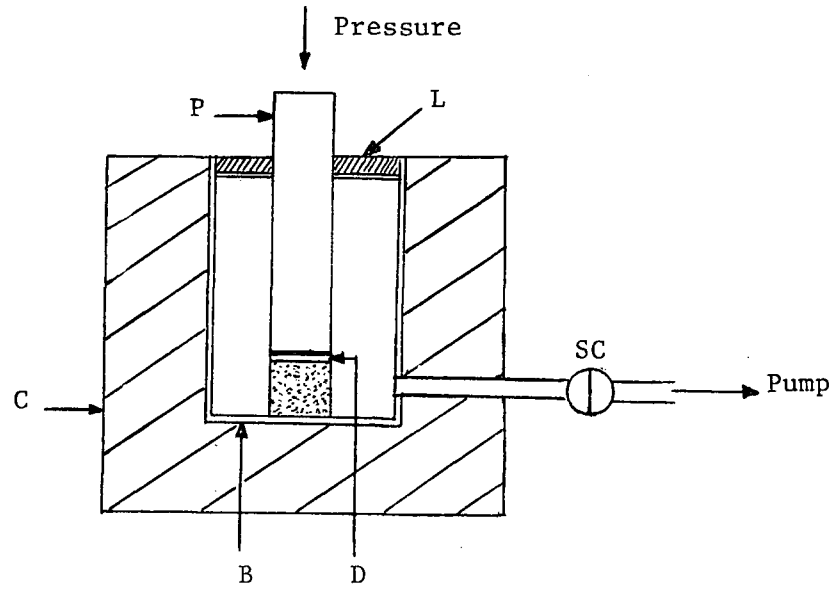

FIGURE II.13

PELLET-MAKING DIE ASSEMBLY

The pellet was prepared in the following manner. 0.5 - 0.8 gm of finely ground powder sample was transferred to the die in a dry box. The whole assembly was removed from the dry box and placed in a hydraulic press. It was evacuated for seven minutes with P, D, and the powder bed just in contact with one another. Afterwards, a pressure of 8,000 p.s.i. was applied for three minutes. It was removed from the press and by opening the stopcock SC, the part B was detached from casing C. The pellet was immediately released and stored in a dry box. The thickness of the pellet was later measured in a dry box by means of a micrometer. The area of pellet is the same as the area of D which is 1.326 cm^2.

The charging of the pellet into the conductivity cell was also performed in a dry box.

(ii) Measurement of Conductivity

After the conductivity cell assembly was anchored in position, evacuation was effected by opening SC 1 to the vacuum line (see Figure II.10). The pellet was usually heated in vacuo and maintained at a temperature of approximately 160°C for more than fifteen hours. The conductance of the pellet was then measured at successive intervals of temperature of approximately 10°C. The time allowed between successive reading was 80 minutes. This was found sufficient to establish thermal equilibrium in the pellet as indicated by its steady temperature. Readings were taken over a number of cycles of heating and cooling, depending on the reproducibility of results.

Besides the relationship between σ and T, the polarization effect was also studied.

The E_2 values were found to behave in a manner shown in Figure II.14. After the switch was turned on (at positive polarity say), the E_2 recorded dropped from the peak P+ value through C+. As the polarity was reversed, E_2 value rose to P− and then dropped to C− and the process repeated itself as polarity was reversed again.

It should be noted that the time interval of 80 seconds was adopted simply because of convenience and the peak values did not need to be the same. The final values of E_2 adopted were the average of $(P\pm + C\pm)/2$ values, and the polarization factor is defined as the average of $\frac{P - C}{(P + C)/2}$ values.

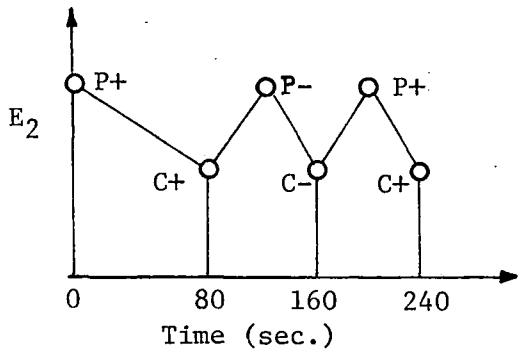

FIGURE II.14

TIME DEPENDENCE OF E_2

II.(4) X-RAY POWDER TECHNIQUE

(A) Equipment

X-ray powder photographs of solids were obtained using a General Electric powder camera of 14.32 cm diameter with Straumanis loading. CuK-α radiation was used with an Ni filter to reduce K-β radiation. A pinhole collimator of 0.8 mm was used in order to obtain photographs of sharp lines. In addition to the supplied equipment, a device was designed to align the position of the capillary tube properly. This can best be described with the aid of Figure II.15. A piece of white paper P is inserted between the capillary sample S and beam catcher. Light is allowed to shine on P by means of a lamp. The sample capillary is seen by eye through the collimator; what the eye sees is exactly what the X-ray will "see". A device D is attached to the head of the motor assembly (not shown) which can be moved in both the X and Y

directions. Thus if the capillary is not vertical w.r.t., the movable support disc M (seen as inclined), D can be moved to a position corresponding to the free end of capillary and then downwards to make the capillary vertical. If the capillary is off centered (seen as moving up and down while the motor is making a 360^{o} turn), D can be placed right above M and then moved downwards to adjust position of M until over a 360^{o} turn, the capillary stays stationary.

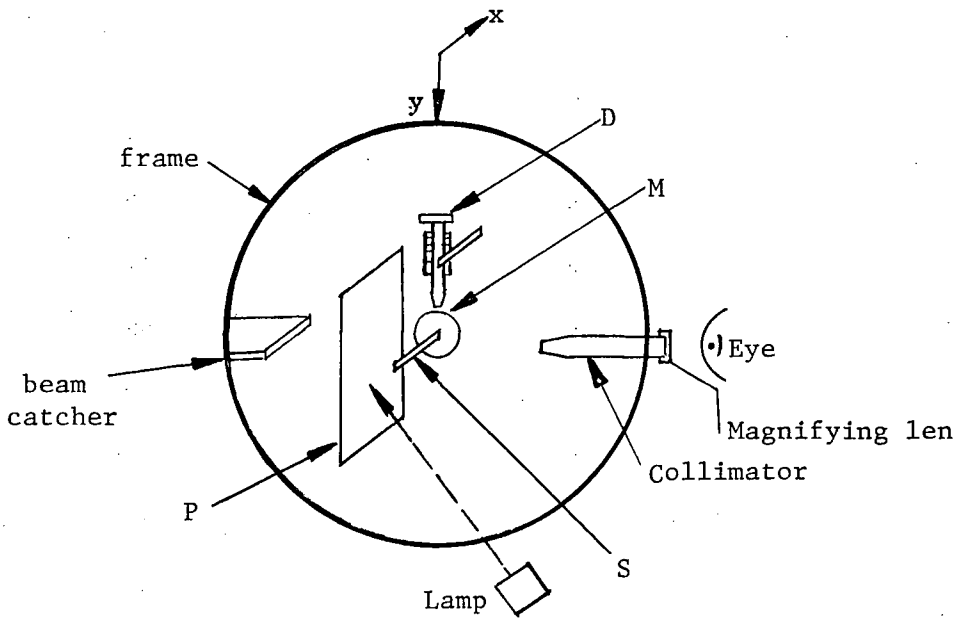

FIGURE II.15

ALIGNMENT OF SAMPLE CAPILLARY

(B) Internal Standard

In this work, since it is aimed at detecting minute changes in lattice parameters of catalysts, the internal standard method was adopted to ensure accurate estimation of the position of

diffraction lines. This method involves the mixing of the compound to be studied with a material which has well-defined positions of diffraction lines (generally not interfering with the diffraction lines expected for the compound) and hence can serve the purpose of calibration of position in the film. Such material is referred to as "Internal Standard." In our case, NaCl was taken as the internal standard. The value of the lattice parameter was taken as 5.6287 Å[12].

The calibration is achieved by plotting the deviation of lattice spacing, $\frac{d_t - d_e}{d_e}$ (d_t and d_e being the true and observed d values) against a certain function of θ. For all the observed NaCl lines, the deviation of the position of diffraction line can then be estimated from this curve. In practice, various functions such as θ, $\sin\theta$, $\cos\theta$, $\frac{1}{2}\left(\frac{\cos^2\theta}{\sin\theta} + \frac{\cos^2\theta}{\theta}\right)$ (the Riley function)were tried. It was found the simple θ function was the most reasonable one to be used since none of the other functions could linearize the plots. Two typical calibration curves plotted in Figure II.16 show the occurrence of uneven shrinkage of a film and therefore the necessity for using the simple function. At the low angle region, the value of $\frac{\Delta d}{d}$ is usually less certain; especially when θ is less than 13.8°, extrapolation heavily depending on the last two low angle points has to be made. In fact, it was found that a weighing scheme using $\sin\theta$ yielded slightly better results in the calculation of the lattice parameters of $CuCl_2$ (in terms of standard deviation), as compared with those using weighing scheme of equal weight. This was so presumably due to the fact that the allowance for the slight uncertainty of the low angle points had been made in the $\sin\theta$ weighting scheme.

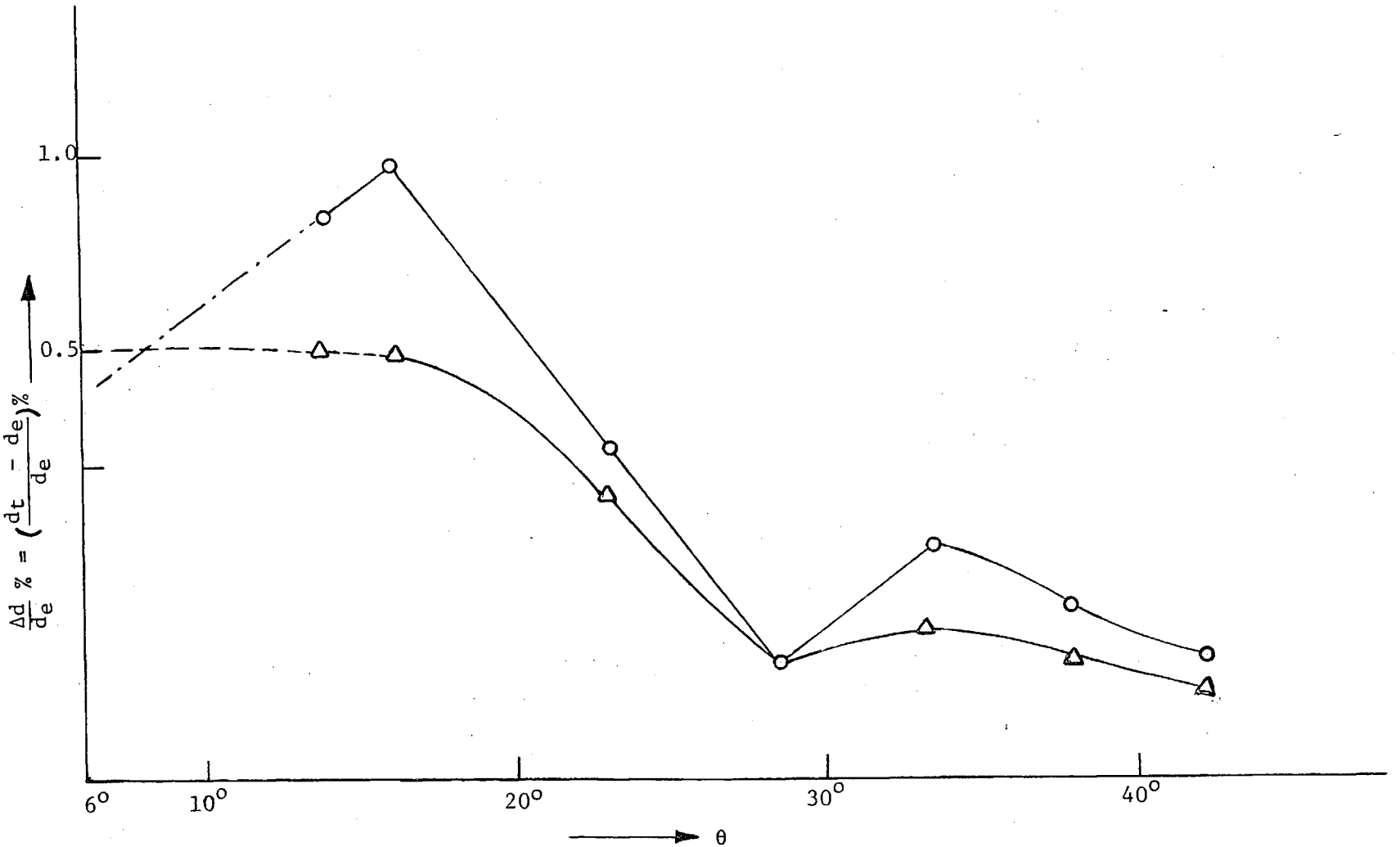

FIGURE II.16

CALIBRATION CURVES FOR X-RAY POWDER MEASUREMENTS

B#20 O (1st Sample)
B#20 Δ (2nd Sample)

(C) Procedure

(i) Sample Preparation and Mounting of Sample Tube

Samples for X-ray powder photographs were mounted in 0.5 mm quartz (or Lindeman Glass) capillaries. The capillaries used were heated @ 180°C for about 24 hours before they were introduced into a dry box. Small amounts of catalyst sample (the same type as that used for conductivity measurements) and AR NaCl were mixed and ground with an agate mortar and pestle and then loaded into the capillary tube with gentle tapping inside a dry box. The top of the capillary was sealed with Kel-F grease and flame-sealed immediately after removal from the dry box. The capillary was then mounted in the camera for X-ray exposure.

(ii) Exposure, Development and Measurement of Photographs

The film was exposed to X-rays (voltage 40 KV and current 15 Amp.) for approximately 50 hours. It was then removed from the camera in a dark room and developed with Agfa Dektol D-19 developer and fixed with Kodak Rapid Fixer.

X-ray powder photographs were measured on a light box provided with a steel scale of mm, to which was attached a measuring slide assembly containing a vernier and a magnified cross-hair for location of the diffraction lines (commercially known as "Film Illuminator and Measuring Device", type No. 52022/1, Philips Electronics, Inc.). The accuracy in reading the position of a line was ± 0.003 cm.

(iii) Computation

The distance between a pair of lines measured is proportional to the angle of diffraction of the X-ray beam by a certain set of planes in the crystal. This value is readily converted to the distance between the planes in this particular set. A simple computer programme was written for this conversion. The d values so obtained were readily converted to the "real" values by means of the calibration curve as described earlier. These "real" d values were then used to calculate the values of parameters by means of another computer programme (Celdim [13] , stored in memory deck at the Computing Centre of University of British Columbia) which employs a least square method.

Calculation of Lattice Parameter of CuCl

For pure CuCl, five lines corresponding to 111, 220, 400, 331, and 002 planes were clearly observed in order of decreasing intensity. As the composition of copper chloride varies from $CuCl_{1.0}$ to $CuCl_{2.0}$, the number of lines observed decreases. In fact, for copper chlorides with a value ($CuCl_x$) greater than 1.608, only two lines (111, 220) could be clearly seen. The reported value of lattice parameter was therefore taken as the mean over the values calculated from the individual d value.

Calculation of Lattice Parameters of $CuCl_2$

For the pure $CuCl_2$, twelve lines could be observed clearly (some lines too close to NaCl lines were disregarded). They were indexed with the aid of the single crystal results reported by

Wells[10] . A comparison in the d value and intensity for various planes between Wells and our results is given in the following table:

TABLE II. 1

COMPARISON OF X-RAY RESULTS FOR $CuCl_2$

hkl	Wells' Results			Present Results	
	Intensity		d	Intensity	d
	Calculated	Observed			
001	202	v.s.	5.744	v.s.	5.7573
20T	97	s.	3.427	s.	3.4336
200	309	v.s.	2.937	v.s.	2.9124
112	185	v.s.	2.352	v.s.	2.3703
111	44	m.s.	2.346	m.	2.3369
312	112	s.	1.855	v.s.	1.8634
113	26	w.	1.820	w.	1.8321
112	106	s.	1.816	s.	1.8068
403	20	w.	1.647	m.	1.6456
404	47	m.s.	1.474	m.	1.4841
004	45	m.s.	1.438	m.s.	1.4351
312	38	m.	1.234	w.	1.2215

For copper chlorides with intermediate composition, the number of planes observed decreases as the x value (in $CuCl_x$) becomes smaller. Thus , the same twelve lines were only observable in copper chlorides

with $x \geqslant 1.50$. For $x = 1.32$, only eight lines were distinctly observed. It was found that a longer time of exposure did not improve the visibility of the lines as the background's intensity was also raised. Therefore calculation were performed on the basis of the data of twelve as well as eight planes. While the former set of results give smaller limits of error, the latter set enable the comparison of results over a wider range of composition.

(D) Materials

The film used was Ilford "Ilfex Safety Base, for use without intensifying screen" supplied in sheets 35.6 x 43.2 cm which was carefully cut in a dark room to approximately 4.4 cm x 43.2 cm for use in the powder camera.

The developer used was DEKTOL D-19 by Agfa.

The fixer used was KODAK rapid fixer.

NaCl used was A. R. NaCl.

II.(5) MAGNETIC SUSCEPTIBILITY TECHNIQUE

Magnetic susceptibility was determined by the Gouy Method. The apparatus used was made available by courtesy of Dr.R.C. Thompson and his research associates. Essentially, it consists of a pair of electromagnets, a balance of high precision (Oertling balance) and a temperature control device enabling measurements to be made over the range of temperature of 77^{o} - $420^{o}K$. The Gouy tube was calibrated using $CuSO_4 \cdot 5\ H_2O$ as standard as described by Figgis [14]. Catalyst samples used for studies were the same as those used for conductivity measurements. Finely ground sample was packed into the tared Gouy tube in a dry box. The

tube was removed from the box and weighed together with a tared jacket tube. Afterwards, it was returned to the dry box for sealing off (using plasticene). The Gouy tube with a known amount of sample was placed in the apparatus for susceptibility measurement. Two field strengths of magnetic field were employed viz. 4,000 oerst and 7,800 oerst.

II.(6) E.S.R. TECHNIQUE

(A) Apparatus

(i) A Varian E_3 spectrometer was used for all E.S.R. work in this thesis. Essentially, the spectrometer is made up of four main parts:

(a) A console system which contains a console power supply, a 100 KC/Sec. modulation unit (for choosing appropriate line width), a magnetic field regulator and a recorder.

(b) A 9.5 KC/sec. microwave bridge which consists of a microwave system for excitation and observation of E.S.R. signal, an AFC which stabilizes the Klystron, a Klystron d.c. power supply and a preamplifier for signal amplification.

(c) A 4 inch water cooled magnet system which has an accessible air gap of 1.2 inches in which the cavity sits.

(d) An oscilloscope for observation of signal when the recording unit is not used.

The spectrometer provides good resolution and is convenient to operate.

(ii) Sample Handling Systems

There are two types of E.S.R. studies in this work. The first is a simple type involving the powder catalyst alone at ambient and liquid nitrogen temperatures. The second type involves studies of E.S.R. with the catalyst in situ in a reactor system specially designed for E.S.R. studies. This type can be further classified into three sub-types:

1. Catalyst in contact with C_3H_8
ii. Catalyst in contact with Cl_2
iii. Catalyst in contact with both C_3H_8 and Cl_2.

They were all carried out at elevated temperatures including the reaction temperature viz. $130^{o}C$.

(a) E.S.R. Studies in the Absence of Gas(es)

The E.S.R. spectra for the powder catalysts alone were obtained with a simple quartz tube sample holder as shown in Figure II.17.(a)

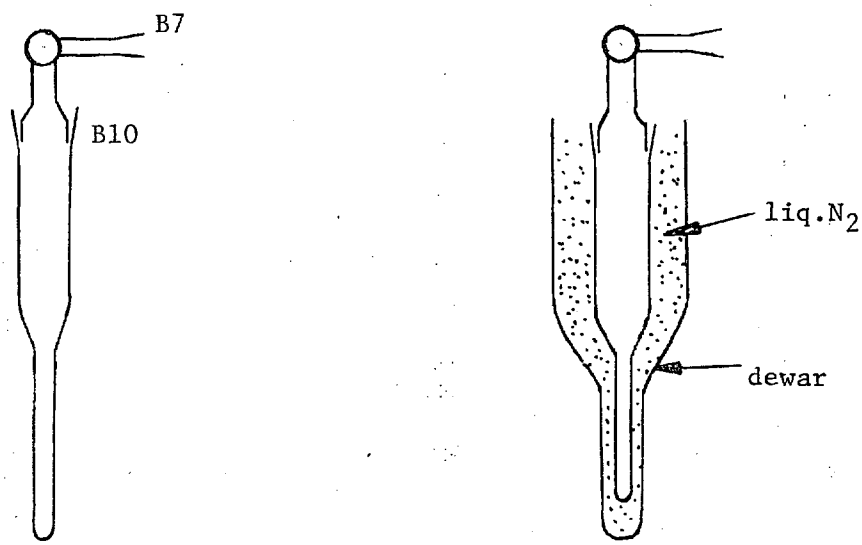

(a) E.S.R. PROBE (b) E.S.R. PROBE WITH DEWAR

FIGURE II.17

E.S.R. PROBES

When the E.S.R. signal at liquid nitrogen temperature was required, a specially designed dewar was employed Figure II.17 (b) .

(b) E.S.R. Studies in the Presence of Gas(es)

The apparatus used for obtaining this type of spectra is more elaborate. It consists of four components described as follows.

(m) Evacuating System

The system is built on a movable rack. High vacuum is provided by a mercury diffusion pump coupled with a rotary pump. The system is equipped with an ionization gauge to measure vacuum as described under "Kinetic Studies".

(n) Storage Area

This part is shown in Figure II.18. The diagram is self-explanatory. The reason for this part to be removable from the evacuating system is that the storage of the gases has to be carried out with aid of the apparatus used for kinetic studies. Only when the gases have been admitted are they pumped on at liquid N_2 temperature by the evacuating system described in (m). It should be noted that SC 9 and 10 are Teflon SC whereas SC 8 and 9 are greased with Kel-F.

(o) Connector

This is a simple U-Shape tube with B-10 socket and a S 13 ball joints at both ends. It connects component n and p as described in the next paragraph.

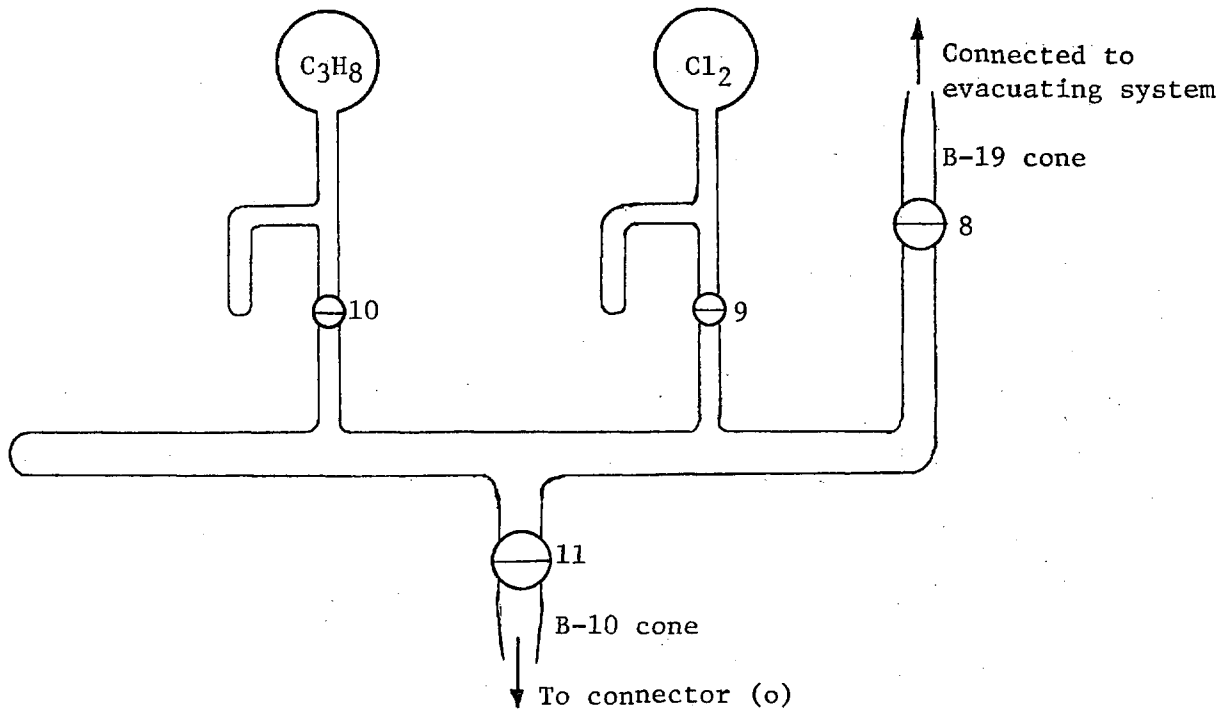

FIGURE II.18

COMPONENT n OF E.S.R. STUDIES

(p) Probe Assembly

The probe assembly is shown in Figure II.19. The main part of the assembly is a triple jacket made of quartz (the shaded part was evacuated for insulation) enabling the sample containing tube S to be heated. (This is also the part sitting in the probe cavity of the E.S.R. spectrometer). It is connected to the rest of the system by a quartz/pyrex graded seal G. The sample can be charged from the joint at the top with a long stem funnel and then evacuated through SC 13 before this component (p) is attached

through connector (o) to the storage area (n).

Hot air from an air heater is allowed to pass from the bottom to top of jacket as shown. A thermocouple is also incorporated.

At a steady state, because of the high degree of convection mixing, the temperature recorded by the thermocouple should correspond very well to the temperature of the sample.

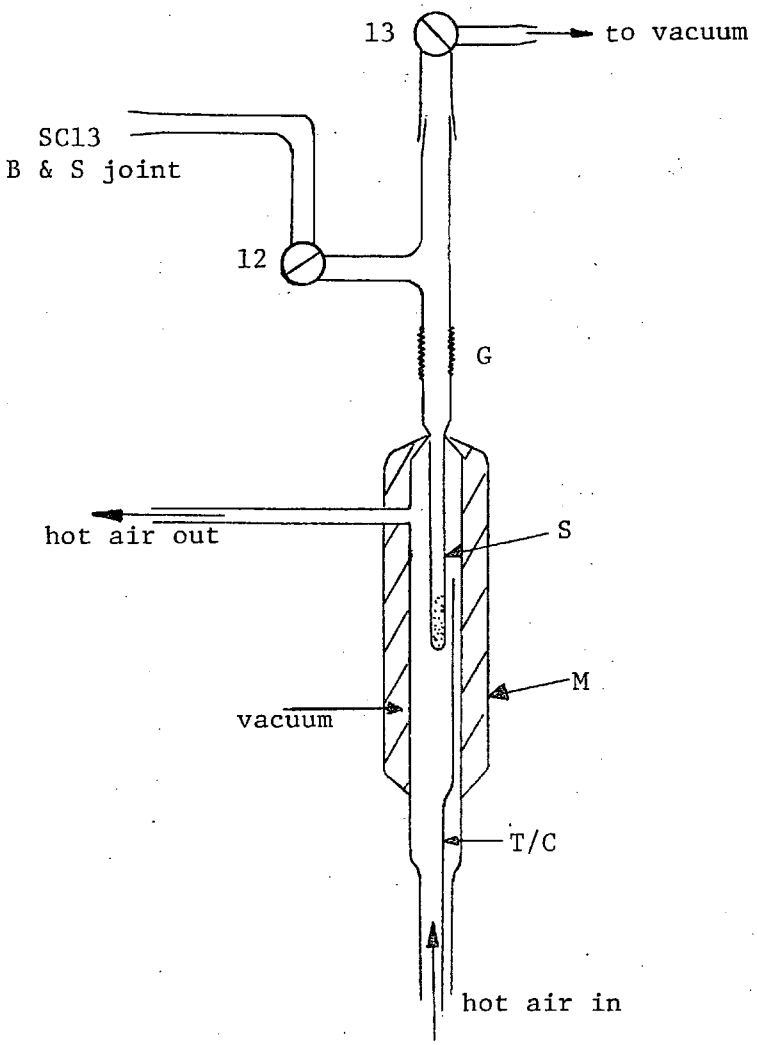

FIGURE II.19

PROBE ASSEMBLY

(B) Procedure

(i) E.S.R. Studies in the Absence of Gas(es)

Powdered catalyst (small lumps were also used but results show no difference) was charged with the aid of a funnel into the probe shown in Figure 17 (a), which was stoppered in a dry box, removed from the dry box, evacuated, and placed in the cavity of the E.S.R. spectrometer.

(ii) E.S.R. Studies in the Presence of Gas(es)

(a) Storage of Gases

The transfer of gases was effected with the B-19 cone shown in Figure II.18 connected to the point just outside the SC 8 of the Kinetic Studies apparatus in Figure II.1. Gases were transferred from the storage bulbs in the latter apparatus to bulbs in the former apparatus (approximately 20 cm Hg of gases were in the storage bulbs). When the gases were stored, the component m (Figure II.18) was then connected to component 1 at the B-19 joint. The gases were trapped in the side arms of the respective bulb with liquid nitrogen and pumped on by the evacuating system.

(b) Charging of Sample and Positioning of all Components

Powdered catalyst was charged in a dry box into the probe assembly (Figure II.19) through the joint A by means of a long stem funnel. It was stopped by closing SC 12 and 13 before the removal of the assembly from the dry box. The probe assembly was placed in the cavity of E.S.R. spectrometer and connected by means of the connector (n)

to the component (m). The overall system was evacuated to 10^{-5} mm Hg and the sample was heated by allowing flow of hot air.

(c) Scanning of E.S.R. Spectra

After all components were placed in position, the apparatus was ready for scanning of E.S.R. spectra. A blank run with the catalyst alone was normally taken for comparison purpose. Then depending on what type of E.S.R. spectrum was required, appropriate gas was admitted into the sample-containing tube.

II.(7) MICROSCOPIC TECHNIQUE

Non-stoichiometric copper chlorides were examined under microscopes. Two microscopes were used; one with a magnifying power of 40 times (binocular, stereoscopic, Cenco Model No.512-I), another with a magnifying power of 75 times (Bausch & Lomb, Model No. LN 4041). Various ways of illumination were attempted. Samples of catalyst (in lump and powdered forms) were loaded into a container which is shown in Figure II.20 in a dry box. The container was then stoppered and removed from the dry box and viewed under microscopes. Lumps were subsequently cut up and pressed between two thin glass slides.

On the other hand, the particle size distribution of CuCl was determined in the following manner. Commercially supplied CuCl was spread over a slide with the aid of another slide shearing over it. Films were taken with the eye piece of the microscope adapted for a camera (Pentax). The films were developed and

enlarged in the usual way. The final magnification factor came up to ∿ 140 times. The particles of various size (in terms of area) could then be counted and a distribution curve be drawn.

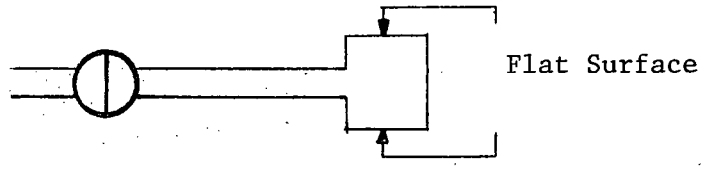

FIGURE II.20

SAMPLE CONTAINER FOR MICROSCOPIC STUDIES

II.(8) ANALYSIS OF CATALYST AFTER USE

After each complete series of runs, the catalyst was removed from the reactor system. The composition was then determined by chemical analysis. Copper was determined by the copper pyridine complex method [15]. Chlorine was determined by the Volhard Method. The only thing calling for comments is that the test solution was made up by dissolving sample in conc. NH_3, and then acidifying with HNO_3 because dissolving by acid directly would cause a loss of chlorine in the form of HCl. Carbon, hydrogen, and oxygen contents were determined by the microanalysis laboratory in the Dept. of Chemistry, University of British Columbia to determine whether irreversibly - adsorbed products from the chlorination of propane were present. However, it was found in a few samples that

the catalyst did not contain any significant amount of these elements, hence microanalysis was not carried out for the subsequent catalyst samples.

The composition of the catalyst during a series of runs was estimated by the amount of Cl_2 taken up irreversibly by the catalyst which in turn was measured by pressure decrease with the spiral gauge. The values of the final composition estimated by such method and that by analysis are in close agreement (to within $\pm$ 0.02 in x in $CuCl_x$).

CHAPTER III

EXPERIMENTAL RESULTS

III. (1) KINETIC STUDIES

Two reactions proceed simultaneously in the system.

The gas-phase reaction $C_3H_8 + Cl_2 \longrightarrow C_3H_7Cl + HCl$ -- (I)

and the gas-solid reaction $CuCl + \frac{1}{2} Cl_2 \longrightarrow CuCl_2$ -- (II)

Since none of the materials in the system remains unchanged, there is no true catalysis; but since the presence of the solid phase accelerates reaction (I), while the presence of propane accelerates or decelerates reaction (II), each reaction may be regarded in a loose sense as being catalysed. The discussion of kinetics and mechanism is not in any essential way different from that appropriate to a case of true catalysis; but the fact that no material remains unchanged presents a difficulty in accumulating experimental data. In particular, that the activity of the solid (which will often be referred to for convenience as the "catalyst") changes with extent of conversion to $CuCl_2$ is both the principal subject of this thesis and a serious obstacle to obtaining, for example, kinetic data at two different pressures or temperatures on solid samples of the same catalytic activity.

A major part of the kinetic work was therefore devoted to studying the activity of the catalyst $CuCl_x$ as a function

of x, at a fixed temperature (130°C) and fixed initial pressures of gaseous reactants (5 cm Hg each). Reproducibility was rather low, but by carrying out series of reactions on many different catalyst samples (each one studied, as far as possible, from CuCl to about $CuCl_{1.85}$), the compositions corresponding to maximum catalytic activity were established fairly definitely.

Data for temperature and pressure dependence were obtained only for the case of $CuCl_2$, for reasons just mentioned. The former was used to calculate the activation energy of the process whereas the latter was used to establish the order of the reaction. In fact, the order of the reaction could only be established in this way (initial rate method) as rate curves could not be used because of the reaction (II) occurring simultaneously; in the time for a sample of propane to be more than half consumed as required for the determination of order, the catalyst composition could have undergone a change large enough to affect its activity significantly.

The rate of uptake of chlorine by CuCl was measured manometrically in two ways:

(i) with chlorine present as the gas phase

(ii) with propane - chlorine mixtures present.

On the other hand, the gravimetric method was employed to study the former case only; the results obtained by this method are much less fruitful and therefore used only for comparison purpose.

Since results obtained in case (i) indicate that the uptake of Cl_2 was usually very close to linear over the duration of one run (except for $CuCl_x$ of low x value), chlorine uptake rates in case (ii) were calculated very often from only two experimental points, viz. at the beginning and end of the standard twenty-minute run used in fixing the catalytic activity curve.

Data on the Chlorination of Propane

(a) Products of Reaction

The reaction between propane and chlorine was found to yield hydrogen chloride, 2-chloropropane and 1-chloropropane in approximately 1:1 ratio. Such a ratio is commonly found although the ratio predicted from a probability consideration should be 1:3 if all hydrogens are equally readily attacked (two secondary hydrogen atoms and six primary hydrogen atoms in propane).

For runs followed for longer times, isomerisation of 2-chloropropane to 1-chloropropane was found to occur. However, no dichloropropanes were detected (up to a reaction time of 100 minutes.)

(b) Rate of Blank Runs

For any catalytic work, it is always important to have knowledge about the rate of the reactions studied in the absence of catalyst in order to establish that the apparent effect of the catalyst is genuine.

It is well-known that owing to the inertness of alkanes, homogeneous (gaseous phase) halogenation of alkanes in the absence of light proceeds slowly at low temperature (lower than $\sim 300^{o}C$), and the reaction mechanism is of a free radical type. According to Yuster & Reyerson [16], who studied chlorination of propane using a flow system with pyrex glass as the material for reaction vessel, the rate of blank runs was of the order of 0.029% of reactant reacted per minute at $130^{o}C$. (This figure was calculated by the author by extrapolating their data, and assuming a continuous stirred tank system). These authors considered that the homogeneous gas phase reaction had a chain mechanism and that the catalytic effect of the glass wall was due to its ability of initiating and breaking such chains.

In our case, the rate of blank runs (after allowing for removal of reactants due to sampling) was found to vary slightly from time to time, and was of the order of 0.05 - 0.1% per minute. That was why blank runs were performed before and after each series of catalytic runs to ensure the observed catalytic rates were properly corrected. Thus the rate of blank runs in our case was reasonably close to the extrapolated value from Yuster and Reyerson's results. That the rates of blank runs are quoted in percentage of reactant reacted per minute is quite arbitrary as the order of blank runs has not been studied and consequently the rate constant could not be worked out. Thus there is some uncertainty in comparisons with reported data.

(c) Order of Reaction

As remarked earlier, the order of the reaction could only be determined definitely for $CuCl_2$ catalyst, by the method of initial rates.

The data are summarized in the following two tables.

TABLE III.1

DETERMINATION OF ORDER IN Cl_2

Initial propane pressure = 10.0 cm Hg

No. of moles of $CuCl_2$ = 4.60×10^{-2} moles

P (Pressure of Cl_2) (cm Hg)	r (rate) (cm Hg/min)
2.03	0.628×10^{-2}
4.90	1.475×10^{-2}
9.40	2.980×10^{-2}

TABLE III.2

DETERMINATION OF ORDER IN C_3H_8

Initial chlorine pressure = 10 cm Hg

No. of moles of $CuCl_2$ = 4.60×10^{-2} moles

P' (Pressure of C_3H_8) (cm Hg)	Log P'	r (rate) (cm Hg/min)	Log r	$\frac{P'}{r}$	$\frac{(P')^{\frac{1}{2}}}{r}$
1.40	0.146	8.25×10^{-3}	$\bar{3}.917$	169	13
2.92	0.465	1.60×10^{-2}	$\bar{2}.204$	181	13.5
5.78	0.762	2.65×10^{-2}	$\bar{2}.424$	218	14.8
10.22	1.005	3.70×10^{-2}	$\bar{2}.568$	276	16.6

The results are also plotted in Figures III.1 - 3. Figure III.1 shows that the rate is directly proportional to P. Chlorination of propane in the presence of $CuCl_2$ is therefore a first order reaction w.r.t. chlorine pressure.

Figures III.1 and 2 show that neither the rate vs. P' nor the log (rate) vs. log P' plot is linear. In fact, both show that the increase of rate slows down as pressure increases. This means that the dependence of rate on propane pressure is quite complicated. The flattening of the curves at higher pressure strongly suggests that a maximum of rate may occur if the reaction is carried out at even higher pressure. If that be the case, the process may be a typical bimolecular reaction proceeding by a Langmuir-Hinshelwood mechanism with one of the reactants very weakly adsorbed (Cl_2 in this case)[17] . The rate equation would then be

$$r = \frac{k K K' P P'}{(1 + K'P)^2} \quad \ldots . \quad (1)$$

Where P and P' are the pressures of Cl_2 and C_3H_8,

K and K' are the adsorption constants of Cl_2 and C_3H_8, having the dimensions of the reciprocal of pressure,

and k is the rate constant, having the same dimensions as the rate (amount of reactant per unit time),

According to equation (1), the rate is proportional to the pressure of chlorine (if P' is kept constant) as found experimentally.

FIGURE III.1

RATE VS. PRESSURE PLOTS

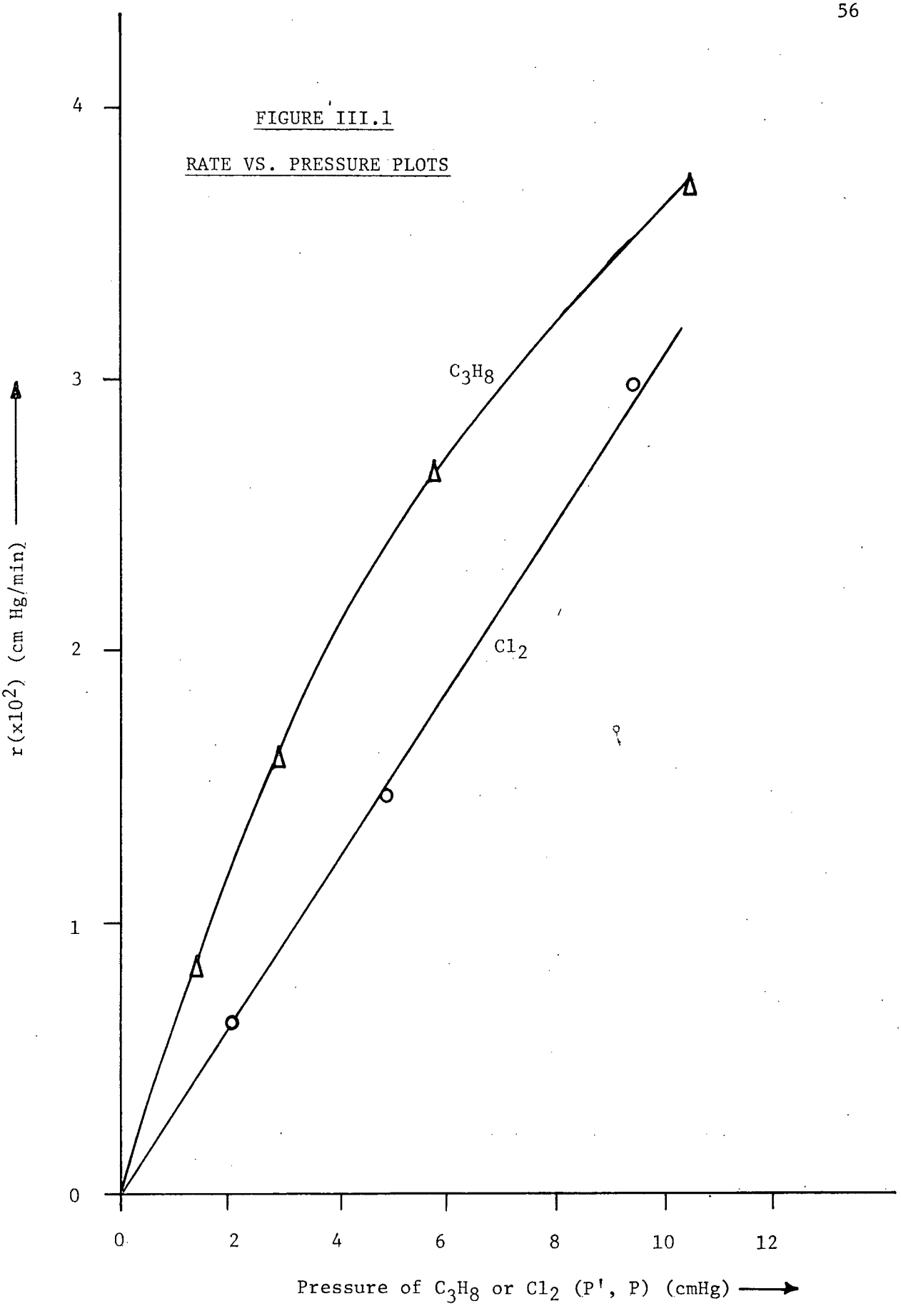

FIGURE III.2

Log r vs. Log P' PLOT FOR C_3H_8

Initial Cl_2 pressure = 10.0 cm Hg

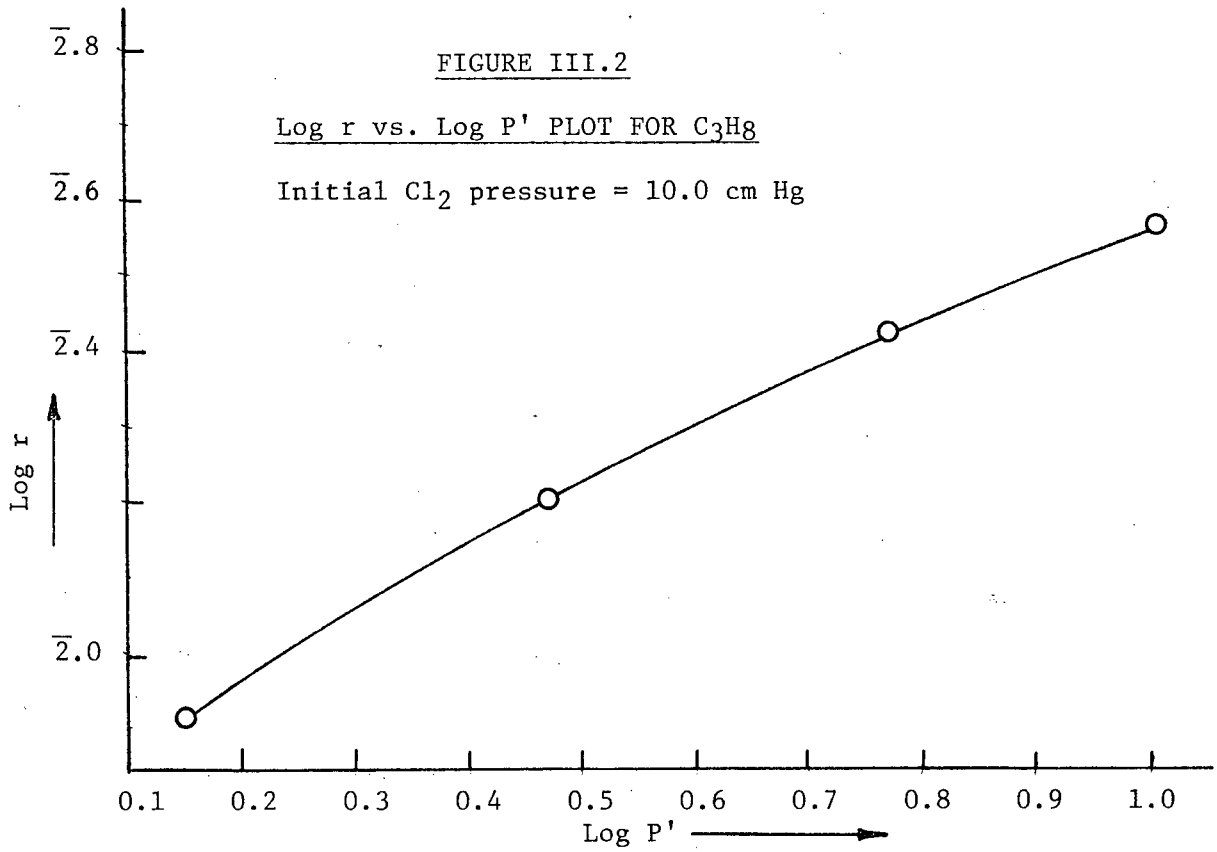

FIGURE III.3

LANGMUIR-HINSHELWOOD MECHANISM

PLOT FOR C_3H_8

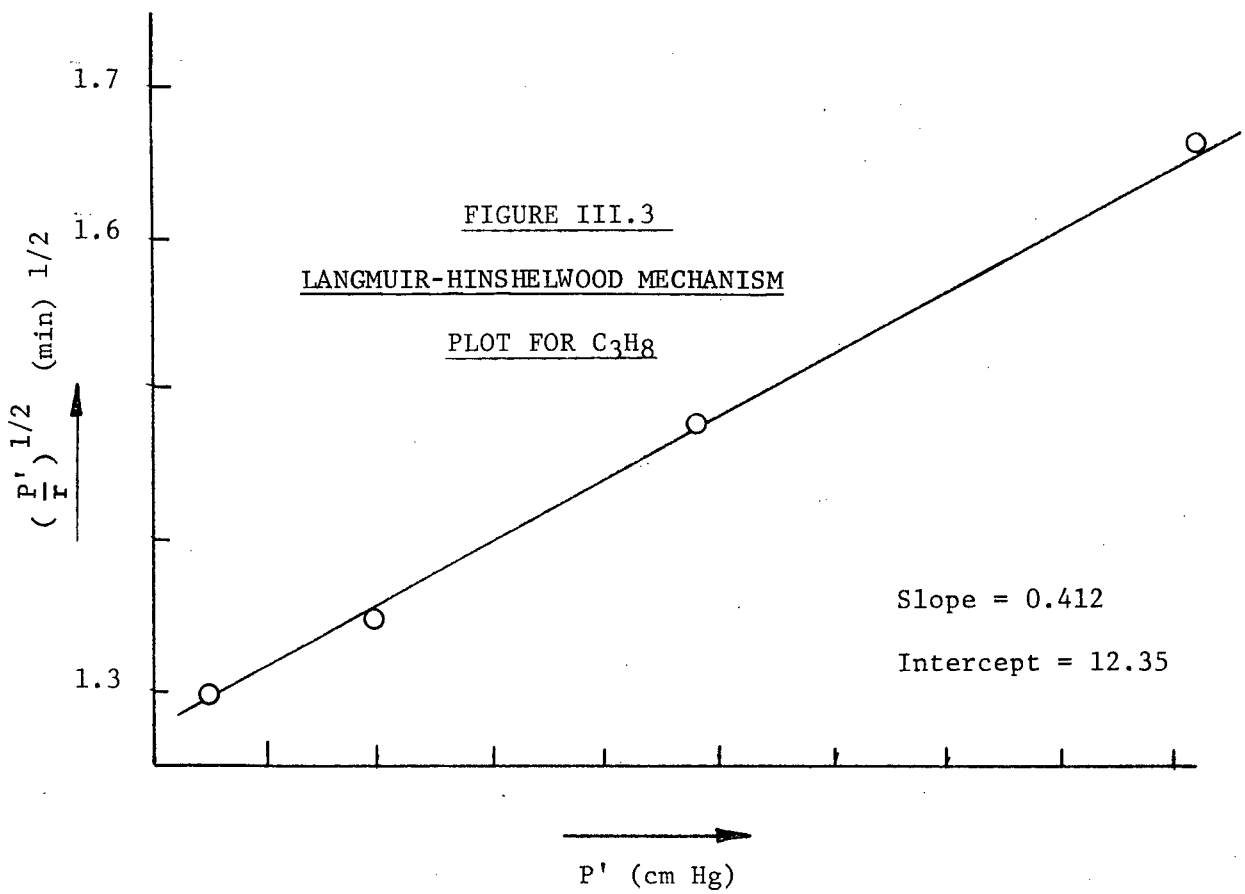

One can rearrange equation (1) into the form

$$\left(\frac{P'}{r}\right)^{1/2} = \left[\frac{1}{k\,K\,K'\,P}\right]^{1/2}(1 + K'P') \quad \ldots . \quad (2)$$

Thus if one plots $\left(\frac{P'}{r}\right)^{1/2}$ vs. P', a straight line with a slope $\left[\frac{1}{k\,K\,K'\,P}\right]^{1/2}$ should be obtained. This was found indeed to be the case as shown in Figure III.3.

The value of the ratio of the slope to the intercept is the value of K', and was calculated as 3.34×10^{-2} cm Hg^{-1}.

To sum up, the chlorination of propane in the presence of $CuCl_2$ was determined to be first order w.r.t. pressure of chlorine but no simple order relationship was found to exist w.r.t. the pressure of propane. The kinetics were found to be consistent with a Langmuir-Hinshelwood mechanism with the chlorine molecules weakly adsorbed onto the surface of $CuCl_2$, and propane much more strongly adsorbed.

(d) The Catalytic Activity as a Function of Composition x

As remarked earlier, great difficulty was experienced in obtaining results of high reproducibility. However, by averaging data for a number of different series of runs, the pattern of behaviour could be established fairly reliably.

In Fig.III.4,the apparent rate constant k_2 [k K K' in Eqn (1)] for four series of runs (10, 12, 16, 17) at 130°C is plotted against the composition x. The length of the vertical line passing through each point represents the standard deviation of the mean. In each of the four series of runs, peaks in catalytic activity appeared at

FIG. III.4 CATALYTIC ACTIVITY OF $CuCl_x$

FOR THE CHLORINATION OF C_3H_8

Average of Results of 4 Series of runs at 130° C

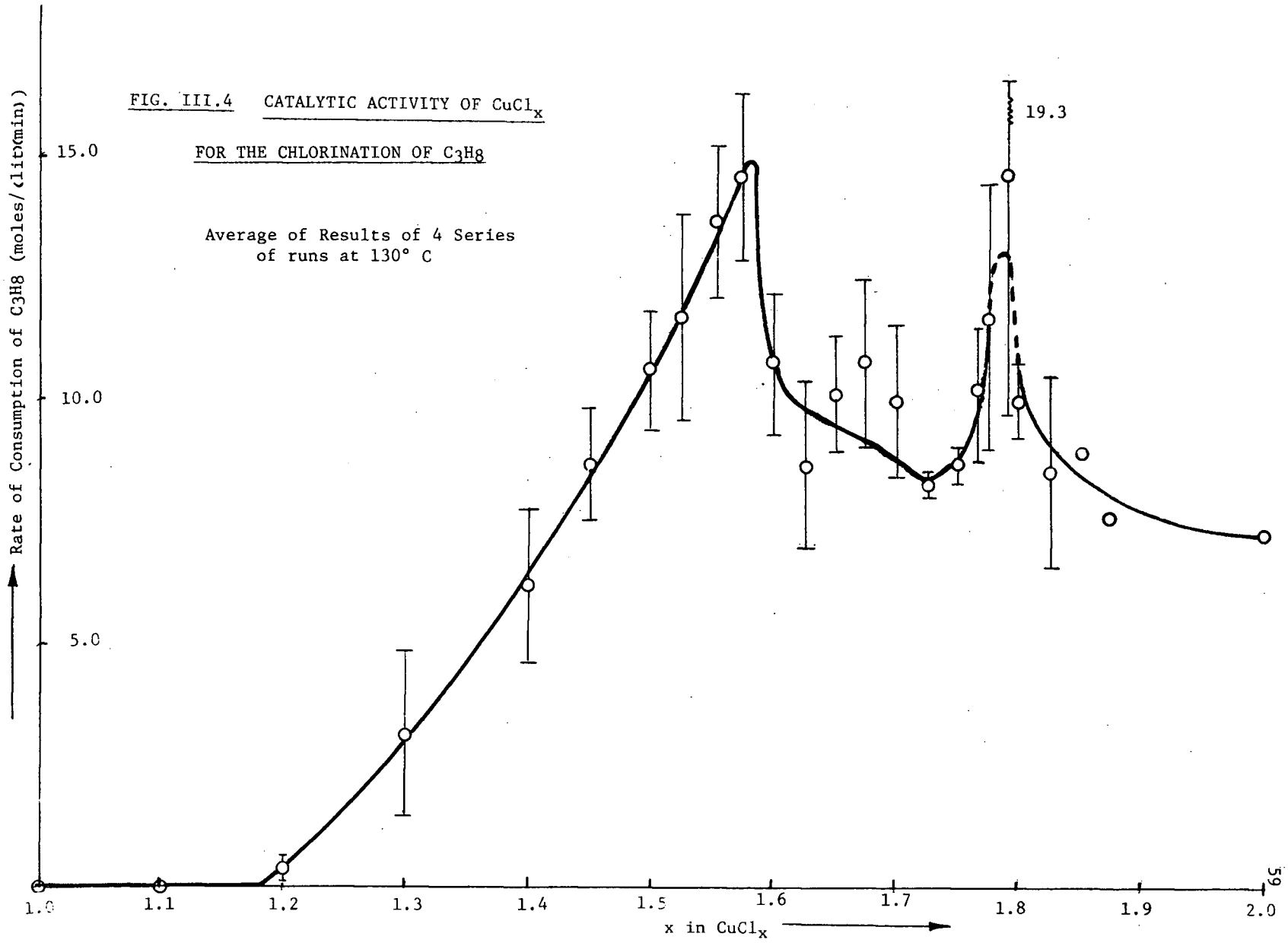

roughly the same compositions, but the absolute values of the reaction rates varied widely from one series to another, the rates being, e.g. all high in one series and all low in another. Thus, as implied by drawing vertical lines through the points, the possible error in absolute activity of the catalysts is large, but the error in positions of the maximum on the composition scale is quite small.

The curve exhibits two maxima. The first one occurs at $x \sim 1.57$. The second maximum is less well established as implied by the large value of standard deviation of the mean around the region of maximum rate. Nonetheless, the peak probably occurs in the range $1.775 < x < 1.795$. This is supported by the fact that the results of one series of runs carried out at 105°C (and therefore not included in the average which is for data at 130°C) exhibit similar behaviour to that shown in Fig.III,4with the second peak occurring at $x \sim 1.79$.

The error in composition is of a cumulative type. In other words, the points at the latter part of the curve (excepting $CuCl_2$) are more uncertain than the earlier points in so far as composition is concerned. Moreover, while each point may have an uncertainty of about $\pm$ 0.005 (the deviation in the end product from the analysis figure was about $\pm$ 0.02 in x as pointed out in Chapter II), the interval between successive points is known much more accurately than this, because each successive chlorination of the catalyst shifts the composition by an amount which follows a definite rate law (see next section of results). In other words, one cannot adopt

very well a random error approach like that for the rate to represent the errors of composition. Consequently, no attempt was made to indicate the limit of error in the composition in Figure III.4.

(e) Temperature Dependence of the Catalytic Activity

The only consistent data on temperature dependence were obtained for the case of $CuCl_2$. For copper chlorides of other compositions, attempts were made to obtain Arrhenius plots for some series of runs at temperatures at 15° intervals from $75^{\circ}C$ to $120^{\circ}C$. The results were very scattered, and the effects of temperature and of varying composition were not adequately separated. Up to $CuCl_{1.5}$, the best value for the activation energy appears to be 0 ± 3.5 Kcal/mole (0 ± 0.15 eV). From $CuCl_{1.5}$ to $CuCl_2$, there appeared to be a definite but small positive temperature dependence, but the activation energy could not be found at all accurately and can be quoted only as 2.3 ± 1.2 Kcal/mole (0.10 ± 0.05 eV).

(f) Effects of Grinding the Catalyst and Re-using It

In order to determine the effect of improving gas-solid contact and of exposing fresh CuCl surface, a catalyst (composition $CuCl_{1.611}$) was removed from the reactor system, ground up in a dry box, and then returned to the reactor for further study. The results show that while the chlorine uptake was greatly enhanced by such treatment, the catalytic rate was hardly affected. The data are summarised in Table III.5 in the next section where the results of the effect of grinding of catalyst on chlorine uptake are also presented.

(g) Delayed Release of HCl

In many catalytic runs, hydrogen chloride was not observed in the first twenty minutes of reaction. When it was first observed in a given run, its amount was usually less than that expected from the amount of C_3H_8 consumed. While there was an uncertainty in the chromatographic analysis of hydrogen chloride in the lower concentration region as pointed out in Chapter II, there were some cases in which the discrepancy in the amount of HCl exceeded the uncertainty inherent in the method of analysis. The effect was most striking at low temperatures in the region of 75°C to 90°C. The results of some such runs are shown in Table III.3.

TABLE III.3

DETENTION OF HCl IN CATALYST

AFTER 20 MIN. REACTION

Series	Run	T°C	Amt. C_3H_8 Consumed (cm Hg)	Peak Height	Amt. of HCl Observed* (cm Hg)	Amt. of HCl Detained cm Hg	Amt. of HCl Detained Mole($\times 10^5$)
3	39	90	0.81	0	0 - 0.6	0.21-0.81	4.6 - 17.9
3	49	75	0.89	0.1	0.7	0.19	4.2
3	44	75	1.09	0.1	0.7	0.39	8.7
6	13	75	0.60	0	0 - 0.6	0 - 0.6	0 - 13.3
6	14	75	0.72	0	0 - 0.6	0.12-0.72	2.7 - 16.0

* Since the calibration curve for HCl pressure vs. peak height (Figure II.8) did not go through the origin, absence of a peak means only that HCl pressure was < 0.6 cm Hg.

It can be seen from Table III.3 that a small amount of HCl (varying from 2.7 - 8.7 x 10^{-5} moles if taking the conservative values) is detained in the lattice for a certain time during reaction. The detention is only temporary because the final product of a series of runs was shown to contain no significant amounts of carbon or hydrogen as pointed out in Chapter II. If the amount of HCl detained was large, it would contribute significantly to the overall pressure drop and cause error in estimation of Cl_2 uptake and hence in the composition of $CuCl_x$. The amount of HCl detained is, however, sufficiently small that such error is negligible. (As mentioned earlier, the value of composition of the final product obtained by weighing or chemical analysis was within ± 0.02 of the x value estimated by the accumulated pressure decrease in the whole series of runs.)

It is interesting to note, however, that in terms of moles of HCl per mole of catalyst, the amount of HCl held up temporarily in the lattice observed could in some cases be about o.13%.

Unfortunately, from the available data, no definite relationship could be established between the amount of HCl detained and either temperature or catalytic activity.

Data from Cl_2 Uptake Studies

The rates of chlorine uptake were followed manometrically and gravimetrically by apparatus as described in Chapter II. The manometric method was used more extensively because the experimental conditions involved (the apparatus used was the same as that for kinetic studies) were very close to the conditions in which kinetic studies were performed and consequently more relevant for the present purpose.

(a) The Dependence of Rate of Uptake on Composition

Many series of manometric runs were carried out at 130°C. The general behaviour was found very reproducible as compared to the catalytic results; the absolute values of rates of uptake, however, were found to vary slightly from one series of runs to another. Typical results are given in Figures III.5 and 6. In Figure 5, the chlorine pressure is plotted against time for the first four runs of series A#4; whereas Figure 6 shows two runs followed over longer time selected from another series of runs.

The striking feature of the curves shown in Figure 5 is that they are all parallel straight lines after a short initial period of rapid uptake ($\sim$ 1 minute) indicating that the rate of uptake of chlorine reaches a fairly steady value which is independent of composition up to $CuCl_{1.2}$. The steepness of the curves in the initial period decreases from Run 1 to 4 (curves A to D). In fact, for Run 4, the plot becomes almost a straight line throughout. Thus, it appears that the rate of uptake of chlorine

FIG.III.5 Cl_2 PRESSURE VS. TIME

(A # 4 Series)

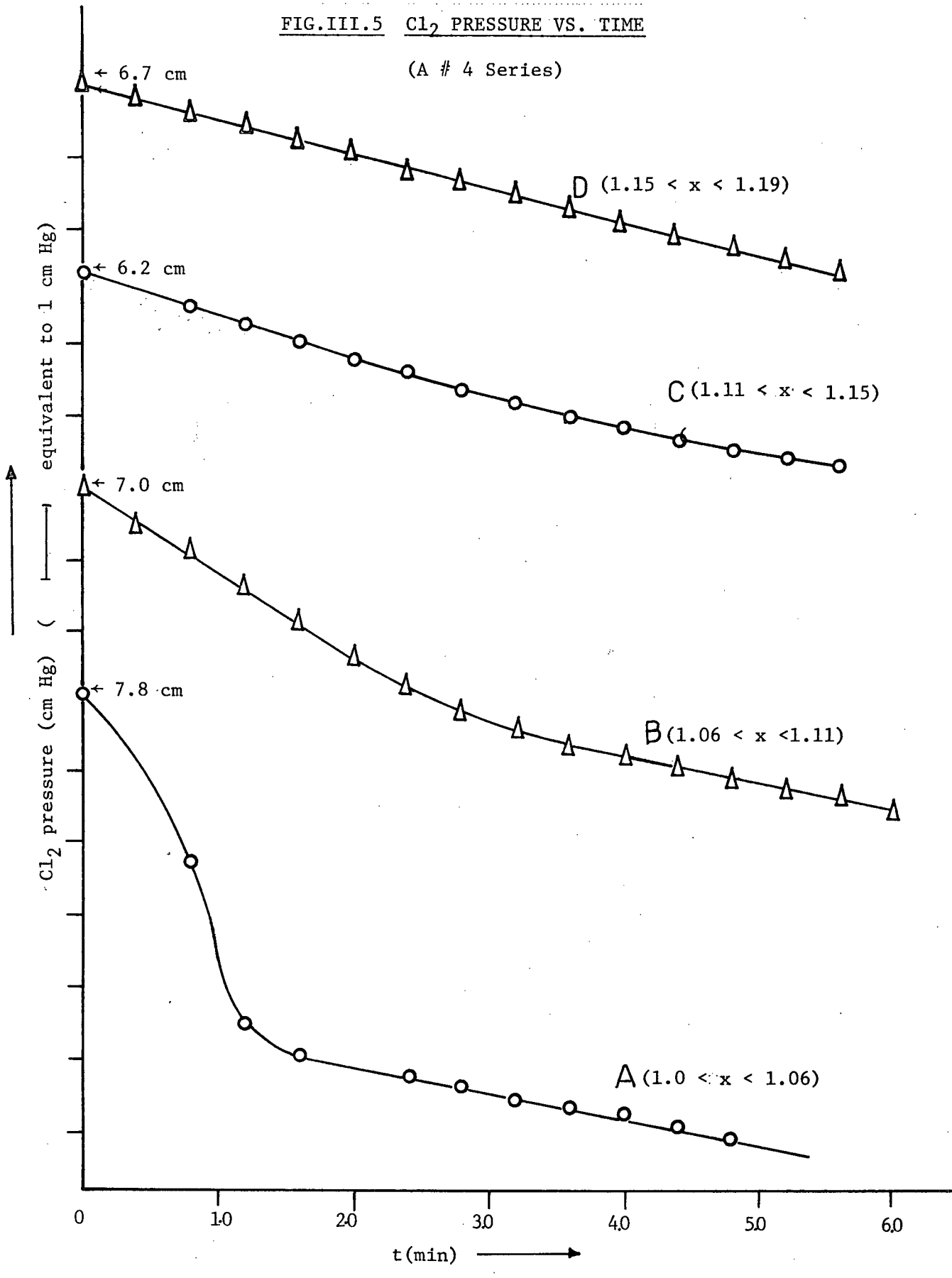

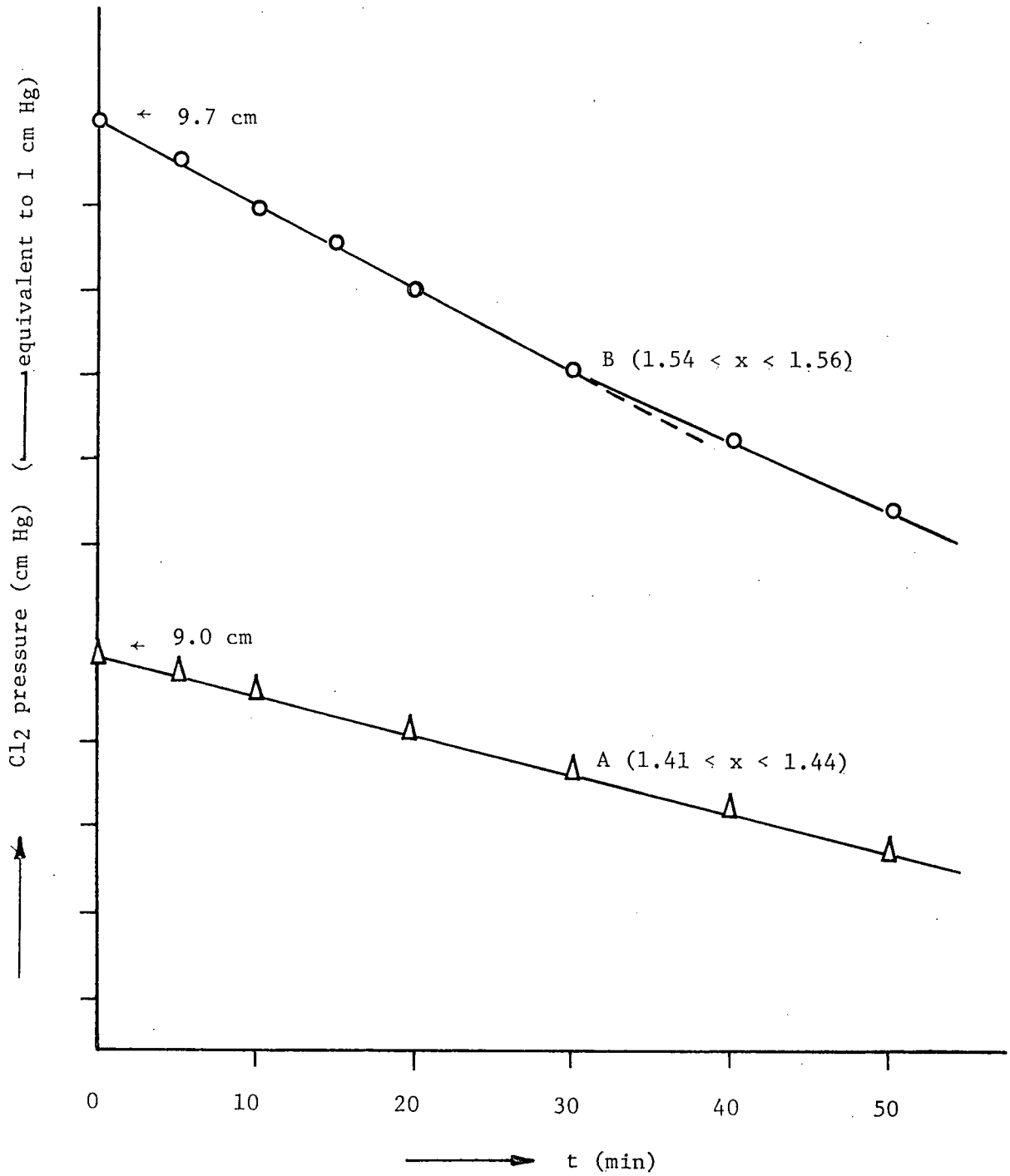

FIG. III.6 Cl_2 PRESSURE VS. TIME

(Series 10)

is independent of chlorine pressure. Behaviour at higher compositions is illustrated in Figure 6 which shows graphs of two runs that were followed for more than 40 minutes. The curves in Figure 6 have much smaller slopes than those of Figure 5. In general, the rate of chlorine uptake decreased markedly at a certain composition and continued to decrease throughout the remainder of the reaction. Such composition was generally found to be about $CuCl_{1.20}$; but a composition as low as $CuCl_{1.16}$ was also observed. Each run appears to give a linear plot because the range of composition covered is small; but the plots are seen to be slightly curved if they extend over long periods (Figure 6, curve A), and they are all actually small portions of a continuous curve of the extent of reaction ($\alpha = x - 1$) against time such as that shown in Figure 7. The kinetic analysis of such a curve is given in detail in the next chapter. In the present account, some qualitative features of the data will be discussed in terms of the rate of reaction, $d\alpha/dt$, rather than α.

Since the chlorine pressure vs. time plots sometimes have a non-linear initial portion, it is necessary to choose parameters for the purpose of comparison of results. Accordingly, two types of rates are chosen, viz. the maximum rate (r_M) and the rate in the linear portion of a chlorine pressure vs. time plot (r_L).

Values of r_M and r_L are shown in Figures III.8 (a) and (b). The significant features of this diagram are that r_M is markedly higher than r_L only up to a composition of about $CuCl_{1.2}$ and that in the region in which the two curves approach each other closely, there

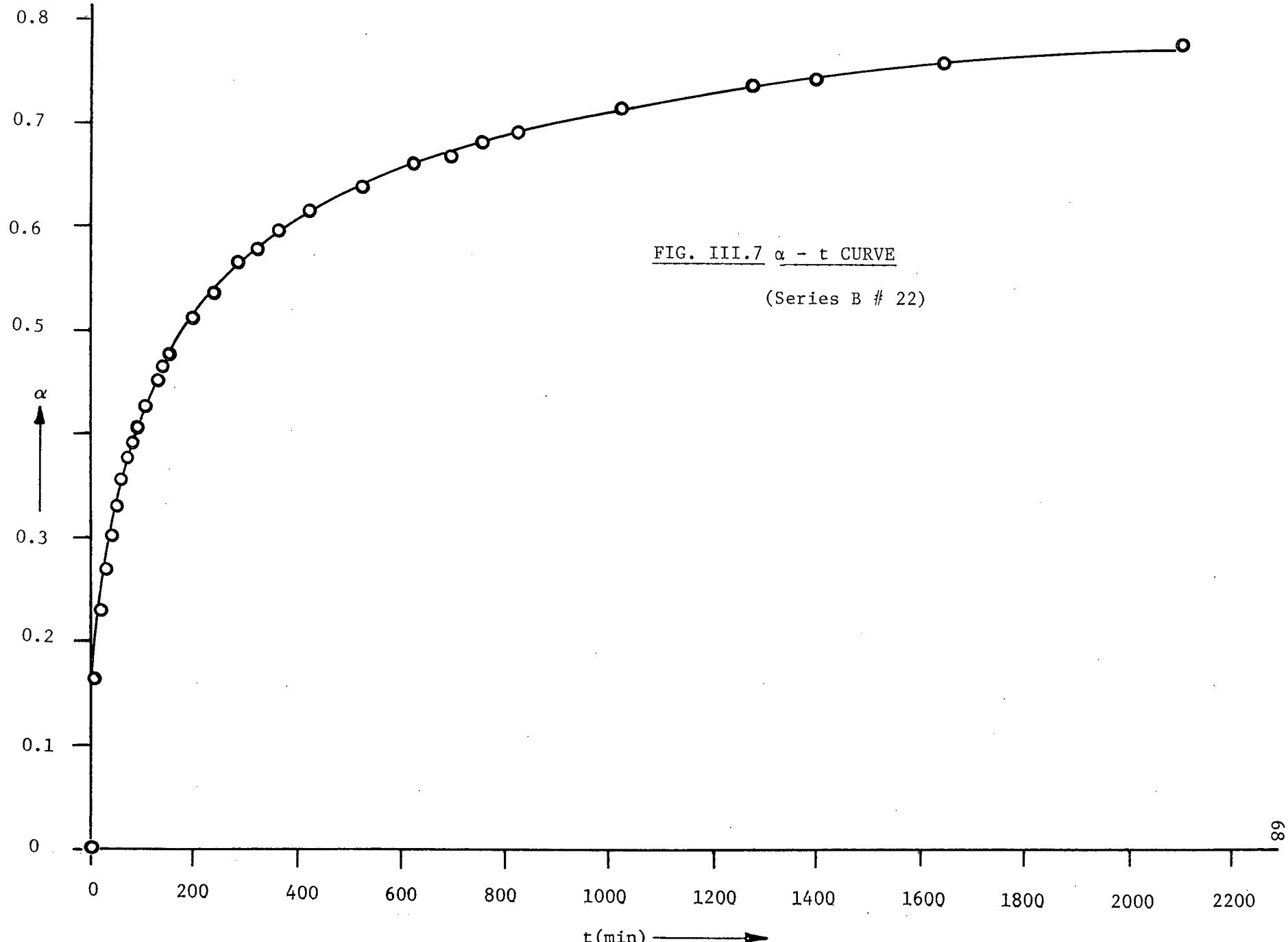

FIG. III.7 α - t CURVE

(Series B # 22)

FIG. III. 8 Cl_2 Uptake rate vs. Composition

(Series B # 22)

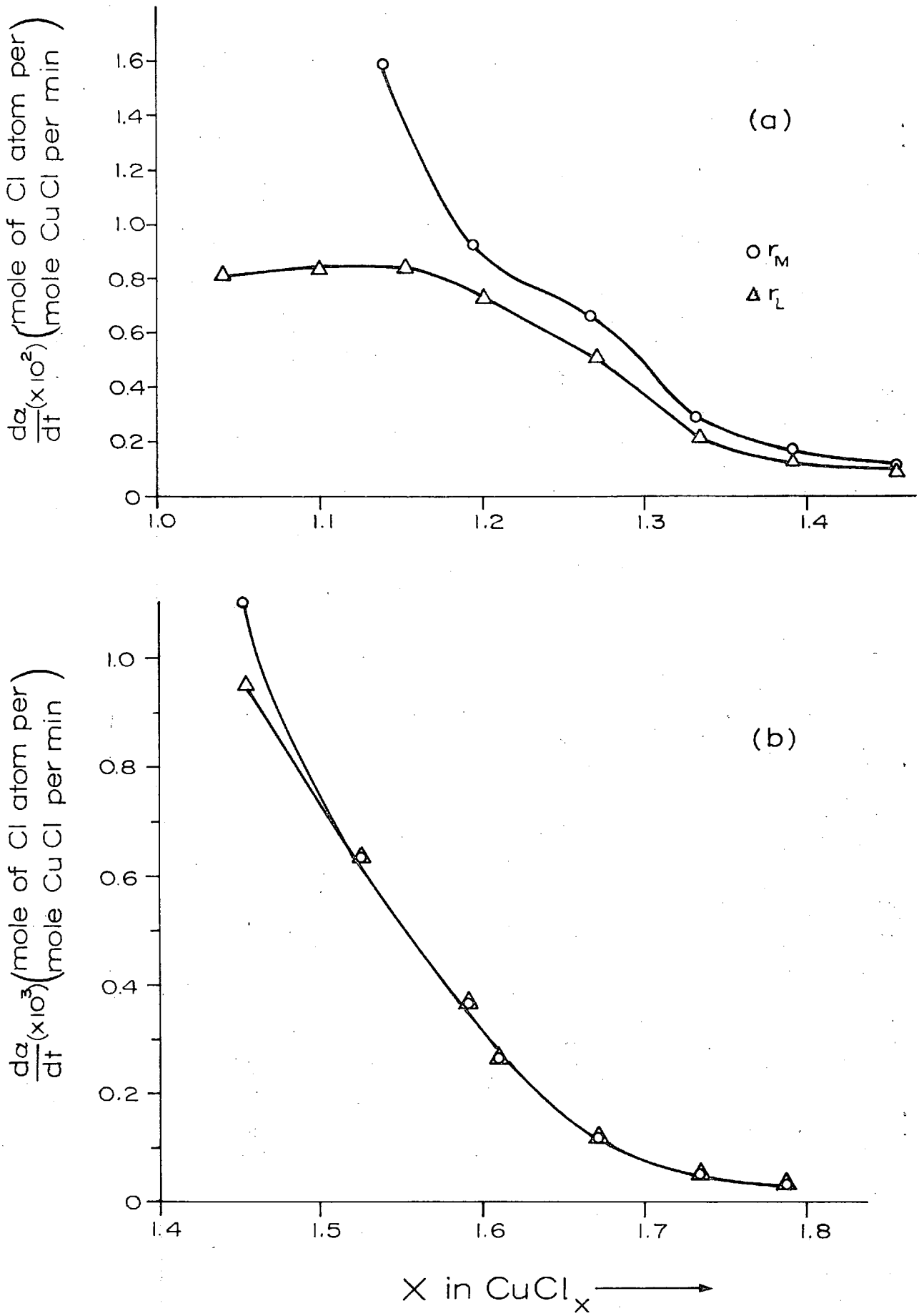

is a shoulder in the curves after which the combined curve is concave throughout. These features suggest a change in mechanism occuring not very sharply but over a range of composition between $CuCl_{1.2}$ and $CuCl_{1.3}$. It is shown in the next chapter that the second part of the curve beyond $CuCl_{1.3}$ can be analysed in terms of diffusion-controlled kinetics.

(b) Dependence of Rate of Uptake on the Presence of Propane

In some series of runs, Cl_2 only was used throughout to study Cl_2 uptake kinetics. In others, every successive gas phase to which the solid was exposed was a mixture of Cl_2 and propane, for catalytic studies. Still in some other cases, the gas phase used was sometimes Cl_2 only and sometimes a Cl_2/C_3H_8 mixture in the same series of runs. In these cases, it was evident that propane affects the Cl_2 uptake rate. Since in these runs catalysis and uptake were being followed simultaneously, it was difficult to make the uptake measurements as complete as in the studies without propane described above. Measurements were usually made only after two and half minutes and after twenty-two and half minutes.

The rate of pressure change in the first two and half minutes before the first sampling (r_1) and the rate of pressure change during the time elapsed between the first and second sampling (r_2) are therefore used as rate parameters. While the latter should correspond fairly well to r_L, the former is only an average value of rate over the first two and half minutes and therefore need not correspond to

r_M. Hence the comparison between r_M and r_1 can only be regarded as qualitative. On this basis, the interesting feature of the r_1 values is that they were often actually less than the r_2 values, i.e. the reaction in the pressure of propane started with an initial slow portion. This was noticeable particularly beyond $CuCl_{1.5}$. Quantitatively, values of r_1 were very erratic and they are not plotted or discussed further here. [The values of r_M, r_L, and r_2 for series 17 are plotted in Figures III.9 (a) and (b).]

The use of propane in the gas phase clearly affects the rate both of the run concerned and of subsequent runs with Cl_2 only. The latter point may be seen from the appreciably more irregular shape of the r_L curve than that in Figure III.8. The most striking feature of the results, however, is the comparison of the r_L and r_2 curves, which is shown in Figure III.10 by plotting the ratio r_2/r_L. There is a striking correlation between this curve and the catalytic activity curve of Figure III.4, which is reproduced as a dotted line in Figure III.10. The effect of propane on the $CuCl/Cl_2$ reaction is sometimes catalysis ($r_2/r_L > 1$) and sometimes poisoning ($r_2/r_L < 1$) according to the curve in Figure III.10. Another similar series gave a curve of similar form, with maxima in similar phases, but r_2/r_L was < 1 throughout.

Thus there is a sort of reciprocal catalysis between the two reactions in the system in which the rate of the Cl_2/C_3H_8 reaction is affected by $CuCl_x$ and the rate of the $CuCl_x/Cl_2$ reaction is affected by propane in a remarkably similar pattern. This clearly

FIG. III.9

Cl_2 UPTAKE RATE vs. COMPOSITION

(with C_3H_8)

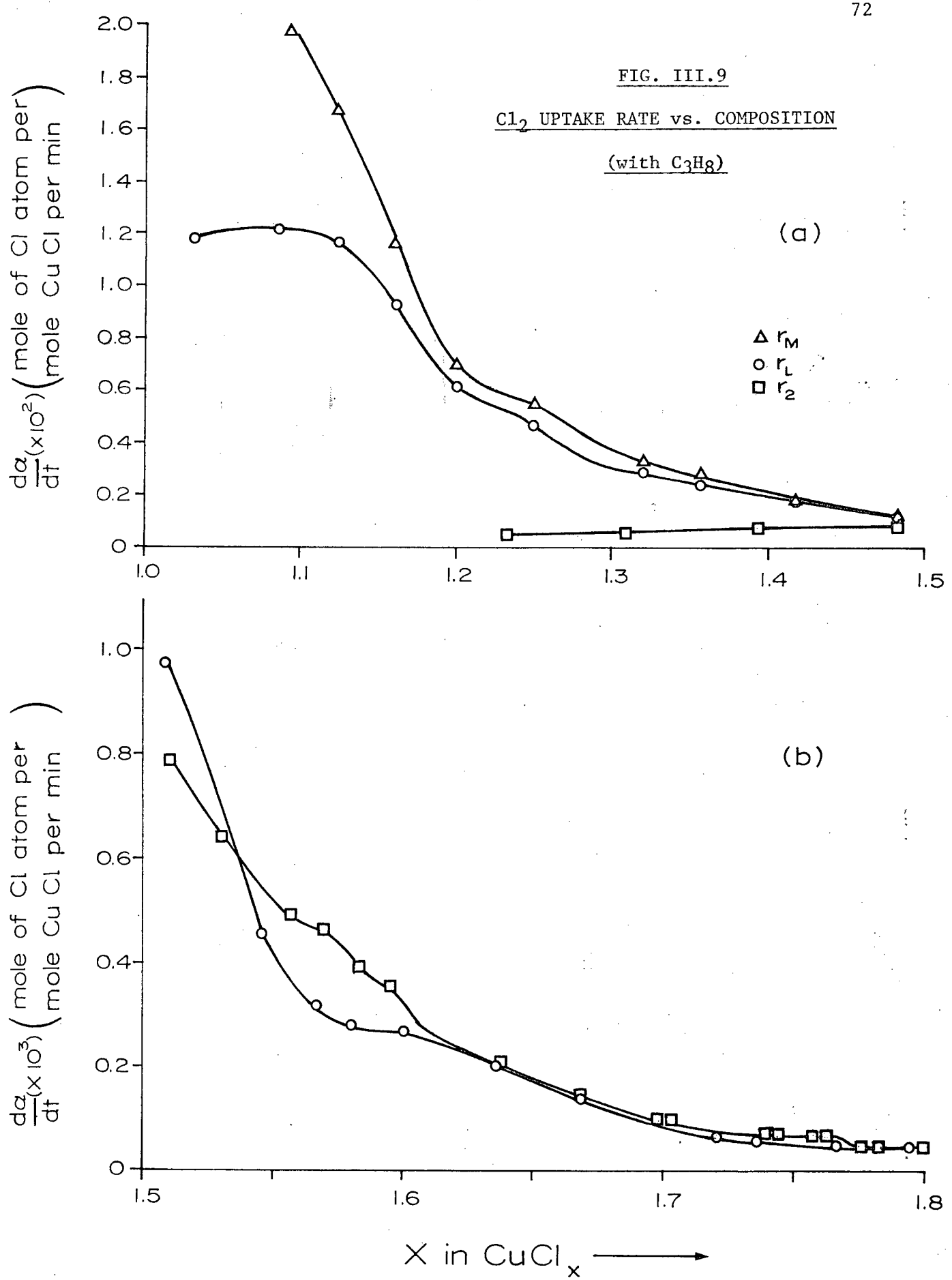

FIG. III. 10

EFFECT OF PROPANE ON

Cl_2 UPTAKE RATE

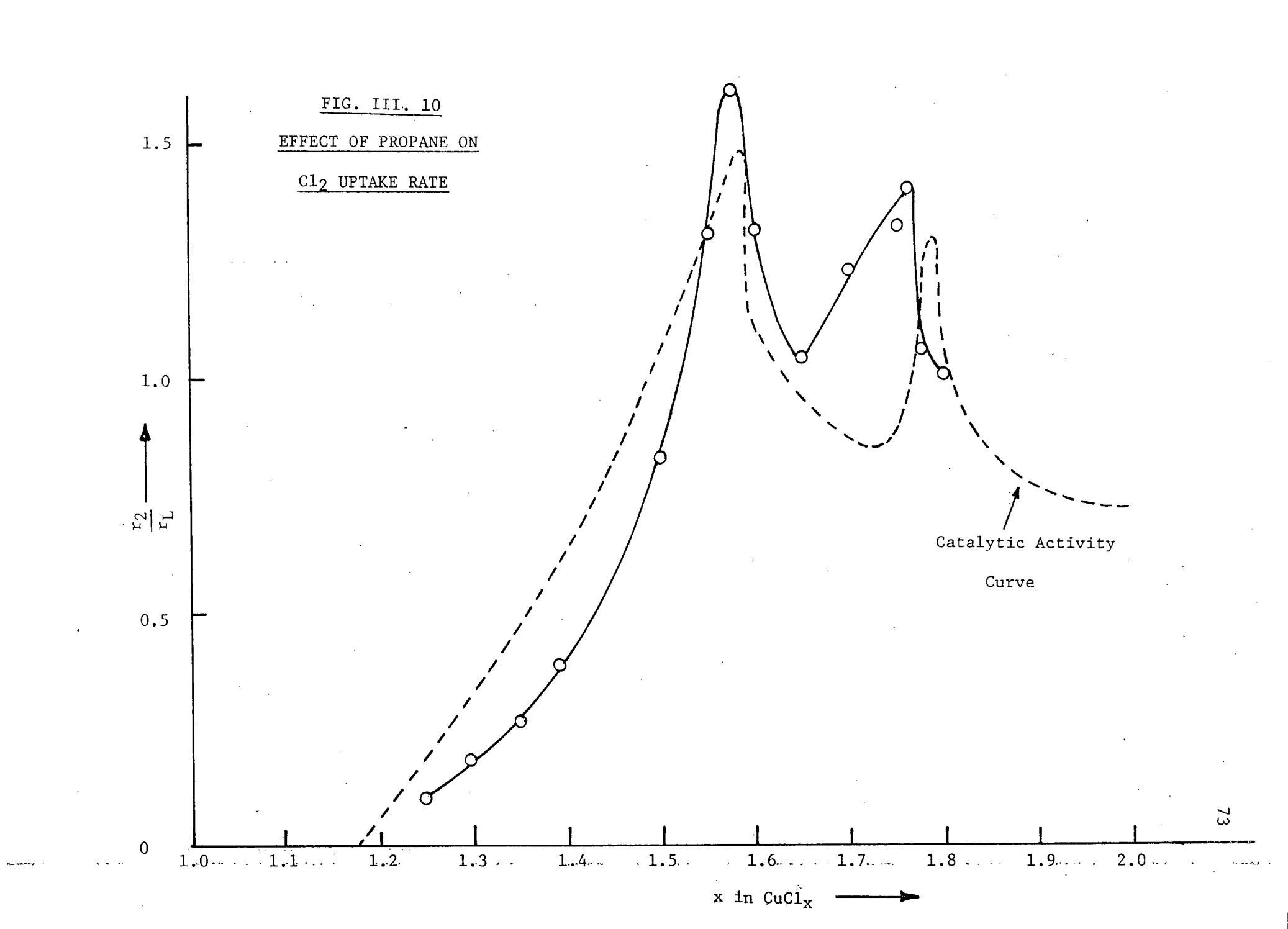

suggests that the two reactions have some active site or reaction intermediate in common.

(c) The Dependence of Rate of Uptake on Time of Evacuation and Grinding Up of the Solid

The effects of evacuation and grinding of catalyst were also studied. Figure III.11 shows the chlorine pressure vs. time plots for some runs of Series B#19. It can be seen from this figure that while Runs 4 and 5 do not exhibit a rapid uptake region, Run 6 does. Therefore, it can be said that prolonged evacuation exposes new surface of CuCl and hence gives rise to a rapid uptake region in a chlorine pressure vs. time plot. The pair of Runs 11 and 12 shows similar behaviour except that the effect is much less pronounced. In fact, among all series of runs, it was found that the highest value of x at which Cl_2 uptake rate was still dependent (very slightly) on the time of evacuation is 1.59, but prolonged evacuation was found to restore the rate (r_M) of uptake to a value as high as those in the $1.0 < x < 1.2$ region only when $x < 1.32$. The slopes in the linear portions in Runs 6 and 12 are actually slightly less than their counterparts in the previous runs, as would be expected from the normal slope of the r_L - composition curve. In other words, values of r_L are not very susceptible to change of evacuation time.

The values of r_M and r_L obtained from Figure III.11 for Run 6 (curve C) are compared with the value of r_L interpolated from the type of curve shown in Figure III.4 in Table III.4.

FIG. III.11 EFFECT OF EVACUATION TIME ON Cl_2 UPTAKE RATE

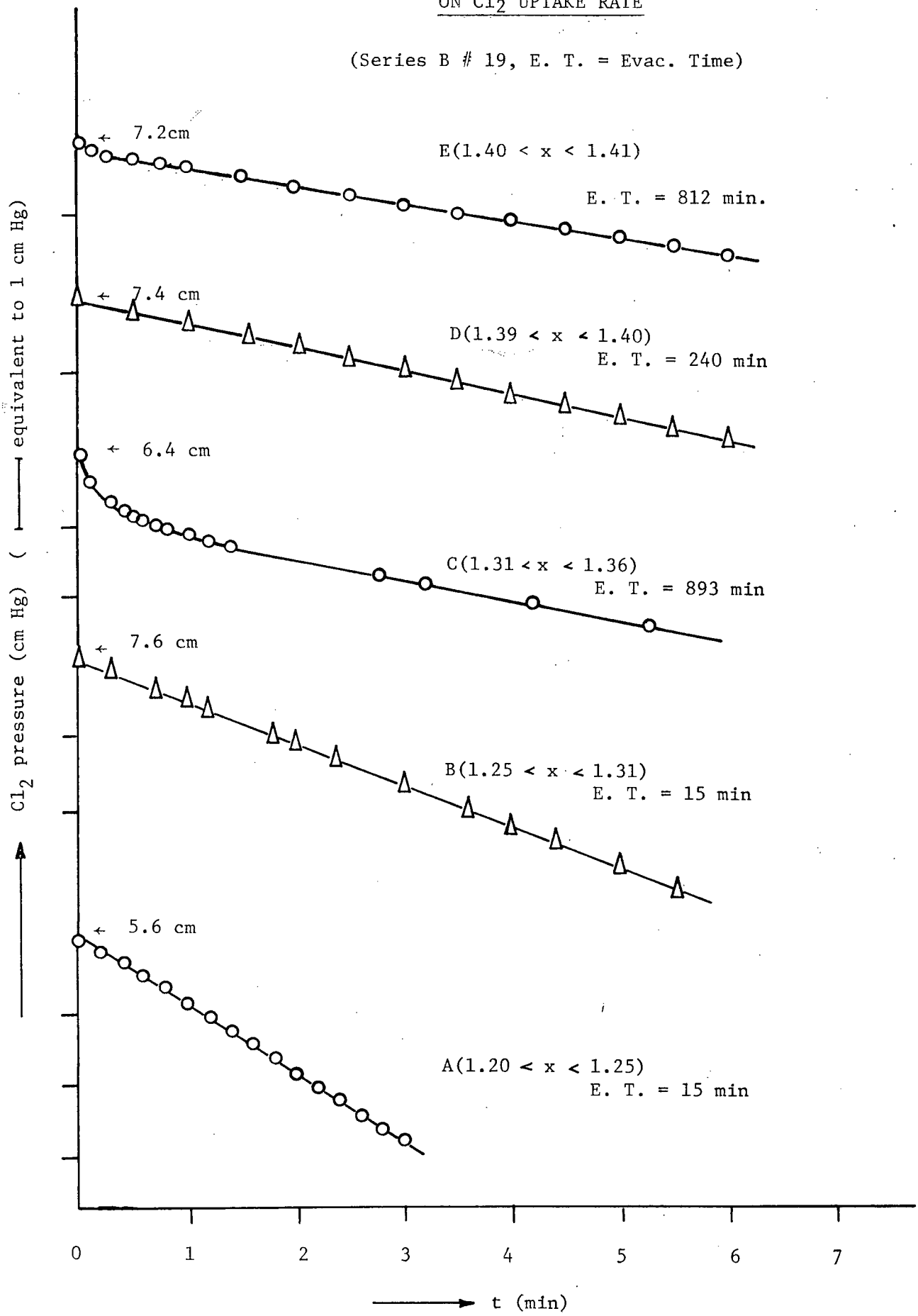

T A B L E III.4

"ANOMALOUS" RESULTS OF RUN 6 (B#19)

DUE TO LONG EVAC. TIME

r_M Observed (Mole of Cl atoms per mole of CuCl per min.)	r_2 Observed (Mole of Cl atoms per mole of CuCl per min.)	r_L Expected (Mole of Cl atoms per mole of CuCl per min.)
3.8×10^{-2} (Corresponding to r_M at x = 1.04)	2.58×10^{-1}	2.62×10^{-1}

As seen from this table, the r_M value obtained corresponds to the r_M value with normal evacuation time when x = 1.04.

The effect of the grinding of the catalyst can be seen from the following table.

T A B L E III.5

EFFECT OF GRINDING OF CATALYST

ON UPTAKE RATE

Run No.	Conditions of Catalyst	x in $CuCl_x$	Evacuation Time (min.)	r_1 (cm Hg/min.)	r_2 (cm Hg / min.)	Catalytic rate (cm Hg/min.)
22	Before grinding	1.611	120	7.28×10^{-3}	1.578×10^{-2}	2.10×10^{-3}
23	After grinding	1.614	600	9.35×10^{-2}	3.24×10^{-2}	2.05×10^{-3}
24	Same catalyst as in Run 23	1.623	60	7.28×10^{-2}	1.457×10^{-2}	1.93×10^{-3}

It can be seen that grinding of catalyst definitely raises the rate of uptake of chlorine. For the r_1 value, it is an increase of the order of 10. For the r_2 value, the increase is about twofold. That the result of Run 24 also appears in Table III is to show that the increase in r_1 in Run 23 was not just due to longer evacuation time but rather, grinding of catalyst. This is consistent with results of Runs 19-22 (not shown), in which it was found that the values of r_1 and r_2 did not appear to be dependent on the time of evacuation. The catalytic rate, however, can be seen to be unaffected by grinding of catalyst.

(6) The Dependence of Rate of Uptake on Temperature

Since the rate of uptake varies from sample to sample, it is impossible to estimate the effect of temperature from different series of runs performed at different temperatures. A more reasonable approach appears to be the study of the rate of uptake at various temperature for a given batch of catalyst. However, such a method also suffers from the disadvantage that the rate of uptake depends on composition. Nevertheless, such a method was found to yield much more informative results. Figure III.12 shows a typical plot of data obtained from a series (No.6) of catalytic runs of which the order of experiments calls for a little comment. The runs were carried out in the sequence that the temperature of reaction was initially at 75°C, then it was raised successively to 120°C at an interval of 15°C. Such runs were referred to as a group of runs. Then the temperature was lowered to 75°C before another group of runs was performed.

TABLE III.6

APPARENT ACTIVATION ENERGY AND COMPOSITION

Composition Range	E_1† (Kcal/mole)			E_2† (Kcal/mole)	
	Series 3	Series 6	Mean	Series 3	Series 6
1.01 - 1.19	-	-2 to +1 *			
				0.2	1.3
1.19 - 1.29	0.24	-4.0*,2.5			
				3.5	-0.4
1.30 - 1.36	-0.7,7.5	-1.7, 2.6			
1.36 - 1.41	0, 8.9	-	8.9	7.4	4.6
1.42 - 1.47	0, 11.3	-1.7,11.6	11.3	9.2	
				11.9	6.1
1.49 - 1.53	11.6	-1.7, 9.1	9.9		
				12.9	7.5
1.54 - 1.59	13.4	4.5,12.4	12.9		
				12.2	12.4
1.60 - 1.63	11.6	10.0	10.8		
				11.3	12.2
1.64 - 1.66	9.3	12.4	10.9		
					11.8
1.67 - 1.68	9.3	13.4	11.4		
				8.5	9.4
1.69 - 1.70	10.3	13.4	11.8		
					13.8
1.71 - 1.73	10.3	11.3	10.8		

† E_1 from solid lines in Figure III.12

E_2 from broken lines.

* Corrected for the composition effects represented by lines AC & DG.

The results are summarized in Table III.6 and in Figure III.12 where log $d\alpha/dt$ is plotted against the group of experiments, the intervals being arranged to correspond to 1/T intervals so that the diagram is a set of Arrhenius plots. Each solid line represents a group of runs; a positive slope of the line means positive activation energy (temperature increasing). Each broken line, on the other hand, represents the cooling from the end of a group of runs to the beginning of the following group of runs; a negative slope therefore means positive activation energy. Apart from sign, the 1/T scales are the same for solid and broken lines.

For the earlier points, dependences of rate on temperature and on composition are not adequately separated. Thus curve AB appears to indicate a negative activation energy, but it almost coincides with the line AC which joins two points at the same temperature and thus displays the effect of composition only. Hence it is probably fairer to say that line AB indicates zero activation energy up to $CuCl_{1.2}$. There is, however, evidence for a negative activation energy in that DE has a larger negative slope than the isotherm DG, and in that EF has a positive slope. The activation energies up to $CuCl_{1.29}$ in Table III.6 have been approximately corrected for the effect of composition.

Physically, a negative activation energy probably means that the reaction rate is controlled by concentration in an adsorbed layer. Figure III.12 and Table III.6 show that negative and small positive activation energies are observed up to a composition of

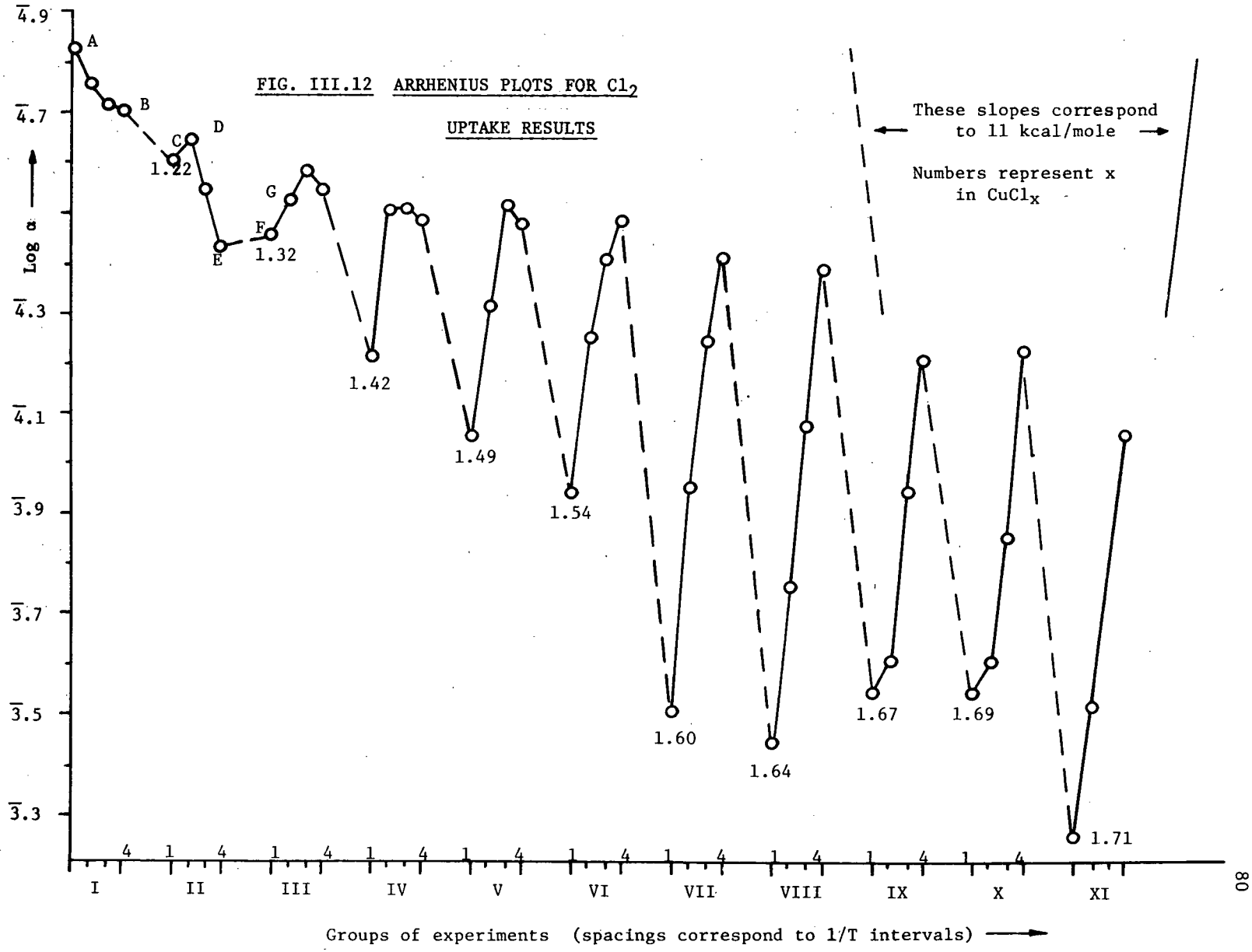
FIG. III.12 ARRHENIUS PLOTS FOR Cl_2
UPTAKE RESULTS
These slopes correspond to 11 kcal/mole
Numbers represent x in $CuCl_x$
Log α
$\overline{4}.9$
$\overline{4}.7$
$\overline{4}.3$
$\overline{4}.1$
$\overline{3}.9$
$\overline{3}.7$
$\overline{3}.5$
$\overline{3}.3$
A
B
C
D
E
F
G
1.22
1.32
1.42
1.49
1.54
1.60
1.64
1.67
1.69
1.71
I
II
III
IV
V
VI
VII
VIII
IX
X
XI
Groups of experiments (spacings correspond to 1/T intervals)

$CuCl_{1.32}$, and that a high positive activation energy then begins to appear and reaches a final value of 11 Kcal/mole (0.48 eV) which is seen from $CuCl_{1.42}$ onwards. The temperature dependence thus suggests that a surface reaction is rate-controlling up to $CuCl_{1.32}$, and that the mechanism then switches over to something with a high activation energy. In the discussion section, it will be shown that the latter is a diffusion-controlled process.

Activation energies were calculated corresponding to both the solid and the broken lines in Figure III.12. These are given, respectively, as E_1 and E_2 values in Table III.6.

The difference between the E_1 and the E_2 values is that while the former may underestimate the actual value of E, owing to the decrease in rate as x increases, the latter may overestimate the actual value of E for the same reason. The best value for the activation energy beyond $CuCl_{1.4}$ is 11.3 ± 0.6 Kcal/mole (0.49 ± 0.03 eV). (Values 6.1 and 7.5 for E_2 in Series 6 were not included in the mean).

Gravimetric Results

The results obtained by the gravimetric method are quite different from those described above. Firstly, after reaction, it was observed that the product consisted of two distinct phases -- brownish $CuCl_2$ at the outside and pale-greenish CuCl at the inside, i.e. only the outer layers reacted.

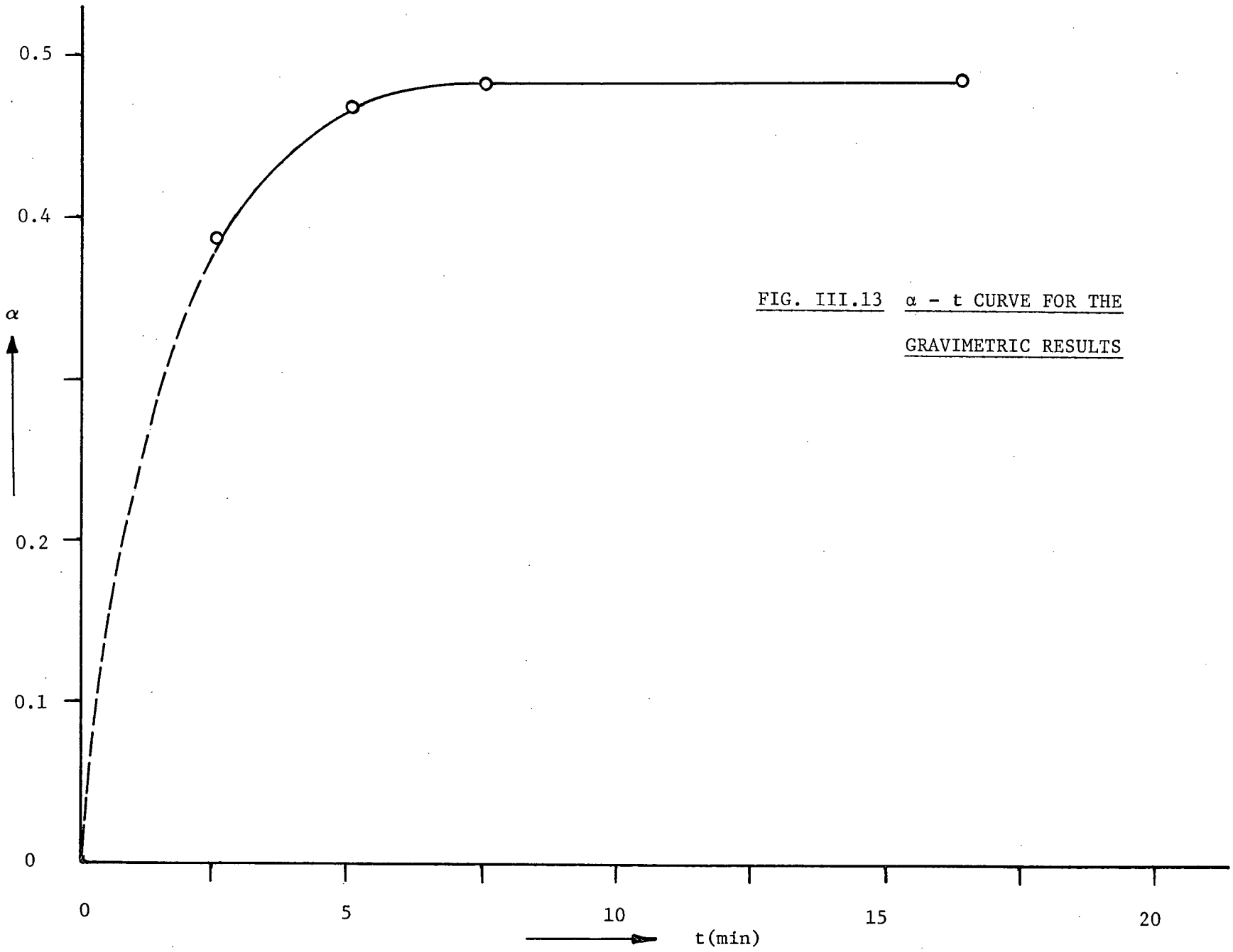

FIG. III.13 α - t CURVE FOR THE GRAVIMETRIC RESULTS

Secondly, it was found that the rate of reaction was much more rapid in the first few minutes; in fact the reaction terminated within a few minutes. It was impossible to measure the rate accurately in the initial period of reaction because of vibration of the quartz spiral balance. This was especially so at elevated temperature (such as 130°C, at which the manometric measurements were carried out). In Figure III.13, the extent of reaction (α) vs. time plot for a typical run at 98°C is given. It can be seen that the reaction virtually stopped at a value of $\alpha = 0.48$.

These results suggest that the course which the reaction takes at the outset is determined by the rate at which gas can reach the sample. The slow reactions observed in the reaction vessel used for catalytic and manometric studies develop only if the access of gas to the solid is initially restricted. But the rate of reaction very soon becomes independent of the transport of gas to the solid and can be interpreted in terms of rate-determing processes at the gas-solid interface or in the solid phase even from compositions as low as $CuCl_{1.06}$.

III.(2) RESULTS OF CONDUCTIVITY MEASUREMENTS

Plots of log σ_{sp} vs. 1/T are shown in Figure III.14 for samples in different ranges of composition. These plots were obtained by carrying out runs on each sample until the individual points at each temperature in two successive runs agreed, if possible, to within 15% (or 0.06 on a logarithm scale). In general, for $x > 1.7$, reproducibility was achieved rapidly, but for lower x often not until the third and fourth runs, and in some cases the best reproducibility which could be attained was about 25% (0.1 on a logarithm scale). The lower reproducibility was also tolerated in many runs for points at the highest temperatures.

No extensive study was made on the effect of using different types of contact between electrodes and pellet, but some measurements on pure CuCl by another worker in this laboratory (M. Prasad) showed no significant difference between silver-painted samples and ones without paints. Consequently, in the present work, the electrodes were secured to the sample by pressure only and without painting the sample.

Three different types of behaviour were observed in different ranges of composition. In addition to the Arrthenius plots shown in Figure III.14, activation energies are plotted in Figure III.15, values of specific conductance (σ_{sp}) at 130°C and the polarization factor Δ at 130°C are plotted in

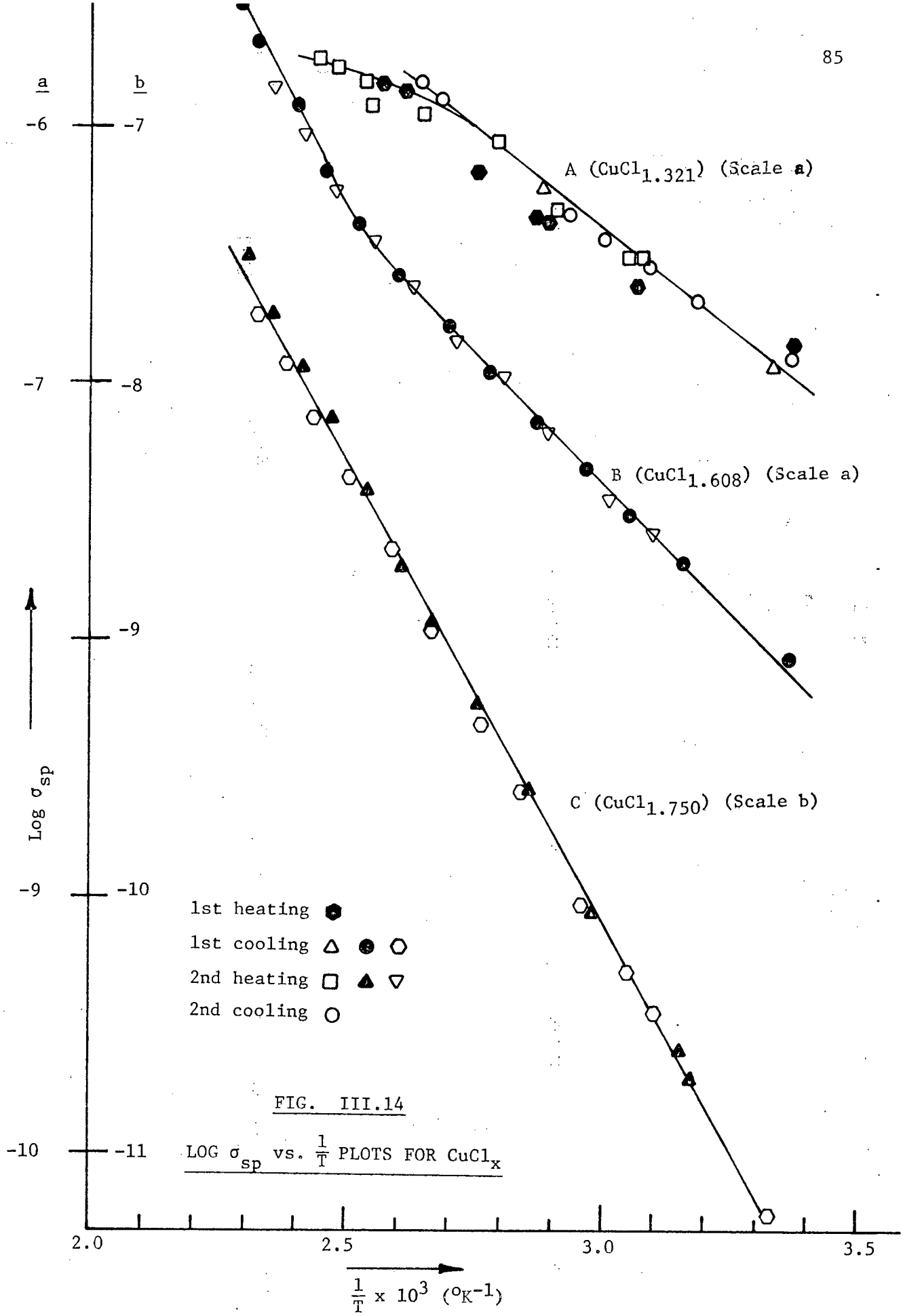

FIG. III.14

LOG σ_{sp} vs. $\frac{1}{T}$ PLOTS FOR $CuCl_x$

FIG. III.15

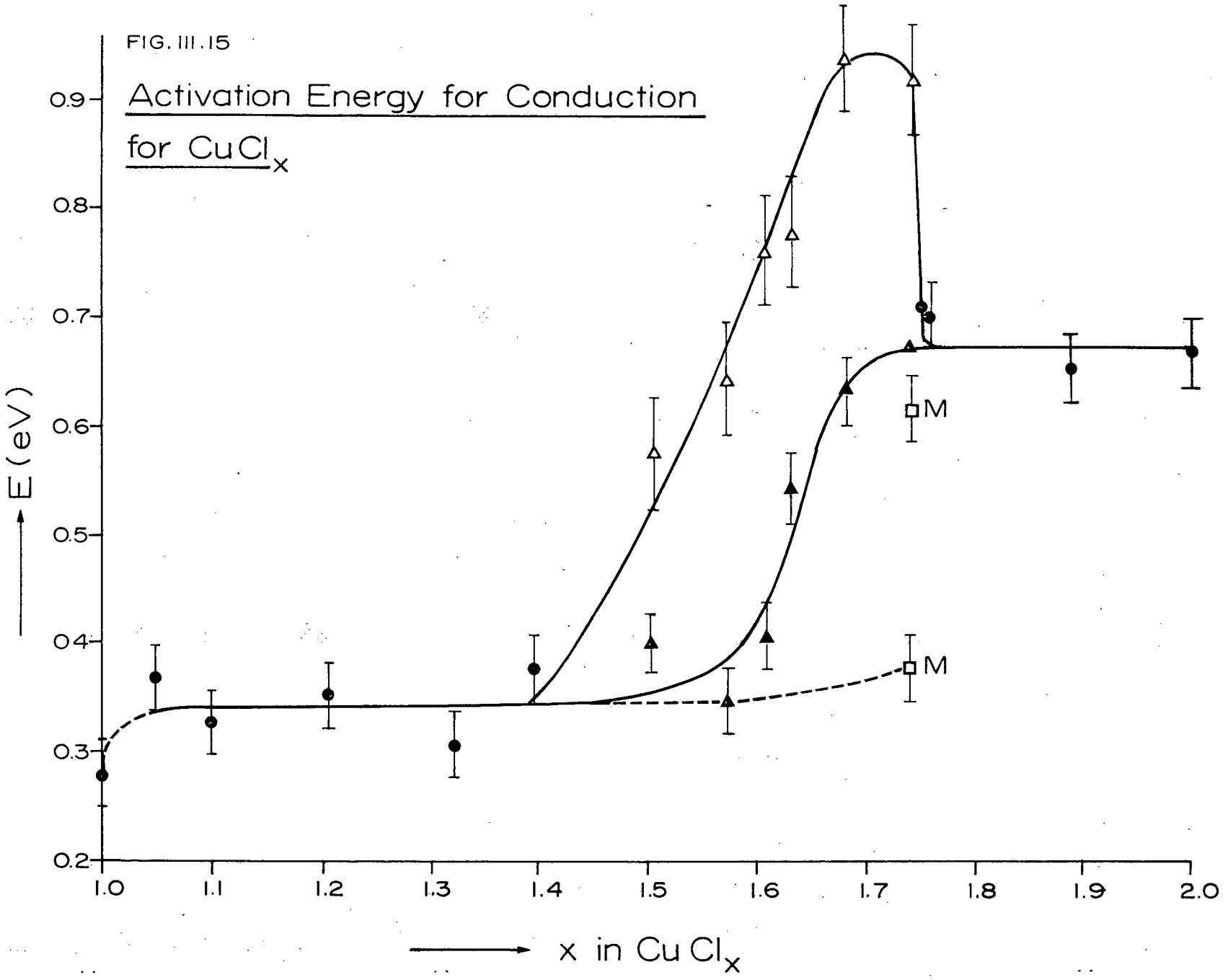
Activation Energy for Conduction
for CuCl$_x$
E (eV)
0.9
0.8
0.7
0.6
0.5
0.4
0.3
0.2
1.0
1.1
1.2
1.3
1.4
1.5
1.6
1.7
1.8
1.9
2.0
M
M
x in CuCl$_x$

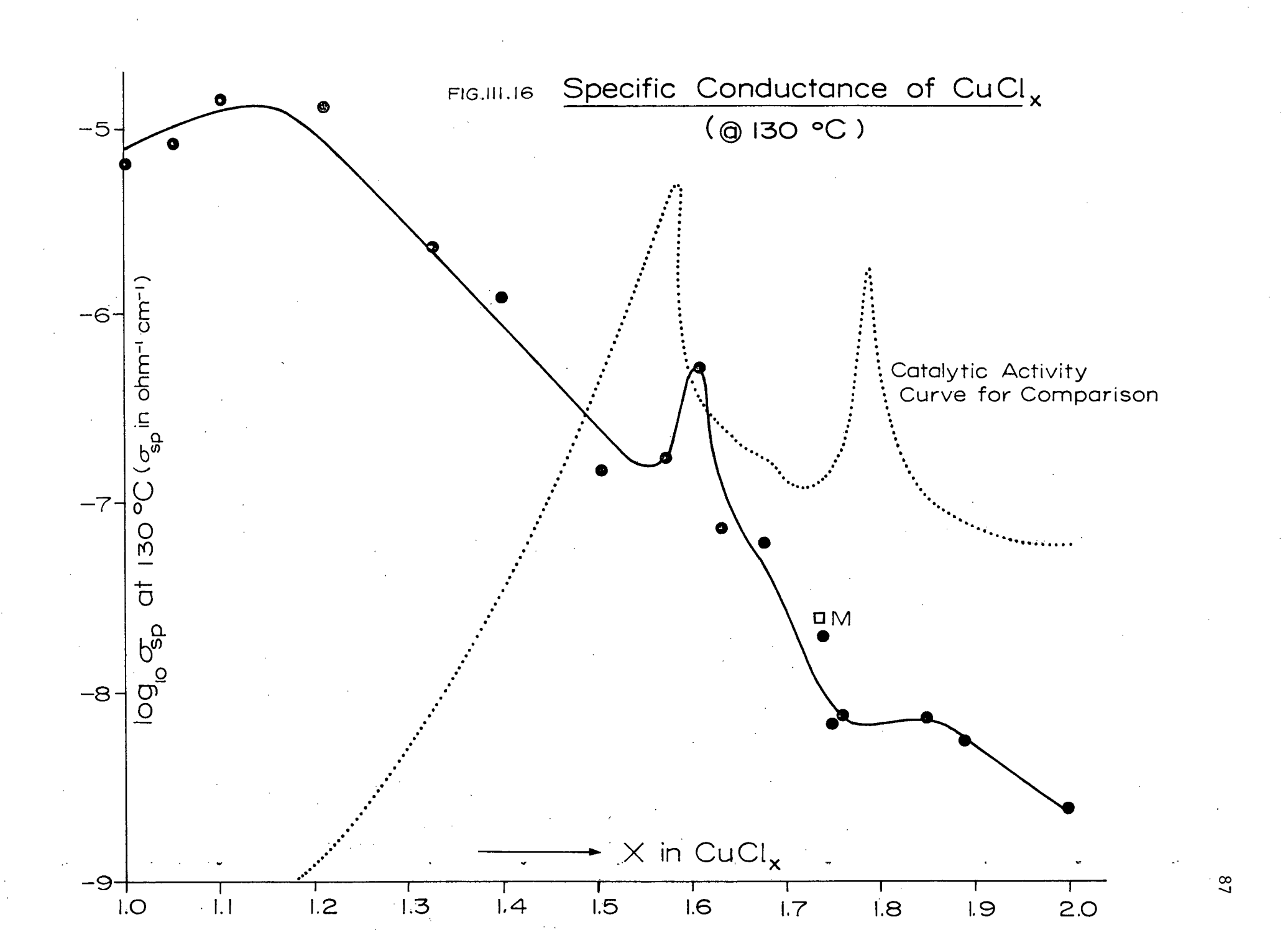
FIG.III.16 Specific Conductance of $CuCl_x$
(@ 130 °C)
$\log_{10} \sigma_{sp}$ at 130 °C (σ_{sp} in $ohm^{-1} cm^{-1}$)
-5
-6
-7
-8
-9
Catalytic Activity
Curve for Comparison
M
X in $CuCl_x$
1.0
1.1
1.2
1.3
1.4
1.5
1.6
1.7
1.8
1.9
2.0

FIG. III.17 Polarization effect in $CuCl_x$

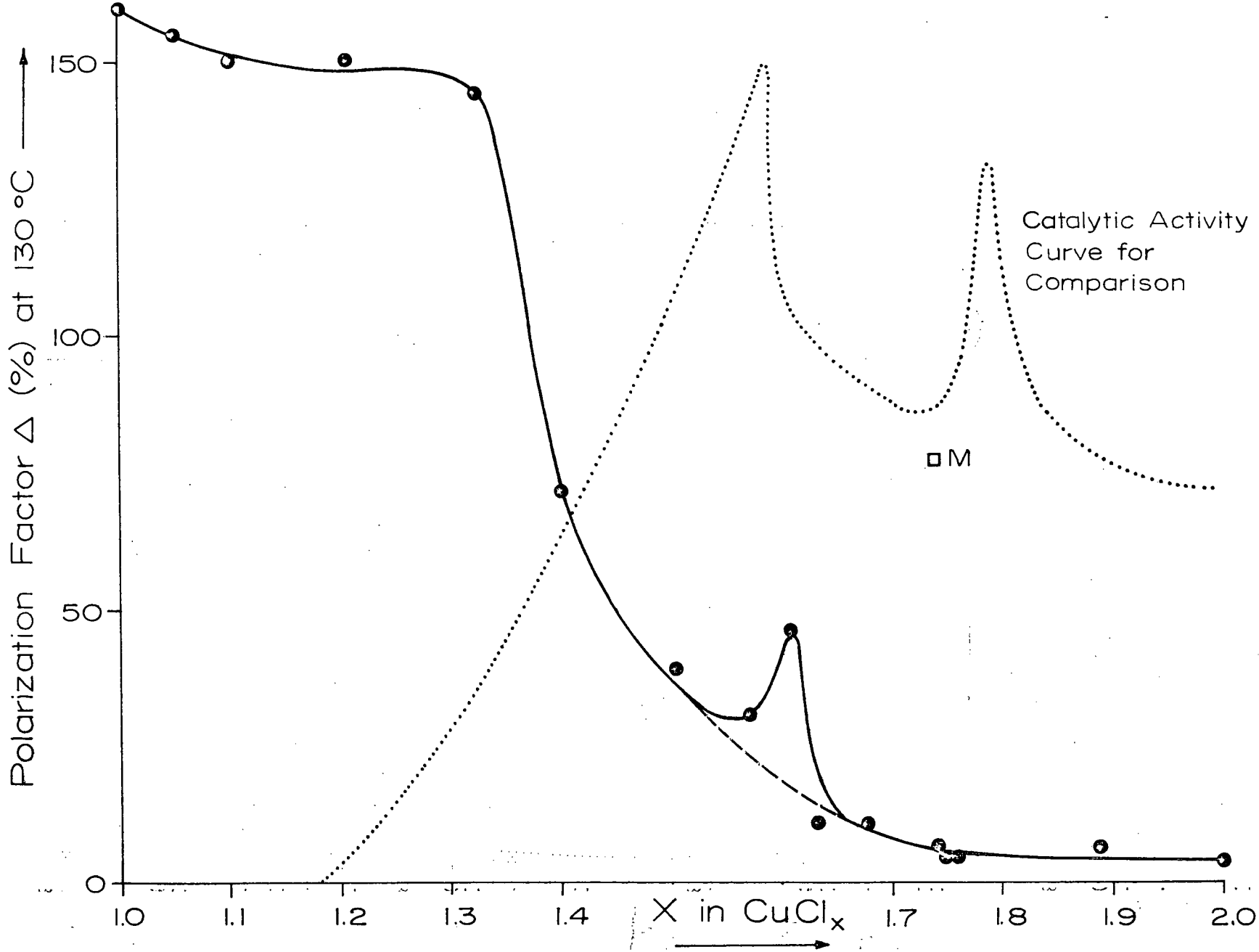

Figures III.16 and III.17 respectively. Table III.7 summarises the numerical values of activation energies, σ_{sp} and Δ.

Type I. ($CuCl$ to $CuCl_{1.4}$, Figure III.14, Curve A)

The log σ_{sp} vs. 1/T plots are linear up to certain temperature (which is ill-defined) above which σ_{sp} becomes less temperature-dependent. The activation energy in the linear portion is about 0.34 eV. The samples show behaviour essentially the same as that of $CuCl$ up to $CuCl_{1.4}$ for activation energy (Figure III.15), up to $CuCl_{1.2}$ for value of σ_{sp} at 130°C (Figure III.16) and up to $CuCl_{1.3}$ for polarization effect (Figure III.17).

Type II. ($CuCl_{1.75}$ to $CuCl_{2.0}$)

Log σ_{sp} vs. 1/T plots are straight lines indicating an activation energy of 0.67 eV, i.e. behaviour essentially that of $CuCl_2$. The value of σ_{sp} throughout this range is within a factor of 3 of that of $CuCl_2$, and the polarization effect is similar to that of $CuCl_2$.

Type III. ($CuCl_{1.4}$ to $CuCl_{1.75}$)

The log σ_{sp} vs. 1/T plots show two distinct linear regions of different slopes. The activation energies vary from one sample to another (Figure III.15) and the transition temperature between the two regions varies somewhat but is generally in the range of 120° - 130°C. The most significant feature of the results is that from $CuCl_{1.57}$ to $CuCl_{1.74}$ the higher temperature region has an activation energy higher than that found for either $CuCl$ or $CuCl_2$.

T A B L E III.7

D. C. CONDUCTIVITY RESULTS

x In $CuCl_x$	Type of Behaviour	Log σ_{sp} @ 130°C	E* (Activation Energy) (eV) (A)	(B)	Polarization Factor Δ (%)
1.000	I	-5.34	0.277 ± 0.03		160.0
1.048	I	-5.16	0.368 ± 0.03		150.0
1.100	I	-4.84	0.328 ± 0.03		150.5
1.207	I	-4.71	0.352 ± 0.03		150.0
1.325	I	-5.63	0.306 ± 0.03		144.0
1.396	I	-5.90	0.378 ± 0.03		72.0
1.503	II	-6.82	0.575 ± 0.05	0.401 ± 0.03	38.5
1.573	II	-6.76	0.640 ± 0.05	0.348 ± 0.03	30.0
1.608	II	-6.27	0.761 ± 0.05	0.409 ± 0.03	45.5
1.631	II	-7.12	0.776 ± 0.05	0.542 ± 0.03	10.5
1.677	II	-7.19	0.935 ± 0.05	0.628 ± 0.03	9.7
1.740	II	-7.69	0.915 ± 0.05	0.615 ± 0.03	6.0
1.750	III	-8.18	0.708 ± 0.03		4.7
1.757	III	-8.12	0.703 ± 0.03		4.6
1.887	III	-8.25	0.655 ± 0.03		6.0
2.000	III	-8.60	0.670 ± 0.03		3.0
1.741(M)†	II	-8.38	0.602 ± 0.05	0.376 ± 0.05	78.0

* (A) For lower activation energy.

(B) For higher activation energy,
Where there is one slope, the E value appears in the middle of this column.

† M was a mechanical mixture.

The activation energy curve rises to a plateau of 0.94 eV from $CuCl_{1.65}$ to $CuCl_{1.74}$.

The value of σ_{sp} at 130°C shows significant deviations from a smooth curve in a similar (but somewhat wider) range of composition. It is not clear precisely how a smooth curve should be drawn to represent "normal" behaviour, and it is thus not clear whether the value at $CuCl_{1.75}$ is anomalously low or whether that at $CuCl_{1.65}$ is anomalously high; but the most striking anomaly is clearly an enhancement in conductivity in the region from $CuCl_{1.55}$ to a composition beyond $CuCl_{1.7}$. For comparison, the catalytic activity curve from Figure III.4 is reproduced as a dotted line in Figure III.16.

The polarization effect shows an anomaly at $CuCl_{1.6}$, extending over only a rather small range of composition. Again, the catalytic activity curve is reproduced for comparison.

In Figure III.15 to III.17, points marked ⊡ M represent the behaviour of a mechanical mixture of CuCl and $CuCl_2$, (prepared by mixing $CuCl_2$ and CuCl together in a dry box). It is interesting to note that sample M has E values very close to those of Type I and Type II. (Figure III.15). If the value of σ_{sp} for sample M is taken as representing "normal" behaviour, then it indicates that the anomaly in copper chloride changes from an enhancement to a diminution in σ_{sp} at $CuCl_{1.74}$. Sample M, however, gives an abnormally high polarization effect (Figure III.17).

III.(3) X-RAY POWDER SPECTRA

None of the X-ray powder spectra obtained exhibits lines which cannot be attributed to cuprous chloride, cupric chloride or sodium chloride (the internal standard). However, the positions of some lines appear to be slightly different from one sample to another, suggesting that the non-stoichiometric copper chlorides contain mixtures of cuprous chloride and cupric chloride with slightly modified lattice parameters. The changes in positions of the lines are very small, and it is necessary first to establish limits of error in order to determine whether the changes are statistically significant.

Limits of Error in the Experimental Results

There are three types of estimation for error in the experimental results. A summary of the typical values of errors so estimated is presented in Table III.8.

The first type is the error estimated from the uncertainty of a single line measurement. The main sources contributing to this type of error arise from the uncertainty in reading the positions of the diffraction lines and the calibration curve (see Figure II.16). This type of error will vary from line to line being higher for the lower angle lines. The magnitude of the error is estimated from experience in using the measuring instrument and the calibration curve, and is not based on a statistical analysis.

TABLE III.8

VALUES OF ERROR ESTIMATED BY DIFFERENT METHODS

Parameter	CuCl	$CuCl_2$				
	a_o (Å)	a_o (Å)	b_o (Å)	c_o (Å)	β (°)	V (A^3)
Error in estimation from a single line:						
(a) 5th line	±0.0005	- *	- *	- *	- *	- *
(b) 1st line	±0.0033	-	-	-	-	-
95% confidence limits from consistency of lines in a single exposure:						
(a) 12 planes	-	±0.0057	±0.0061	±0.0047	±0.0045	-
(b) 8 planes	-	±0.0258	±0.0110	±0.0142	±0.0250	-
(c) 5 planes	±0.0012	-	-	-	-	-
(d) 3 planes	±0.0023	-	-	-	-	-
Observed discrepancy between values from two exposures:						
(a) 12 planes	-	±0.0030	±0.0045	±0.0042	±0.02	±0.15
(b) 8 planes	-	±0.0080	±0.0040	±0.0050	±0.04	±0.30
(c) 5 planes	±0.0008	-	-	-	-	-
(d) 3 planes	±0.0013	-	-	-	-	-
Limits of error indicated on Figures III.18 (CuCl, 3-5 planes) & III.19 ($CuCl_2$, 12 planes)	±0.0015	±0.0050	±0.0050	±0.0050	±0.02	±0.15

* Error in estimation of spacing d between planes is:

1st line	±0.0070 Å
12th line	±0.0005 Å

The second type is the error estimated from consistency of lines in a single exposure.

The range of error is established on the basis of 95% confidence limits[18]. Thus a parameter P will be regarded as having a value ranging from $\overline{P} + \frac{1.96}{\sqrt{n}}\sigma$ to $\overline{P} - \frac{1.96}{\sqrt{n}}\sigma$ ($\overline{P}$ is the mean value of P, σ is the standard deviation and n is the number of measurements).

In the case of CuCl, $\overline{P}$ is simply the average of the a_o values obtained from a number of lines; and n varies from 3 to 5. In the case of $CuCl_2$, $\overline{P}$ is the best fit value for any one of the four lattice parameters calculated by the least square method; and n varies from 8 to 12.

The third type is the error estimated from the observed discrepancy between values from two exposures, i.e. the reproducibility of results.

It can be seen from Table III.8 that the errors estimated from the third method are always smaller than those from the second method. This suggests that there are systematic errors in the positions of lines, which are incorrectly assumed to be random errors in the statistical computation of confidence limits. Moreover, in the $CuCl_2$ case, there is a drastic increase in the values of error estimated by the second method in going from a 12 plane scheme to a 8 plane scheme. This is understandable because the value of confidence limit is inversely proportional to $\frac{1}{\sqrt{n(n-4)}}$. However, it was found the computed values of the parameters change much less than the computed confidence

limits on varying the value of n. To illustrate this, Table III.9 shows the results of $CuCl_2$ calculated from different schemes (values in brackets are 95% confidence limits).

TABLE III.9

RESULTS OF $CuCl_2$ CALCULATED FROM DIFFERENT SCHEMES

No. of Planes Used	a_o (Å)	b_o (Å)	c_o (Å)	β (°)
12	6.8334 (0.0044)	3.3246 (0.0050)	6.7555 (0.0036)	121.81 (0.003)
11	6.8351 (0.0051)	3.3210 (0.0061)	6.7536 (0.0060)	121.80 (0.006)
10	6.8272 (0.0133)	3.3238 (0.0070)	6.7592 (0.0065)	121.88 (0.012)
9	6.8275 (0.0148)	3.3272 (0.0084)	6.7585 (0.0073)	121.88 (0.011)
8	6.8275 (0.0246)	3.3272 (0.0112)	6.7580 (0.0136)	121.87 (0.022)

Thus, while the second and third methods of estimating error (95% confidence limits, and reproducibility of results) are in good agreement for the 12-plane calculation, it appears that the increase in uncertainty for the 8-plane calculation is overestimated by the statistical computations for a single exposure.

In view of the discrepancy between different error estimates for the 8-plane scheme, no limits of error are shown in Figure III.20;

but for Figs.III.18 & 19(CuCl, and 12-plane scheme for $CuCl_2$) limits of error are drawn as summarized in Table III.8.

Results

The values of the lattice parameters are summarized in Tables III.10 and III.11, and Figures III.18, 19, and 20. As shown in Figure III.18, the lattice of CuCl remains more or less the same from CuCl to $CuCl_{1.5}$. A variation in the lattice parameter, (in general, expansion) occurs in the region between $CuCl_{1.5}$ to $CuCl_{1.74}$.

Since the accuracy of the results is insufficient to justify any attempt to draw a detailed curve of lattice parameter against composition, average values have been computed over three ranges. The ranges used are the same for CuCl and $CuCl_2$ results, viz. I. CuCl to $CuCl_{1.45}$; II. $CuCl_{1.45}$ to $CuCl_{1.70}$; III. $CuCl_{1.70}$ to $CuCl_2$. Mean values of lattice parameters for these ranges, together with 95% confidence limits, are shown in Table III.12. The confidence limits are calculated on the assumption that each lattice parameter is actually constant over the ranges concerned. If this is not true, then the confidence limits have been overestimated.

For CuCl, the mean values of a_o for ranges I and II are separated by an amount just greater than the sum of their 95% confidence limits, so that the chance that the true values are not in fact different is only $(1/20)^2 = 1/400$.

In Figures III.19 and III.20, the contraction from the values of the lattice parameters of pure $CuCl_2$ is plotted for the parameters

FIG. III.18 a_o of CuCl in $CuCl_x$

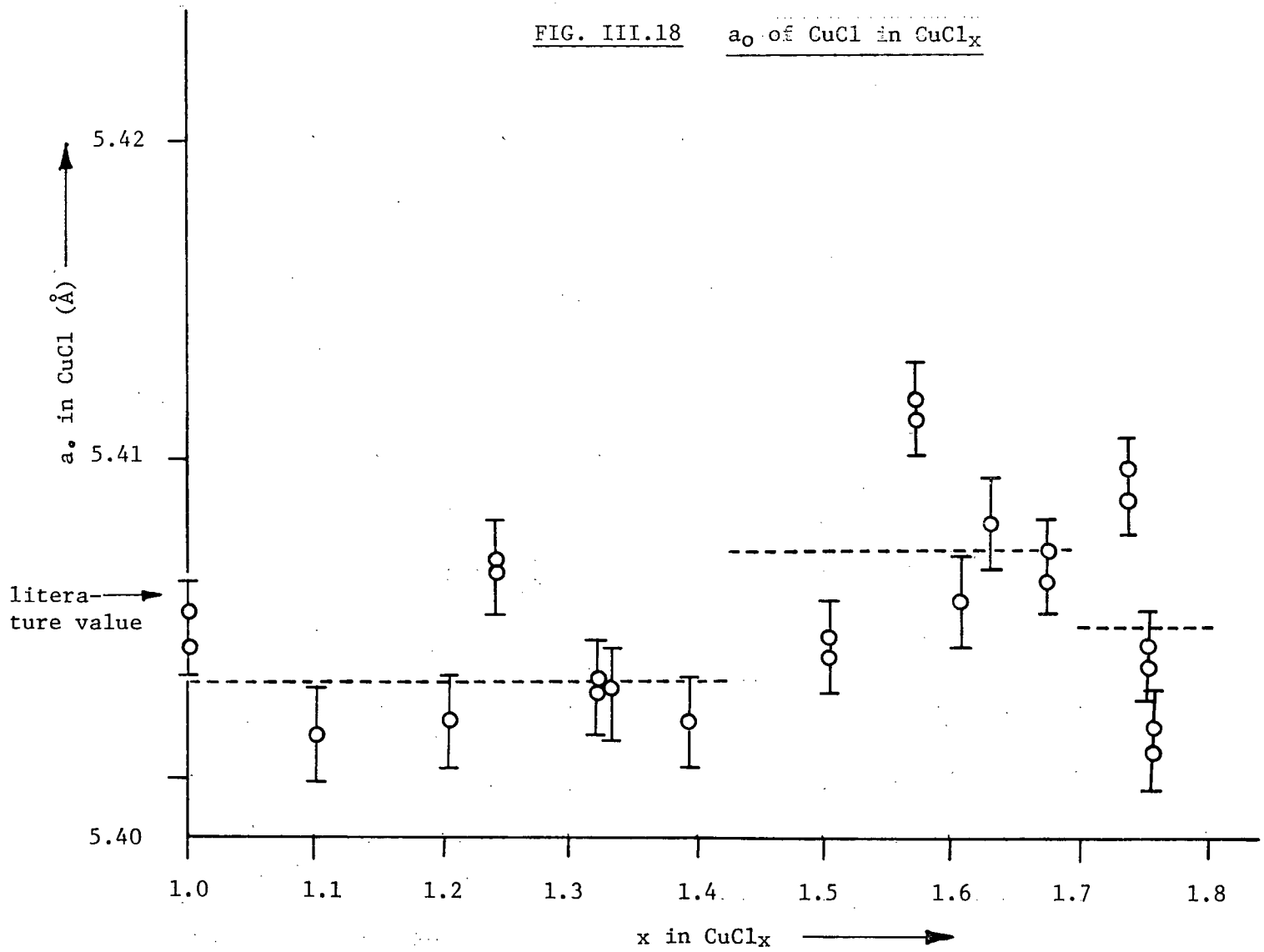

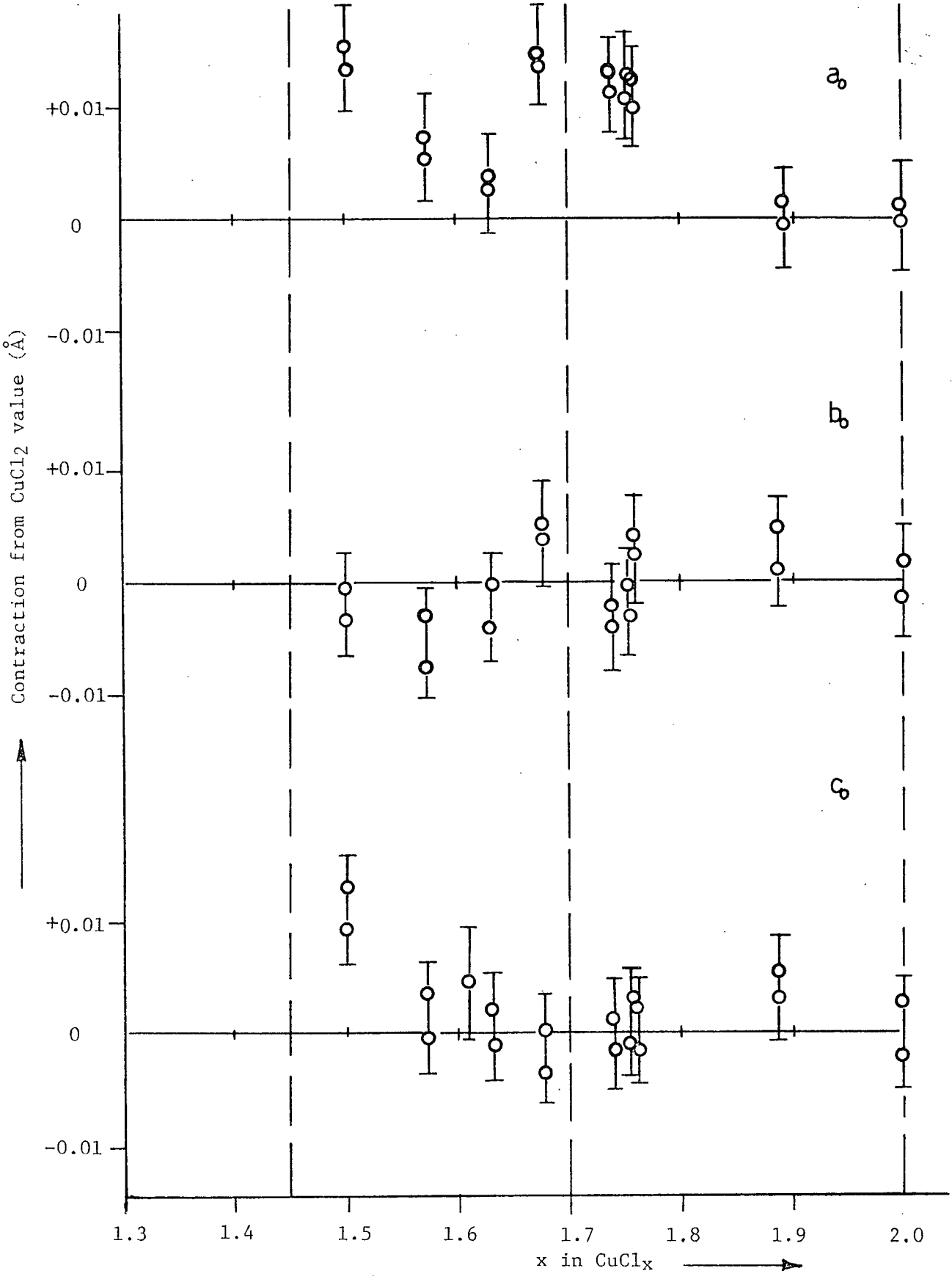

FIG. III.19 LATTICE PARAMETERS OF $CuCl_2$ in $CuCl_x$

(12 plane scheme)

FIG. III.20 LATTICE PARAMETERS OF $CuCl_2$ IN $CuCl_x$

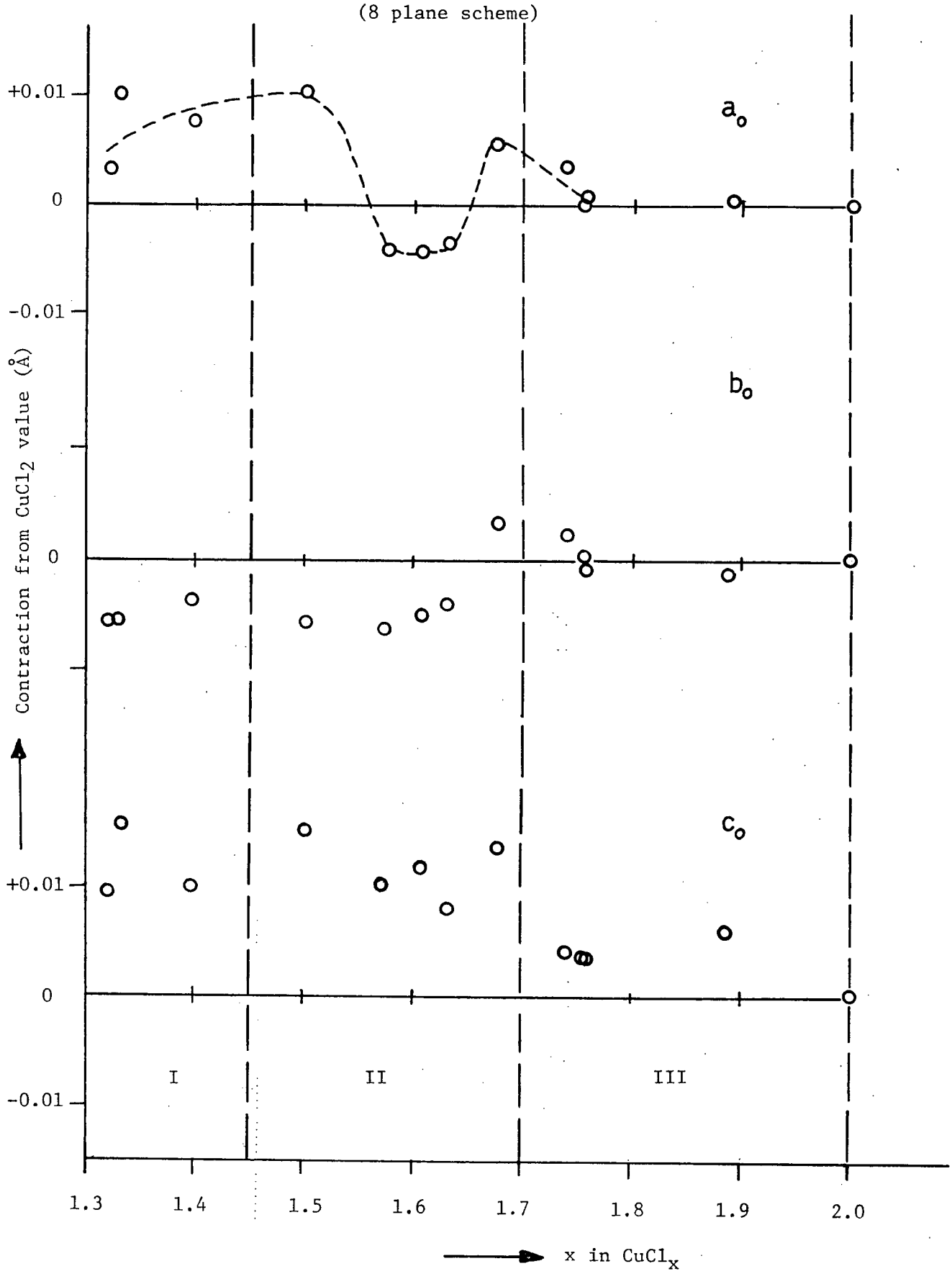

T A B L E III.10

LATTICE PARAMETER a_o OF CuCl IN COPPER CHLORIDES

x in $CuCl_x$	a_o (Å)
1.000 *	5.4057
1.000	5.4046
1.100	5.4012
1.207	5.4017
1.240	5.4065
1.321	5.4027 ± 0.0002
1.331	5.4026 ± 0.0004
1.393	5.4016
1.503	5.4039 ± 0.0006
1.573	5.4114 ± 0.0006
1.608	5.4053
1.631	5.4078 ± 0.0001
1.677	5.4064 ± 0.0010
1.740	5.4090 ± 0.0010
1.755	5.4036 ± 0.0007
1.757	5.4009 ± 0.0008

* Literature value [12].

TABLE III.11

LATTICE PARAMETERS OF $CuCl_2$ IN COPPER CHLORIDES *

x in $CuCl_x$	a_o (Å)	b_o (Å)	c_o (Å)	β (°)
1.321	6.8245	3.3330	6.7465	121.78
1.331	6.8176	3.3329	6.7405	121.84
1.398	6.8200	3.3310	6.7460	121.82
1.503	6.8173 (6.8190)	3.3330 (3.3270)	6.7410 (6.7450)	121.78 (121.81)
1.573	6.8318 (6.8271)	3.3335 (3.3302)	6.7460 (6.7541)	121.75 (121.88)
1.608	6.8320 (6.8295)	3.3325 (3.3290)	6.7445 (6.7515)	121.82 (121.87)
1.631	6.8311 (6.8304)	3.3314 (3.3269)	6.7480 (6.7556)	121.80 (121.87)
1.677	6.8220 (6.8193)	3.3240 (3.3203)	6.7425 (6.7576)	121.74 (121.94)
1.741	6.8240 (6.8212)	3.3250 (3.3280)	6.7520 (6.7563)	121.78 (121.91)
1.755	6.8275 (6.8217)	3.3270 (3.3262)	6.7525 (6.7550)	121.80 (121.90)
1.757	6.8268 (6.8222)	3.3282 (3.3215)	6.7523 (6.7553)	121.84 (121.84)
1.887	6.8272 (6.8332)	3.3285 (3.3220)	6.7500 (6.7518)	121.84 (121.75)
2.000	6.8275 (6.8334)	3.3272 (3.3246)	6.7560 (6.7555)	121.85 (121.81)
2.000**	6.85 ± 0.07	3.30 ± 0.03	6.70 ± 0.07	121.0 ± 1.2

* Values without brackets were calculated by the 8 plane scheme while values in brackets were calculated by the 12 plane scheme.

** Values reported by Wells[10] based on single crystal measurement.

a_o, b_o, and c_o for the two calculation schemes.

It can be seen from Figure III.20 that the value of a_o may possibly vary in a rather complicated way which may not be adequately represented by the averaging procedure in Table III.12. The plot shows possible indications of two maxima and a minimum in the region from $CuCl_{1.45}$ to $CuCl_{1.7}$ (range II).

According to the results for the 8-plane calculation, (Figure III.20), the statistically significant behaviour is a contraction in a_o and c_o and an expansion in b_o, all in region I (below $CuCl_{1.65}$) and probably extending into region II, in which, however, a_o and b_o may not be constant throughout the region. The largest contraction is in c_o; but some doubt is cast on the magnitude of this by the rather large shift in four of the points (between $CuCl_{1.573}$ and $CuCl_{1.677}$) in the 12-plane calculation (compare Figures III.19 and III.20).

Of the two quantities showing a contraction, c_o traverses a plane of normally octahedral holes and a_o is related to the distance between adjacent $CuCl_2$ chains. The quantity showing an expansion, b_o, is the distance between two adjacent Cu^{2+} ions in a chain. The data are thus consistent with displacement of a small number of cations from the chains to octahedral sites in layers which are vacant in the perfect lattice.

The angle β showed no statistically significant changes between the three regions, and it is not very clear how this parameter might be expected to behave on displacement of some of the cations.

T A B L E III.12

MEAN VALUES OF PARAMETERS

IN

DIFFERENT RANGES OF COMPOSITION

Range of Composition	I $CuCl - CuCl_{1.45}$	II $CuCl_{1.45} - CuCl_{1.7}$	III $CuCl_{1.7} - CuCl_2$
CuCl, a_o	5.4030 ± 0.0014	5.4070 ± 0.0024	5.4045 ± 0.0048
$CuCl_2$, a_o	6.8207 ± 0.0040	6.8264 ± 0.0060	6.8266 ± 0.0013
$CuCl_2$, b_o	3.3323 ± 0.0013	3.3309 ± 0.0035	3.3272 ± 0.0012
$CuCl_2$, c_o	6.7443 ± 0.0038	6.7444 ± 0.0024	6.7527 ± 0.0021

III.(4) MAGNETIC SUSCEPTIBILITY MEASUREMENTS

Magnetic susceptibility measurements at various temperatures and two different field strengths viz. 4,000 and 7,800 oerst were performed on copper chlorides over the range of composition from $CuCl_{1.32}$ - $CuCl_{2.0}$. For copper chlorides with composition lower than $CuCl_{1.32}$, owing to the small amount of Cu^{2+} present, the values of magnetic susceptibility could not be determined as accurately as those of higher composition and therefore no attempts were made to measure the magnetic susceptibility of them.

Since Cu^{+} ion is diamagnetic, and if the susceptibility observed for a copper chloride $CuCl_x$ is assumed to be due to the amount of Cu^{2+} ion present, then the molar susceptibility χ'_M (corrected for diamagnetic contribution) can be calculated from the measured gram susceptibility as follows:

The weight of $CuCl_2$ in $CuCl_x$ is given as

$$\frac{(x-1)\ (\text{Mol. Wt. of } CuCl_2)}{(x-1)\ (\text{Mol. Wt. of } CuCl_2) + (2-x)\ (\text{Mol. Wt. of CuCl})} = \frac{134.5(x-1)}{35.5x-63.5}$$

$$\therefore \quad \chi_g = \begin{matrix}\text{gm susceptibility} \\ \text{of } CuCl_2 \text{ in the} \\ \text{substance}\end{matrix} = \frac{\text{Measured gm susceptibility}}{134.5\ (x-1)/(35.5x - 63.5)}$$

$$\therefore \quad \chi_M = \begin{matrix}\text{molar susceptibi-} \\ \text{lity of } CuCl_2 \text{ in} \\ \text{the substance}\end{matrix} = \frac{\text{Measured gm susceptibility}}{(x-1)/(35.5x - 63.5)}$$

and $\chi'_M = \chi_M$ + diamagnetic correction for $CuCl_2$

$= (\chi_M + 40) \times 10^{-6}$ c.g.s. units.

If the copper chloride is only a physical mixture of CuCl and $CuCl_2$, one naturally would expect that the value of its χ'_M (or for greater generality, the value of magnetic moment, μ_{eff}) to be the same as that of pure $CuCl_2$. On the other hand, if the values of χ'_M and μ_{eff} of the copper chloride are different from those of pure $CuCl_2$, a phase of a significant defect structure which does not exist in normal preparations of either $CuCl_2$ or CuCl might well be present. In addition to the values of μ_{eff} and χ'_M, the value of θ, a measure for the deviation from the Curie behaviour is also a quantity popularly used for comparison of magnetic behaviour of different compounds. In our case, since $CuCl_2$ is antiferromagnetic, the Curie temperature (T_c) which is a measure of the strength of exchange of neighbouring paramagnetic ions is also of interest.

The values of μ_{eff}, and θ can be obtained from a plot of $\frac{1}{\chi'_M}$ vs. T. According to Curie-Weiss law,

$$\chi'_M = \frac{C}{(T + \theta)} \quad \ldots\ldots\ldots\ldots\ldots\ldots\ldots\ldots (1)$$

$$\text{i.e.} \quad \frac{1}{\chi'_M} = \frac{T}{C} + \frac{\theta}{C} \quad \ldots\ldots\ldots\ldots\ldots\ldots\ldots\ldots (2)$$

where C = Curie-Weiss constant = $(\frac{2.84}{\mu_{eff}})^2$

T is temperature in ^oK

Such a plot should be a straight line. The slope will be equal to $\frac{1}{C}$ (hence μ_{eff} can be evaluated) whereas the intercept will yield $\frac{\theta}{C}$. In our case, the $\frac{1}{\chi'_M}$ vs. T plot normally is a straight line only

down to a certain temperature below which it becomes a curve. Thus the values of μ_{eff} were extracted from the straight line region. Typical plots of $\frac{1}{\chi'_M}$ vs. T are given in Figure III.21 for a few selected cases.

In principle, if one plots χ'_M vs. T for an antiferromagnetic substance, a curve with a maximum should be obtained. The temperature at which the maximum occurs is referred to as the Curie temperature (or Neel's temperature) below which short range ordering of spins takes place and hence the value of χ'_M decreases. In the present work, except for the cases of $CuCl_{1.503}$ and $CuCl_{1.631}$, no maximum value of χ'_M could be observed, presumably because the values of T_c in these cases are lower than the minimum temperature at which the measurements were carried out, viz. 77.6°K, liquid nitrogen temperature. The value of T_c for $CuCl_2$ reported in the literature[19] is 76° - 78°K which is close to liquid nitrogen temperature. Even for the two cases mentioned, the value of T_c could only be roughly estimated as (82 ± 2)°K because of the lack of data below T_c. A plot of χ'_M vs. T for $CuCl_{1.631}$ is illustrated in Figure III.22.

In other cases for which T_c could not be estimated from a χ'_M vs. T plot, a different procedure was attempted to extract this quantity from the existing data.

Barraclough and Ng[11] derived an equation for the magnetic susceptibility of an antiferromagnetic substance having a linear chain structure. This equation was found applicable in the cases of $CuCl_2$ and $CuBr_2$.

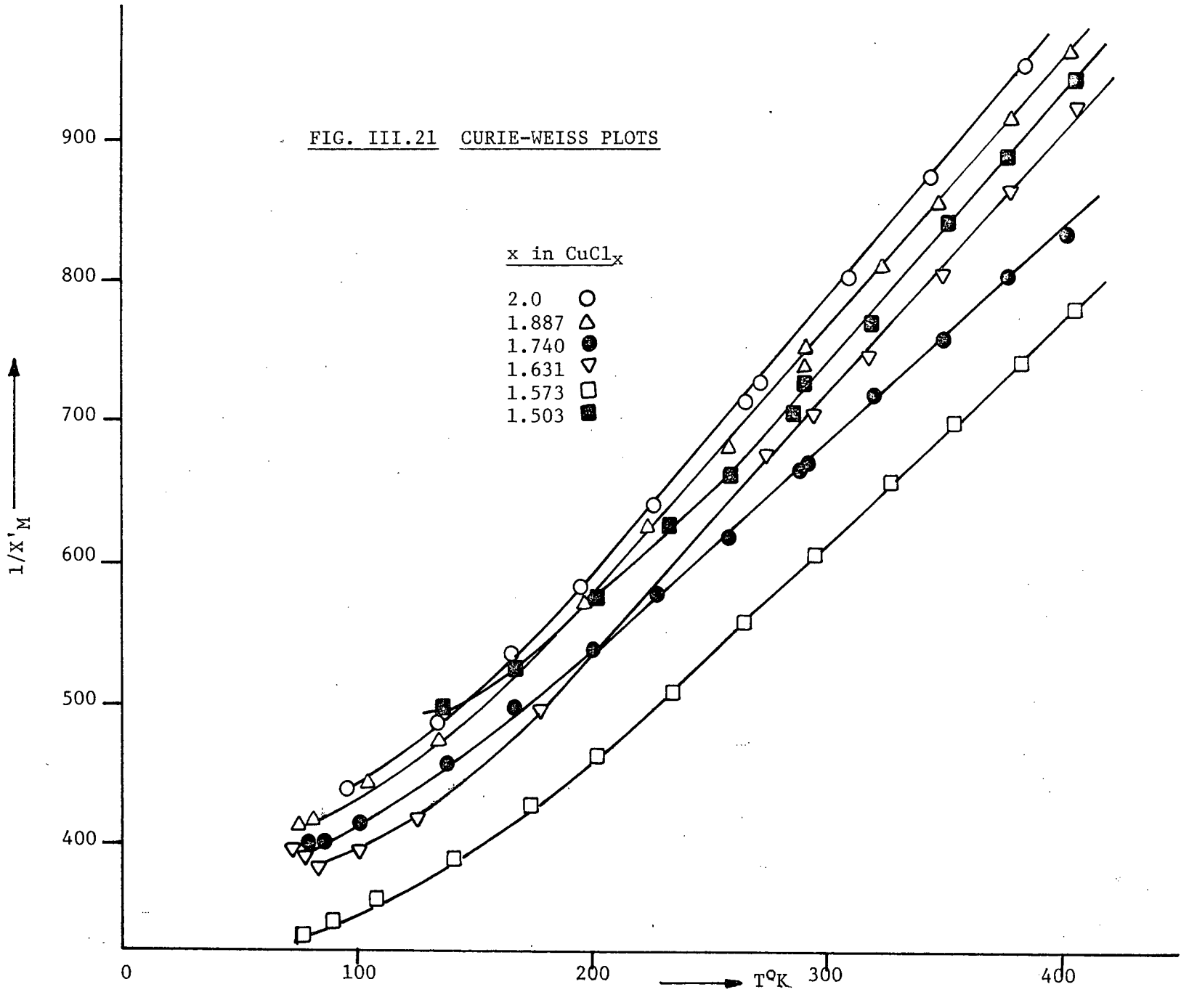

FIG. III.21 CURIE-WEISS PLOTS

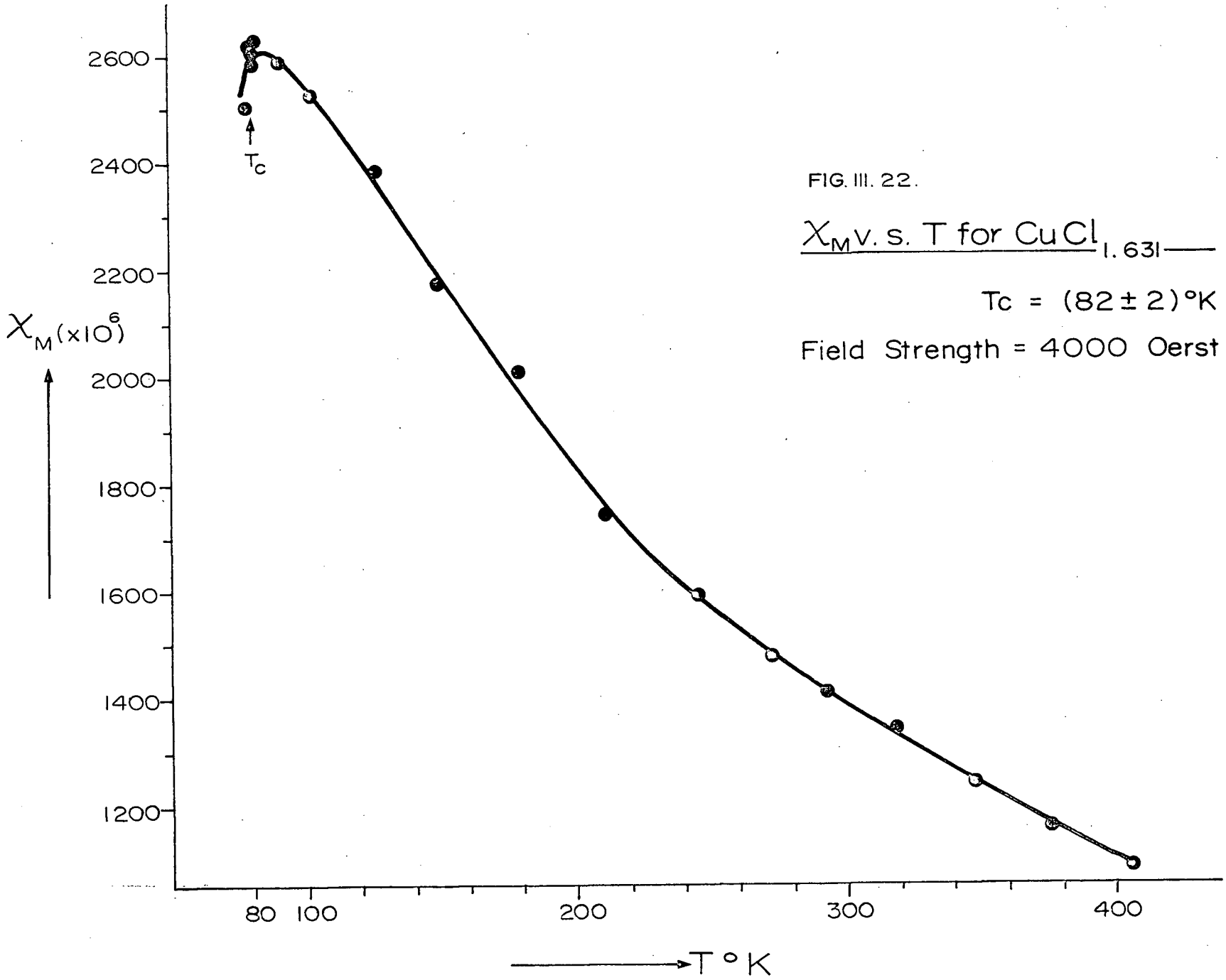

FIG. III. 22.

χ_M v. s. T for $CuCl_{1.631}$

Tc = (82 ± 2) °K

Field Strength = 4000 Oerst

At a temperature equal to or higher than T_c, the equation takes the form:

$$\chi'_M = \frac{Ng^2 \beta^2}{4kT} \exp. \left(\frac{2J}{kT} \right) \ldots\ldots \quad (3)$$

Where N is Avogadro's number

g is the spectroscopic splitting factor

β is the Bohr magneton

k is the Boltzmann Constant

T is temperature in ^oK

J is the exchange energy between neighbouring spins, negative for antiferromagnetic substances.

It follows directly from (3) that when $\frac{d\chi'_M}{dT} = 0$, i.e. at the maximum in χ'_M, the temperature reaches a critical value (Curie temperature).

$$T_c = -2J/k.$$

If one plots log $(\chi'_M T)$ vs. $\frac{1}{T}$, a straight line should be obtained. The slope of the line will be $\frac{1}{2.303}(2J/k)$, i.e. $-\frac{T_c}{2.303}$. In addition to the evaluation of the value of T_c, such plots have another important significance.

A deviation from linearity might imply a structure different from that of linear chains existing in the copper chloride at least in localised regions. (Note, however, that if this be the case, the value of T_c could not be estimated). Figure III.23 shows plots for three different composition.

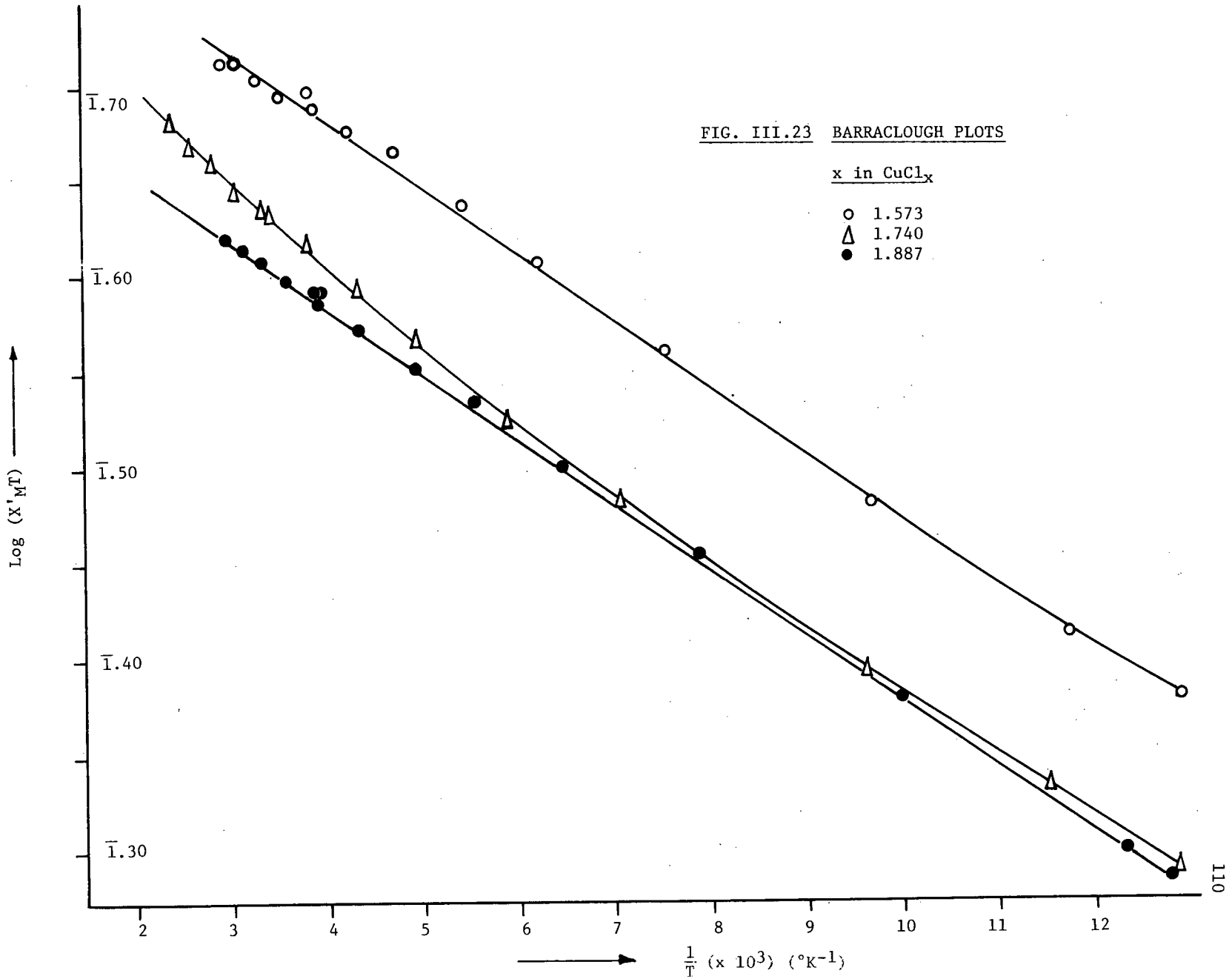
FIG. III.23 BARRACLOUGH PLOTS
x in CuCl$_x$
1.573
1.740
1.887
Log ($X'_M T$)
$\bar{1}$.70
$\bar{1}$.60
$\bar{1}$.50
$\bar{1}$.40
$\bar{1}$.30
2
3
4
5
6
7
8
9
10
11
12
$\frac{1}{T}$ (x 10^3) ($°K^{-1}$)
110

The results (summarised in Figure III.24 and Table III.13) show that all samples with compositions from about $CuCl_{1.32}$ to $CuCl_{1.75}$ are significantly different in behaviour from $CuCl_2$. For all these samples χ'_M at a fixed temperature and μ_{eff} were higher for most of the samples [Figure III.24 (a) & (b)]. Each of these quantities shows two maxima, the first in the region $CuCl_{1.57}$ to $CuCl_{1.61}$ coinciding roughly with the first maximum in catalytic activity, while the second at $CuCl_{1.68}$ to $CuCl_{1.73}$ coincides with a minimum in catalytic activity. The two peaks in magnetic properties are distinguished in that the properties are all field-dependent in the region of the second peak, but not that of the first; but properties at $CuCl_{1.321}$ were also field-dependent.

A mechanical mixture (points M in Figure III.24) showed behaviour quite indistinguishable from that of $CuCl_2$. χ'_M of M_1 at room temperature was found unchanged after being heated to 130°C for 5 hours followed by gentle cooling. Such results imply that a different phase of structure could not be obtained by simple annealing of a mechanical mixture, in agreement with the results of conductivity measurements.

Except for $x > 1.75$, the Barraclough plot for $CuCl_x$ shows departure from linearity. Also the effect is more pronounced in the low temperature region. Moreover, the effect is greater for $CuCl_x$ whose magnetic properties are field-dependent. ($1.63 < x < 1.75$ and $x = 1.32$).

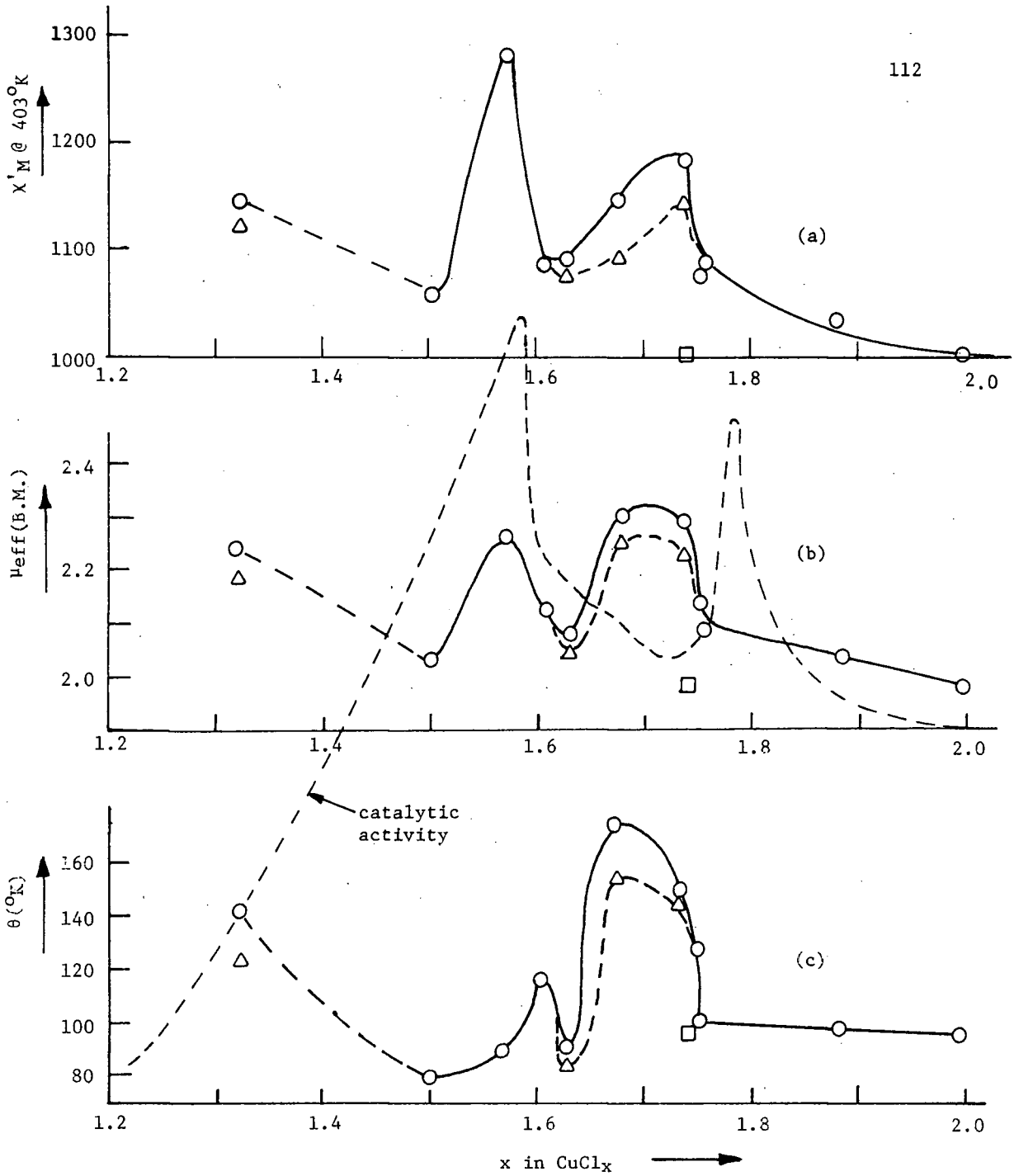

FIG. III.24 RESULTS OF MAGNETIC MEASUREMENTS

In the field-indept. case, O represents the results obtained at 4000 as well as 7800 oerst. In the field-dept. case, O represents the results obtained at 4000 oerst. whereas △ represents results obtained at 7800 oerst. Mixture M (□) is field-indept.

TABLE III.13

RESULTS OF MAGNETIC MEASUREMENTS

Composition x	μ_{eff} (B.M.)		χ'_M (x10^6)@130°C		θ°		T_C (°K)	
	4000 oerst.	7800 oerst.	4000 oerst.	7800 oerst.	4000 oerst.	7800 oerst.	4000 oerst.	7800 oerst.
1.321	2.25 ±0.10	2.20 ±0.10	1144 ± 15	1118 ± 15	142 ± 5	123 ± 5	-	-
1.503	2.02 ±0.10	2.02 ±0.10	1056 ± 15	1068 ± 15	79 ± 5	79 ± 5	82 ± 2	82 ± 2
1.573	2.26 ±0.10	2.26 ±0.10	1282 ± 15	1284 ± 15	88 ± 5	88 ± 5	80 ± 2	80 ± 2
1.608	2.13 ±0.10	2.12 ±0.10	1088 ± 15	1078 ± 15	116 ± 5	115 ± 5	81 ± 2	81 ± 2
1.631	2.08 ±0.10	2.06 ±0.10	1091 ± 15	1072 ± 15	90 ± 5	84 ± 5	82 ± 2	82 ± 2
1.677	2.30 ±0.10	2.26 ±0.10	1145 ± 15	1090 ± 15	174 ± 5	154 ± 5	-	-
1.740	2.30 ±0.10	2.24 ±0.10	1184 ± 15	1142 ± 15	148 ± 5	144 ± 5	-	-
1.755	2.14 ±0.10	2.14 ±0.10	1075 ± 15	1075 ± 15	126 ± 5	126 ± 5	80 ± 2	80 ± 2
1.757	2.09 ±0.10	2.09 ±0.10	1085 ± 15	1090 ± 15	100 ± 5	100 ± 5	77 ± 2	77 ± 2
1.887	2.04 ±0.10	2.04 ±0.10	1035 ± 15	1035 ± 15	98 ± 5	98 ± 5	80 ± 2	80 ± 2
1.744	1.99 ±0.10	1.99 ±0.10	1000 ± 15	1000 ± 15	98 ± 5	98 ± 5	-	-
2.00	1.99 ±0.10	1.99 ±0.10	1000 ± 15	1000 ± 15	94 ± 5	94 ± 5	78 ± 2	78 ± 2
2.00*	(2.05 ± 0.10)		(990 ± 15)		(110 ± 5)		(78)	

* Literature Values [19]

The values of T_c are slightly higher than the normal $CuCl_2$ value only for compositions $CuCl_{1.503}$ and $CuCl_{1.631}$.

Whenever the magnetic susceptability is field-dependent, the values of χ'_M, μ_{eff}, & θ are always higher for lower field (i.e. the opposite behaviour from that normally found in ferromagnetism).

Before leaving the results of magnetic measurement, some words about the limits of error and the reproducibility of results are appropriate.

The limits of error quoted in Table III.13 for μ_{eff}, χ'_M, T_c, and θ are mainly based on the range within which the tangents of the $\frac{1}{\chi'_M}$ vs. T plots could be drawn. The limit of error for T_c, on the other hand, depends on the range within which the tangents of the Barraclough plots could be drawn.

III.(5) ESR SPECTRA

ESR spectra were taken for the following types of sample:

(a) Catalysts of various compositions taken from the reaction vessel and studied in vacuo

  (i) at room temperature

  (ii) at $77^{o}K$

  (iii) at $4^{o}K$

(b) Catalysts of various compositions at $130^{o}C$ in contact with

  (i) propane

  (ii) chlorine

  (iii) a chlorine - propane mixture.

In all cases except (a)(iii), a single broad structureless line was observed, its centre corresponding to a g value of about 2.09. This is attributed to Cu^{2+}. For a series of different compositions at room temperature, the amount of ESR absorption (double integral of derivative spectrum) was closely proportional to the expected amount of Cu^{2+} present according to the stoichiometry of the sample. Cu^{2+} signals usually show fine structure attributable to anisotropy of the g value. The absence of such structure in this case is probably a consequence of antiferromagnetic exchange, which is well known in $CuCl_2$. At room temperature and above the line was symmetrical, of Lorentz type (Figure III.25a). The linewidth W = 352 gauss at room temperature corresponds to a spin-spin relaxation time $T_2 = 2/W\sqrt{3} = 3.3 \times 10^{-2}$ sec.

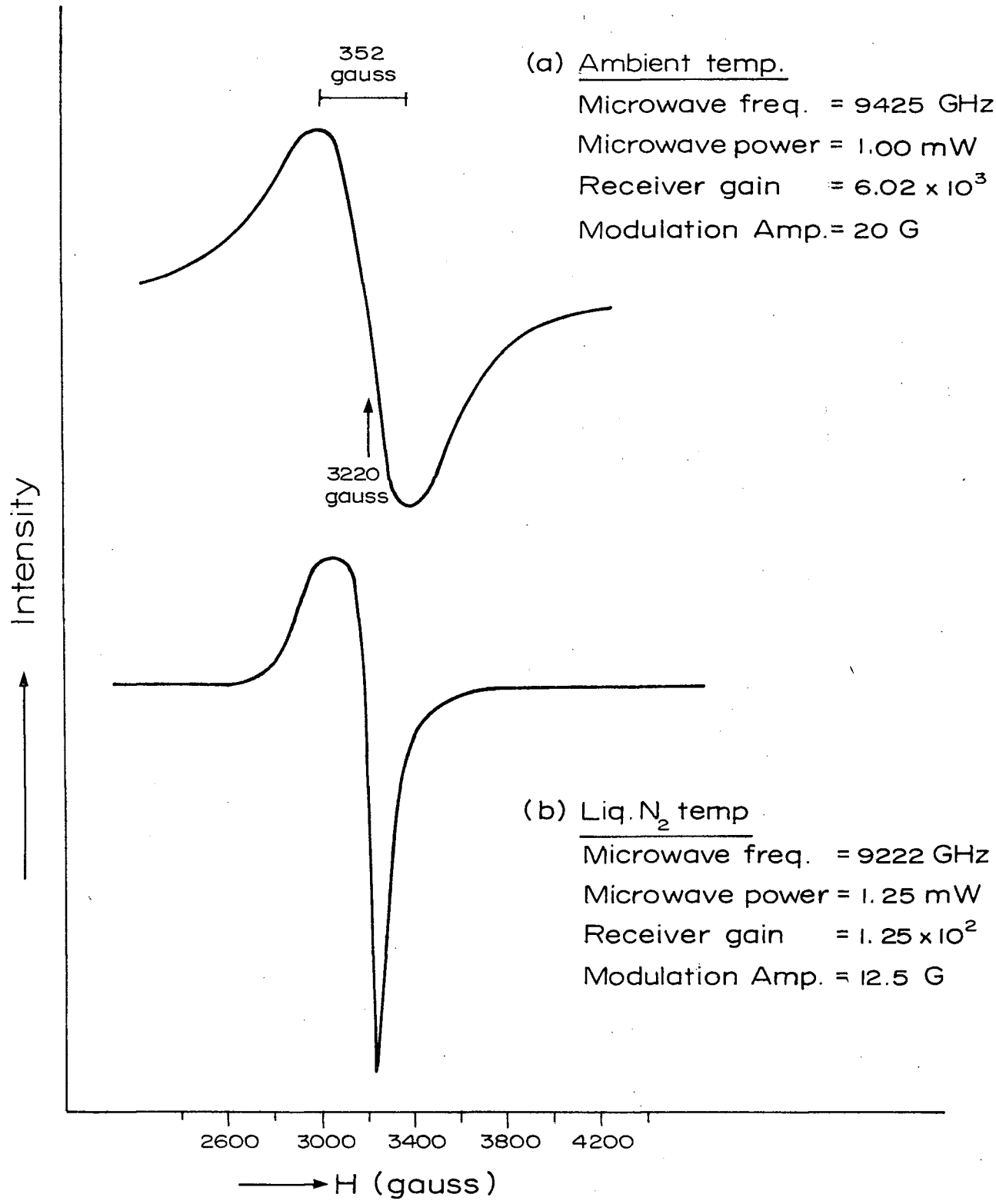

FIG. III. 25. ESR Signal of $CuCl_2$

Lower temperatures were used in an attempt to overcome antiferromagnetic exchange and reveal fine structure; but although the signal at 77°K narrowed and became asymmetric (Figure III.25b), it remained structureless. At 4°K, there was no signal. This may indicate perfect antiferromagnetic ordering, which is equivalent to pairing of all the spins.

No new signals appeared in the presence of the various gas phases, and the Cu^{2+} signal was not affected by the gases.

III.(6) MICROSCOPIC STUDIES

For compositions up to $CuCl_{1.2}$, some unreacted CuCl crystals (pale green) could be seen, together with crystals of various shades of brown representing an increasing fraction of the material as x increased. From $CuCl_{1.2}$ to $CuCl_{1.325}$, all crystals appeared brown, but with noticeably different shades. Beyond $CuCl_{1.325}$, all crystals had the chocolate-brown appearance of $CuCl_2$; but by dark field illumination, different intensities of colour could be distinguished, together with some indication that some crystals had reacted externally but remained CuCl at the centre.

The particle size distribution of CuCl as determined by the microphotographic method covered a range of 3.5 - 63μ. The distribution was adequately represented by a Gaussian curve with the peak at 17.5μ (see Figure III.26).

Some coherent lumps of catalyst (just as it comes from the reactor) were cut with a scalpel under the microscope. This was easily done, leaving a flat surface of shiny appearance, and indicated the softness of $CuCl_2$, to be expected from its layer lattice.

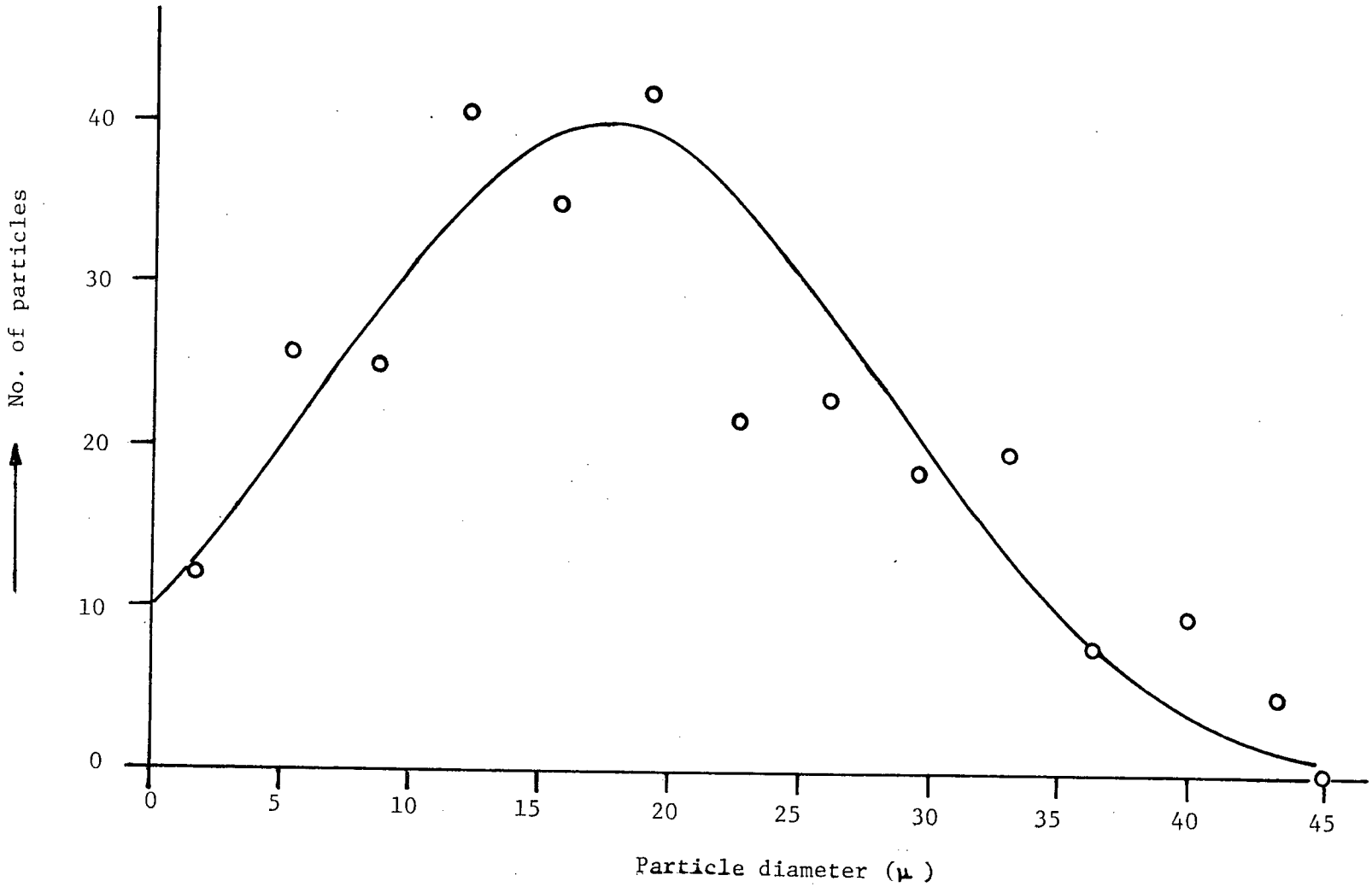

FIG. III.26 PARTICLE SIZE DISTRIBUTION OF CuCl

CHAPTER IV

DISCUSSION OF RESULTS

As the main objectives of this thesis are to study the catalytic activity and the reactivity of copper chloride and in view of the fact that the catalytic activity of copper chloride in the C_3H_8/Cl_2 system appears to be closely related to the reactivity of copper chloride towards chlorine, the discussion will be focused on the kinetics and mechanisms involved in the two reactions. The results of other types of measurement for the characterization of catalysts will be treated as supporting evidence for structural changes in copper chloride in going from CuCl to $CuCl_2$.

IV.(1) KINETICS AND MECHANISM OF THE REACTION OF CuCl with Cl_2

$CuCl_2$ occupies a volume 66% greater than that of the CuCl from which it is formed, and the formation of $CuCl_2$ therefore involves a migration of copper nuclei, presumably as either Cu^+ or Cu^{2+}. If a complete recrystallization occurs starting from small $CuCl_2$ nuclei, then all Cu nuclei may be displaced macroscopic distances from their original positions; but if a layer of $CuCl_2$ builds up on each CuCl crystal, forming a reaction interface which advances into the CuCl, then some of the original Cu^+ ions may not be displaced far, and an electron transport process may occur to convert them to Cu^{2+}.

Much of the evidence suggests that these two mechanisms both occur, as successive stages in the reaction. The transition between them, which is not very sharp, appears to be in the region of $CuCl_{1.2 - 1.3}$. Below this composition, the rate of linear reaction (r_L) is essentially independent of x; its apparent activation energy is zero or slightly negative; the rate of the initial rapid reaction (r_M) is sensitive to evacuation time; electrical conductivity indicates a continuous CuCl phase; and microscopic observation shows separate CuCl and $CuCl_2$ crystals. All these features suggest a surface-controlled reaction, in which the product is continuously removed to form new $CuCl_2$ crystals.

Beyond $CuCl_{1.2 - 1.3}$, the same types of experimental

evidence all show marked changes in behaviour suggesting that a layer of $CuCl_2$ is building up around each CuCl crystal, and that this layer is markedly defective. The rate of reaction slows down greatly with increasing extent of reaction (and the main object of this part of the discussion is to show that these data can be analysed in terms of diffusion through the $CuCl_2$ layer as the rate-controlling step); the diffusion process has a fairly high positive activation energy (11.4 kcal/mole); the rate of reaction ceases to be sensitive to evacuation time; microscopic observation shows no CuCl surfaces; but, although X-ray diffraction shows only CuCl and $CuCl_2$ lattices, electrical conductivity, magnetic susceptibility and catalytic activity become significantly different from those of $CuCl_2$.

To account for these data, it is postulated that the $CuCl_2$ layer contains a fairly high concentration (in relation to "normal" values of defect concentrations in ionic crystals) of Cu^+, which is the mobile species. The following analysis of diffusion kinetics is, however, valid regardless of the identity of the diffusing species.

The Interface Displacement Parameter ℓ

In the first stage of reaction, below $\alpha \sim 1.3$, the reaction interface is the exposed CuCl surface, which may reasonably be assumed to advance at the same linear rate for all particles. Thus we may define a parameter ℓ, the distance which the reaction interface has travelled from time zero to time t, which has the same value for all CuCl particles, regardless of their initial size. For a known

particle size distribution, ℓ is functionally related to the overall extent of reaction α of the whole assembly of particles. Let b_o be the initial size parameter of any particle (the particles will be taken in this account to be spherical, with initial radius b_o, but equation (1) below is independent of particle shape provided that all particles are of similar shape). Let the size distribution be $N(b_o)$, such that the number of particles between b_o and $(b_o + db_o)$ is $N(b_o)\ db_o$. Then the fraction unreacted at any time is

$$1 - \alpha = \int_{\ell}^{\infty} (b_o - \ell)^3\ N\ (b_o)\ db_o \ /\ \int_{\ell}^{\infty} b_o^3\ N\ (b_o)\ db_o \quad . \ . \ . \ (1)$$

For a known size distribution, α can be found at any ℓ by numerical integration according to equation (1).

Figure IV.1 shows the observed data or particle size distribution (points), a Gaussian curve (A) which will be taken to represent the distribution for purposes of computation, and another Gaussian B with half the width of A. Some computations have been done for this "sharp" distribution in order to show which features of the analysis are sensitive to particle size distribution, and which are not.

Figure IV.2 shows computed $\alpha - \ell$ curves: A, for uniform particle size; B, for the "actual distribution" A; C, for the "sharp distribution" B. The $\alpha - \ell$ curves are almost linear up to $\alpha = 0.3$, indicating that the rate of chlorination should be constant up to that value of α. Experimentally, chlorination rates were often roughly constant up to $\alpha \sim 0.2$, but they started to drop markedly

FIGURE IV.1 PARTICLE SIZE DISTRIBUTION (two types)

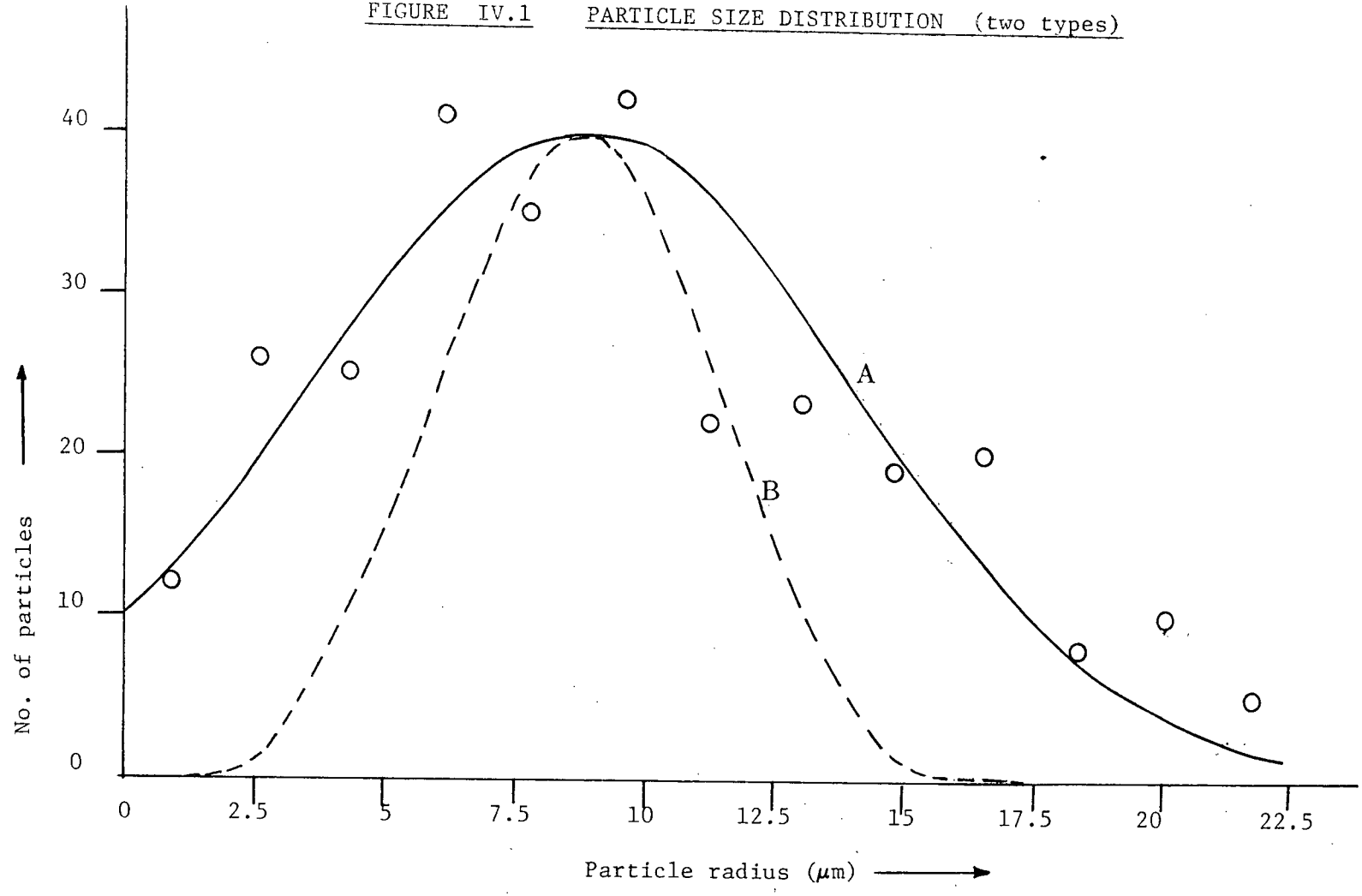

beyond that value. The high rate of chlorination could, however, be restored completely or partially by prolonged evacuation between runs up to at least $\alpha = 0.32$. The region from $\alpha = 0.2$ to $\alpha = 0.3$ is evidently a transition region between the surface-controlled and diffusion-controlled mechanisms.

Beyond $\alpha = 0.3$, the drop in reaction rate is far greater than can be accounted for by the calibration curves of Figure IV.2 with continued linear advance of the reaction front. If the mechanism has now become diffusion across an accumulating product layer then, provided that the product layer is not too thick in comparison to the radius of the remaining reactant, the kinetics of advance of the reaction front may be expected to be given by Wagner's parabolic law for tarnishing reactions. For purposes of kinetic analysis, it is assumed that the diffusion layer starts to build up on each particle at the instant when it has lost an amount ℓ_o of its original radius, ℓ_o having the same value for all particles. Thus all particles of radius $b_o < \ell_o$ are alreayd completely reacted, and diffusion starts effectively in a new assembly of particles of initial radius $b_o' = b_o - \ell_o$ for any particle, and with size distribution $N'(b_o') = N(b_o)$. As long as the parabolic law remains a good approximation, ℓ will continue to have the same value for all particles which are not already fully reacted, and will be given by

$$(\ell - \ell_o)^2 = k_T t \quad \ldots\ldots\ldots \quad (2)$$

where k_T is the "tarnishing constant". In terms of the extent of

FIG.IV.2 α VS. ℓ PLOTS

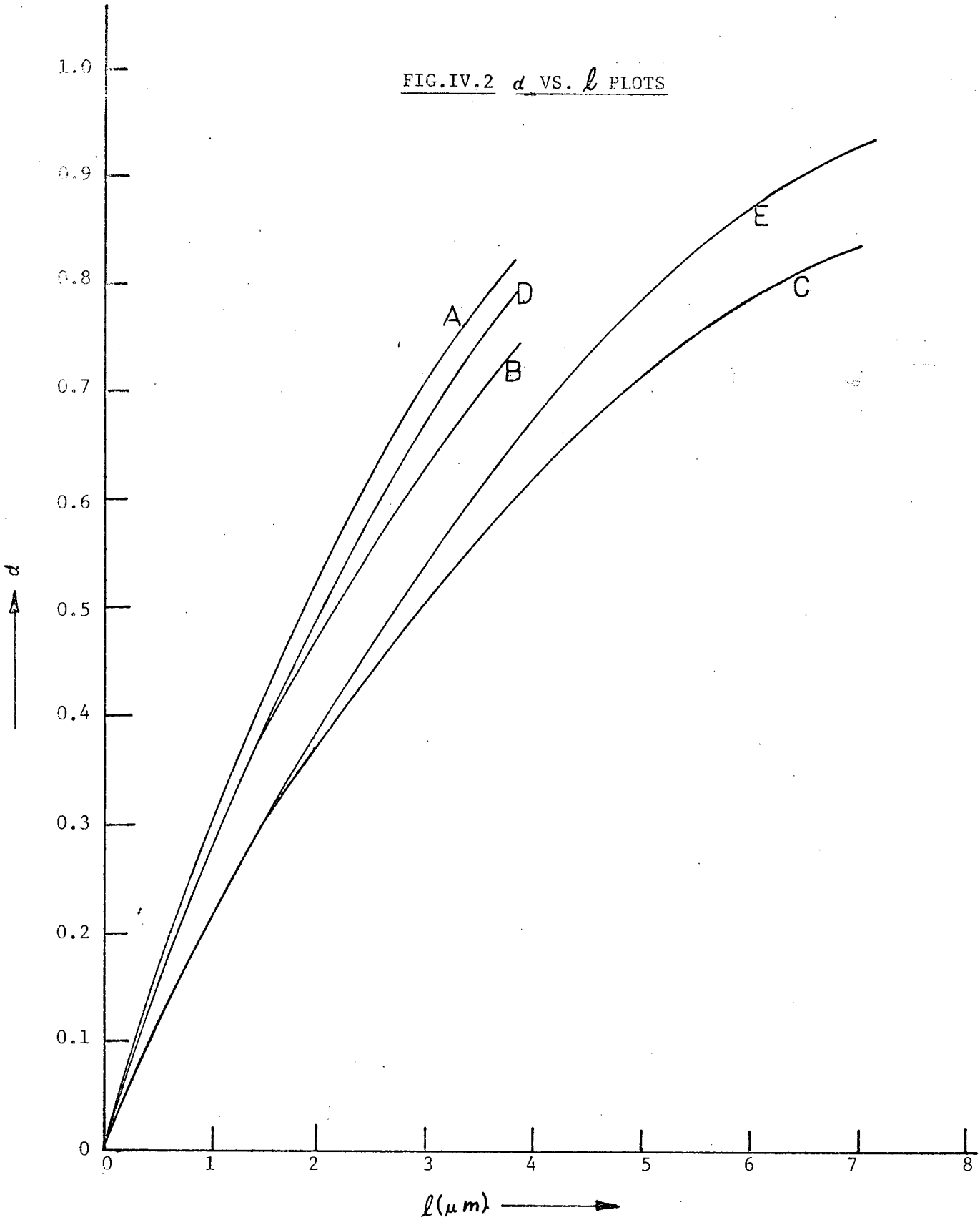

reaction α_J of any spherical particle of initial radius b_o', the Wagner law may be recast in the form of the Jander equation

$$[\ 1 - (1-\alpha_J)^{1/3}\ ]^2 = 2\ D\ C_1\ V_M\ t/(b_o')^2 \quad . . . . . \quad (3)$$

in which the outer surface of the sphere is assumed to remain at b_o' throughout reaction, the diffusing material has concentration C_1 at the solid/solid interface (radius a) and D is its diffusion coefficient. The constants representing reaction rate in the two forms of the equation are related by

$$k_T = 2\ D\ C_1\ V_M \quad . . . . . \quad (4)$$

If the volume of the product is β times that of the reactant, then (see Appendix I) the Jander equation should contain the factor β on the left-hand side:

$$\beta\ [\ 1 - (1-\alpha_J)^{1/3}\ ]^2 = 2\ D\ C_1\ V_M\ t\ /\ (b_o')^2 \quad . . . \quad (5)$$

Equation (4) is correspondingly modified:

$$k_T = 2\ D\ C_1\ V_M\ /\ \beta \quad . . . . . \quad (6)$$

The above equations are derived by the quasi-stationary state method with the concentration distribution appropriate to a semi-infinite solid initially having a plane surface, so that the diffusion layer is at all times a slab with plane parallel surfaces. For a diffusion layer in the form of a spherical shell, the parabolic law is valid only at low extents of reaction α. At higher α, a quasi-

stationary state approximation for a spherical shell must be used which takes into account the convergence of diffusion paths with decreasing radius in a spherical geometry. The correction which must be applied to the parabolic law is obviously a function of particle size, and correspondingly the distance which the reacting interface has moved by time t is no longer independent of particle size. Accordingly, if the distance parameter ℓ is still to be used, it must be redefined. In the present computations, it was found convenient to use a parameter ℓ which is the limit of the actual displacement of the reaction interface as $b_o' \to \infty$. Since a particle of infinite size obeys the parabolic law exactly, ℓ as defined in this way should still obey equation (2), with k_T as given by equation (6).

Plots According to the Parabolic Law (Jander Equation)

The correction for spherical geometry metnioned above is fairly complicated, and has to be recalculated completely for every assumed value of ℓ_o. Since the correction is not important at low α, a simpler procedure is to ignore the correction in the first instance and, with data only for fairly low α, to determine the ℓ_o value which will give a linear plot of $(\ell - \ell_o)^2$ against t. Thus, for a set of experimental α - t data, the calibration curve C of Figure IV.2, being the Jander approximation to the α - ℓ curve for the actual particle size distribution, is used to convert α values to ℓ values. Figure IV.3 shows a typical series of plots (for Series B#22) of $(\ell - \ell_o)^2$ against t for various trial values of ℓ_o. The results are well linearized by ℓ_o = 1.25 μm, with an uncertainty of no worse

FIG. IV.3

DETERMINATION OF ℓ_o

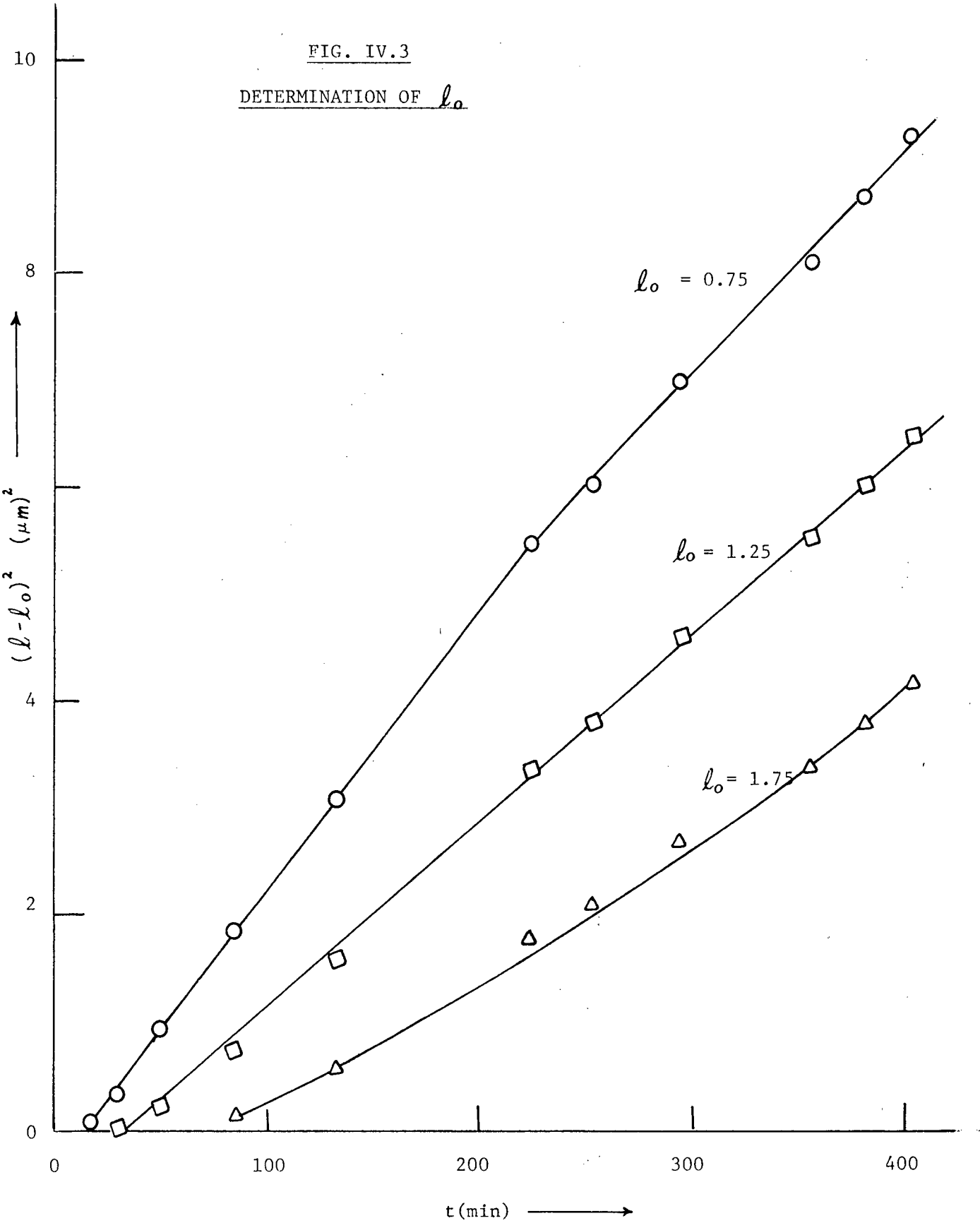

than ± 0.25 μm. The linear plot extends from $\alpha = 0.25$ to $\alpha = 0.63$, i.e. for the first 400 min. of diffusion following about 30 min. of surface-controlled reaction.

Figure IV.4 shows the same plot over a much longer time. The most interesting new feature is a second linear region (B) extending over an even longer time period (430 - 1,030 min.) but only a small α range (0.63 - 0.72). The plot appears to indicate an abrupt transition in the tarnishing constant k_T at $\alpha = 0.63$. This probably indicates [see equation (6)] a sudden decrease either in the diffusivity D or the boundary concentration C_1 of the diffusing material by a factor of ~ 2, which implies a very minor structural change in the diffusion layer. The flattening of the plot at even higher compositions presumably represents a further gradual decline in C_1 or D or both, towards the normal behaviour of stoichiometric $CuCl_2$. No detailed analysis of kinetic data in this region is attempted, however.

Corrected Plots (Ginstling - Brounshtein Equation)

The correct quasi-stationary state equation for diffusion across a spherical shell of reaction product separated from the reactant by a sharp boundary is the Ginstling - Brounshtein equation. It is usually given in a form which does not allow for the volume of the product to differ from that of the reactant, viz.

$$1 - \frac{2}{3}\ \alpha_G - (1 - \alpha_G)^{2/3} = 2\ D\ C_1\ V_M\ t\ /\ (b_o')^2 \quad . \ . \ . \ . \ . \quad (7)$$

where α_G is the extent of reaction of any one particle. Modification

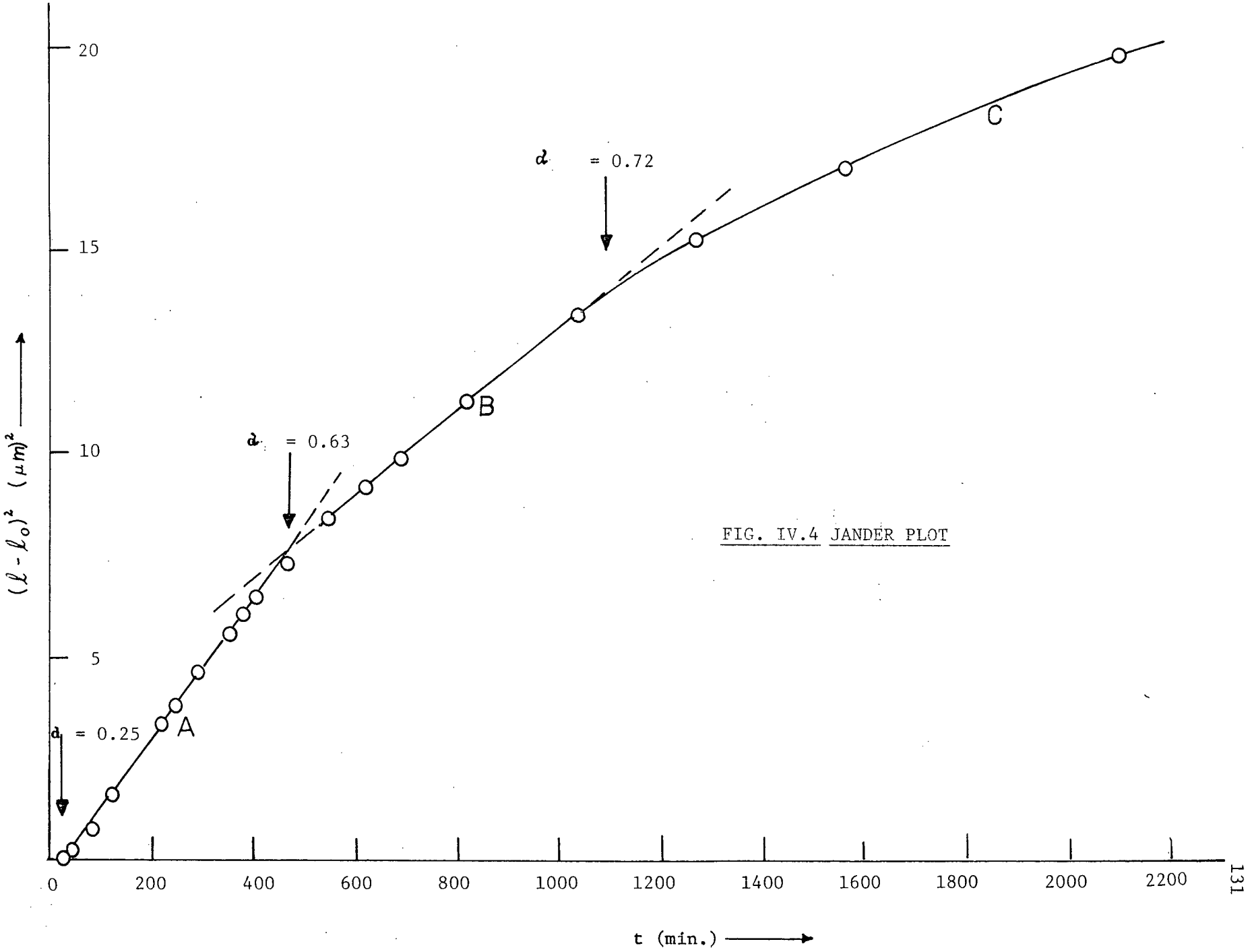

FIG. IV.4 JANDER PLOT

of the equation to allow for expansion by a factor β from reactant volume to product volume (see Appendix I) leads to:

$$1 - (1 - \alpha_G)^{2/3} - [1/(\beta - 1)]\ [\{1 + (\beta - 1)\alpha_G\}^{2/3} - 1]$$
$$= 2\ D\ C_1\ V_M\ t\ /\ (b_o')^2 \quad \ldots\ldots\ldots\ldots\ldots\ldots\ldots\ldots \quad (8)$$

Consider a particle of initial radius b_o' at a time t after the start of diffusion. Since t and b_o' appear only on the right-hand side od the Jander and Ginstling-Brounshtein equations, and since the two expressions in t and b_o' are identical, there is a functional relationship between the extents of reaction α_J and α_G from the two equations, which depends only on β and not on t or b_o'. From equations (5) and (8), this relationship is given by

$$\beta\ [\ 1 - (1 - \alpha_J)^{1/3}\ ]^2$$
$$= 1 - (1-\alpha_G)^{2/3} - [1\ /\ (\beta-1)]\ [\{1 + (\beta-1)\alpha_G\}^{2/3} - 1] \quad \ldots\ldots \quad (9)$$

For the value β = 1.66, α_G is plotted against α_J in Figure IV.5.

The plot of experimental results in Figure IV.4 may now be recalculated in the following way. The diffusion-controlled process is assumed to start at the same point (α_o, ℓ_o, having for series B#22 the values α_o = 0.25, ℓ_o = 1.25 μm) as was determined by the Jander approximation. If α' is the extent of reaction in the diffusion process, then the overall extent of reaction in both processes is

$$\alpha \quad = \quad \alpha_o + (1 - \alpha_o)\ \alpha' \quad \ldots\ldots\ldots\ldots\ldots\ldots\ldots \quad (10)$$

(i.e. for series B#22, $\alpha = 0.25 + 0.75\ \alpha'$).

For a number of values of the displacement distance ℓ, α_J is calculated as a function of particle size, and Figure IV.5 is used to convert the values to α_G. The total extent of reaction in the diffusion process is then obtained by numerical integration over the particle size distribution according to:

$$\alpha' = \int_0^\infty (b_o')^3 \alpha_G N'(b_o')db_o' \; / \; \int_0^\infty (b_o')^3 N'(b_o') \, db_o' \quad . \; . \; (11)$$

Thus from equations (10) and (11), a corrected curve of α against ℓ can be plotted. This is shown in Figure IV.2, as curve D (for the "sharp distribution") and curve E (for the "actual distribution"). Significant deviation from the Jander approximation starts at about $\alpha = 0.4$.

Figure IV.6 shows, as curve A, the corrected version of the plot in Figure IV.4, which is reproduced as a dotted line (curve B) for easy comparison. No qualitative feature of the results is altered by the correction, but there is an appreciable quantitative change in the slope of the second linear region (430 - 1,030 min.). Curve C is the corrected plot for the "sharp distribution". Once again, the same qualitative features are evident, but it is evident that the quantitative values of the tarnishing constant k_T, determined from the slopes of the linear portions, are quite sensitive to the width of the particle size distribution.

Estimation of C_1

The first linear portion of curve A in Figure IV.6 gives the tarnishing constant as $k_T = 1.31 \times 10^{-2}$ $(\mu m)^2$ $min.^{-1} = 2.18 \times 10^{-12}$ $cm^2 sec.^{-1}$ at 130^oC. If the mobile species is a form of copper, its

FIG. IV.5

CONVERSION OF α_J TO α_G

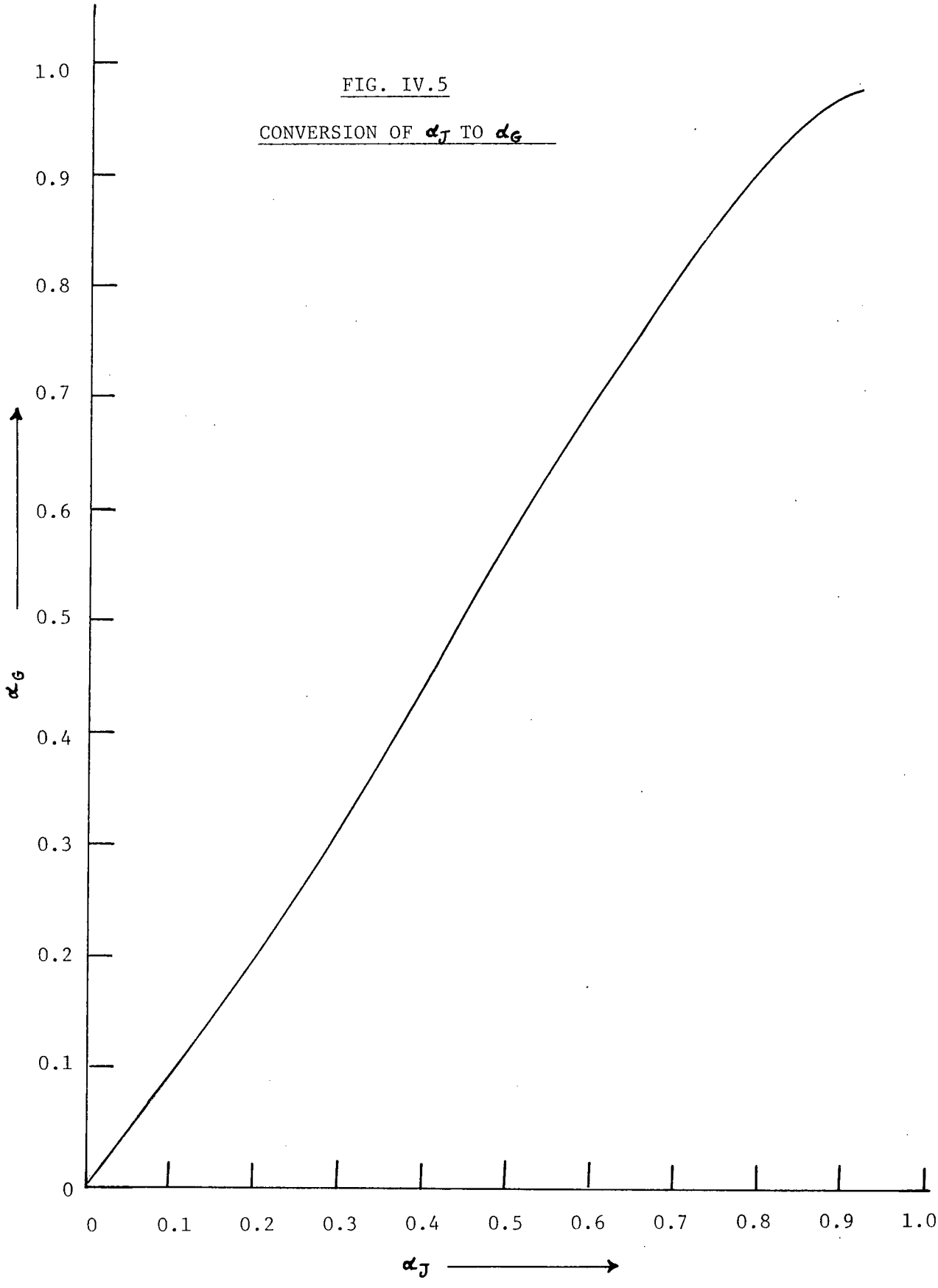

FIG. IV.6

COMPARISON OF PARABOLIC PLOTS

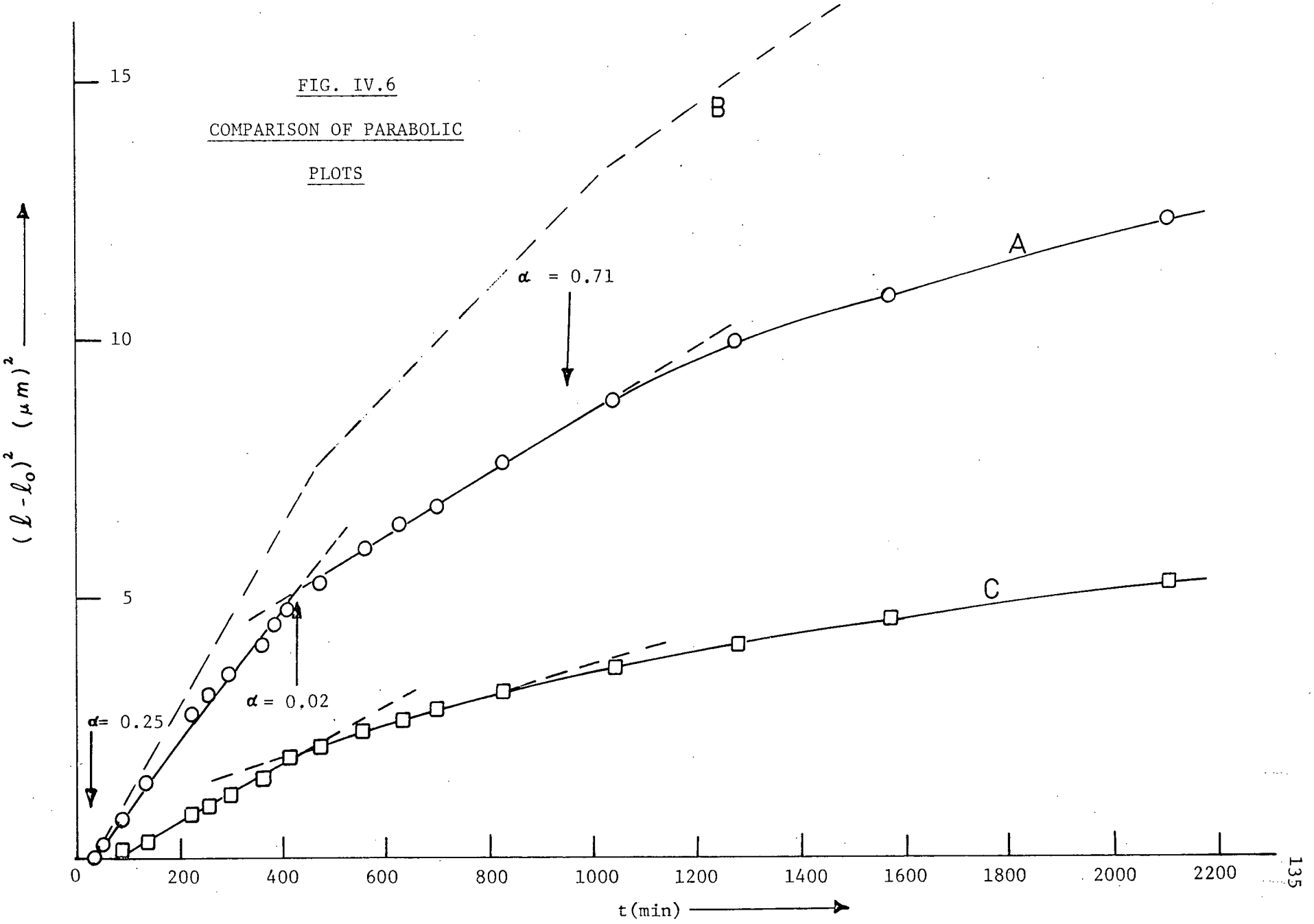

molar volume in the reactant CuCl is $V_M = 23.9$ cm^3 mole^{-1}. Then from equation (6),

$$D\,C_1 = k_T\beta / 2\,V_M = 7.56 \times 10^{-14} \text{ mole cm}^{-1} \text{ sec.}^{-1}$$

Since the activation energy is known, it is possible to estimate D. For diffusion in three dimensions,

$$D = \frac{1}{6} z\, w\, \ell^2$$

where z is the number of directions in which the mobile species can jump, w is its jump frequency and ℓ is the length of a jump. Here, if the diffusion path involves alternate octahedral and tetrahedral sites, z is either 6 or 4 depending on which site the species occupies between jumps. These are here assumed to be tetrahedral sites (see later discussion), so that z = 4. The distance ℓ between tetrahedral sites via an octahedral site is $\ell = 4.4$ Å. The jump frequency w is given by $w = \nu \exp(-E/kT)$ where $\nu \sim 4 \times 10^{+12}$ sec.$^{-1}$ (the frequency corresponding to a Debye temperature of about 200°K), and E = 11.4 kcal/mole from the experimental results. Then $w = 2.5 \times 10^6$ sec.$^{-1}$ and $D = 3.2 \times 10^{-9}$ cm^2 sec.$^{-1}$.

$$\text{Thus} \quad C_1 = \frac{7.56 \times 10^{-14} \text{ mole cm}^{-1} \text{ sec.}^{-1}}{3.2 \times 10^{-9} \text{ cm}^2 \text{ sec.}^{-1}}$$

$$= 2.4 \times 10^{-5} \text{ mole cm}^{-3}$$

The concentration of cations in stoichiometric $CuCl_2$ is 2.5×10^{-2} mole cm^{-3}, so that C_1 is equivalent to about 0.1% of the cation concentration. This is at once much lower than the concentration difference normally expected for a true non-stoichiometric compound, and much higher than normal defect concentrations, and serves

further to confirm that this is an intermediate case between those extremes.

It is interesting to compare our results with those of Cini et al[8,9], who observed (for a different type of CuCl preparation) parabolic law kinetics right from the start of reaction with chlorine. Their quantitative data are quite different from the present ones. They reported $k_T = 5 \times 10^{-8}$ mg^2 cm^{-4} sec.$^{-1}$ at 91.2°C, which converts to $k_T = 2.3 \times 10^{-14}$ cm^2 sec.$^{-1}$, about a hundred times smaller than the present value at 130°C. Their activation energy, however, is 31.5 kcal/mole, and does not seem at all consistent with the quoted rate at 91.2°C. A similar calculation to that given above for the present results gives $C_1 \sim 10^6$ mole cm^{-3}. Some doubt is thus cast on the very high reported activation energy, which was based on measurements at only two temperatures 15° apart.

Correlation with Catalytic Activity

It has been shown above that the rate law of the $CuCl/Cl_2$ reaction is consistent with a mechanism involving diffusion through $CuCl_2$ over a wide range of extent of reaction, and provides some evidence for a minor structural transition at $\alpha \sim 0.62$. It remains to enquire whether any quantity can be found, arising from this mechanism, which passes through maxima at the observed peaks in catalytic activity. A priori, both surface and bulk properties should be considered, e.g.:-

(a) the rate of arrival of diffusing material at the gas-solid interface;

(b) the total amount of diffusing material (M) in the diffusion layer.

Computations, based in the first instant on constant D and C_1 throughout the course of the diffusion, showed that (a) decreases continuously while (b) passes through a maximum at $\alpha = 0.75$, as calculated from the actual particle size distribution (Figure IV.7). Qualitatively, it is evident that the amount of diffusing material is zero at the beginning and end of the process and must go through at least one maximum. A more precise picture is given in Figure IV.8, which shows the development of the concentration gradient at various stages α' in the development of diffusion for a particle of initial radius 10 μm. In studying this diagram, one should bear in mind that the total diffusing material is proportional to $\int r^2 C \, dr$, so that the values of C at high r are the most important. The diagram also illustrates the expansion of the particle from its radius of 10 μm as CuCl to its final radius of 11.8 μm as $CuCl_2$, and the increasing departure from linearity of the concentration profile, which is another aspect of the departure from the parabolic law.

For computation, it is shown in the Appendix I that, for a particle of volume V_o at the start of diffusion,

$$M = \frac{1}{2} V_o C_1 [\, 1 + \alpha (\beta - 1) \,] (\gamma + \gamma^2 - 2\gamma^3) \quad \ldots\ldots (12)$$

where $$\gamma = \left[\frac{1 - \alpha}{1 + \alpha (\beta - 1)}\right]^{1/3} \quad \ldots\ldots\ldots\ldots (13)$$

FIG. IV.7

AMOUNT OF DIFFUSING MATERIAL

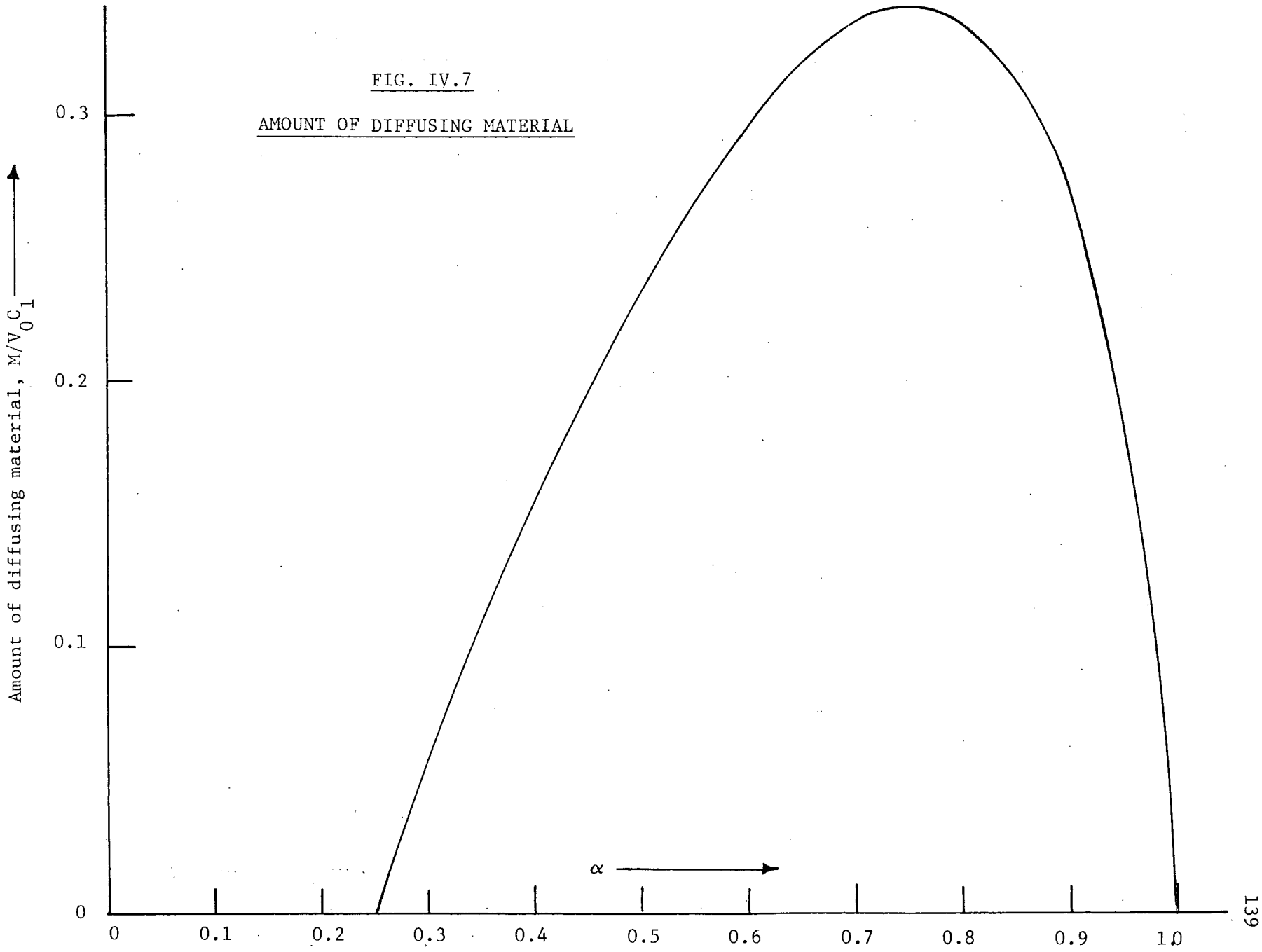

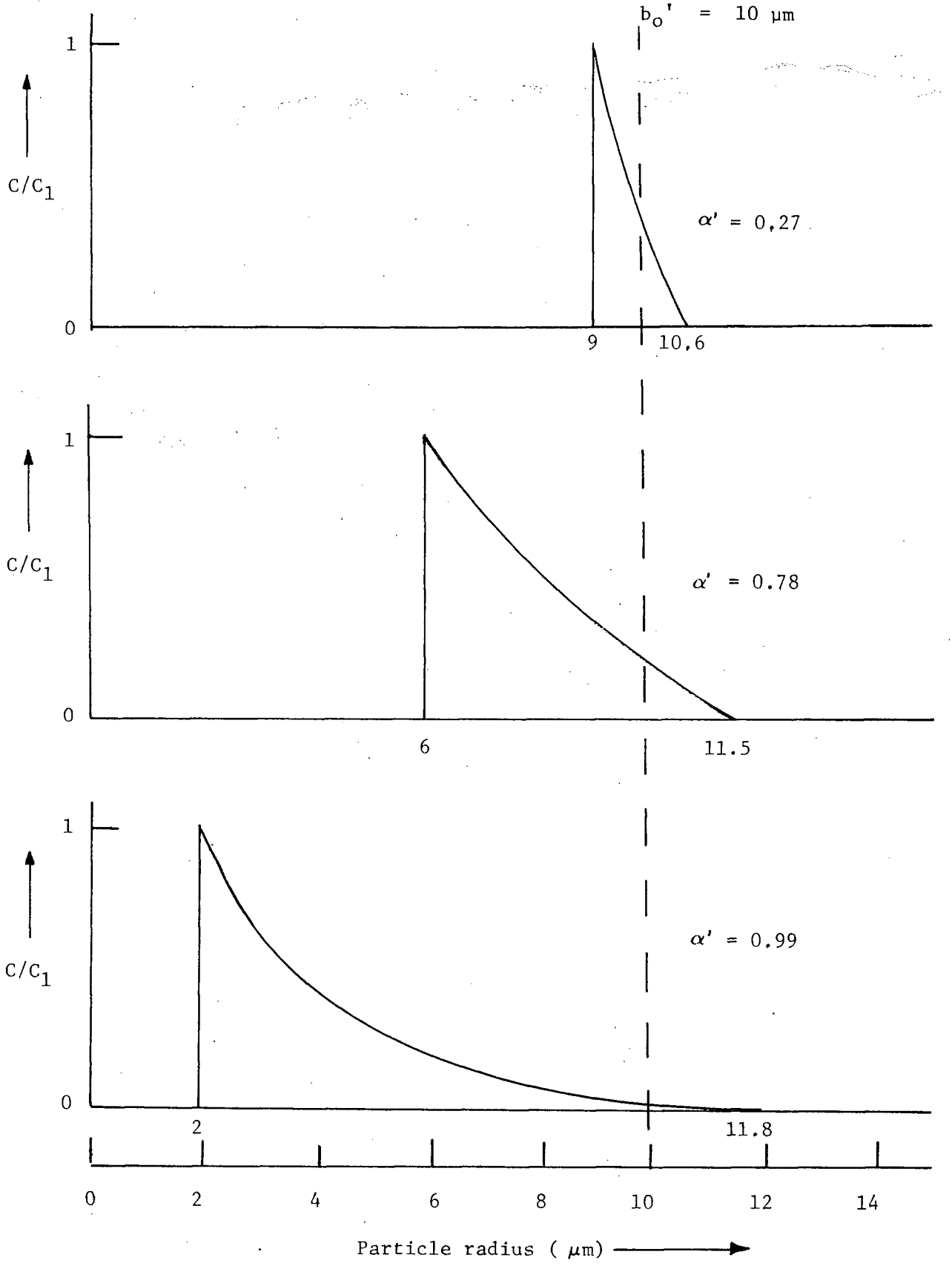

FIG. IV. 8 CONCENTRATION GRADIENT OF DIFFUSING MATERIAL IN PRODUCT LAYER

M values in Figure IV.7 are given as $M/V_o\ C_1$; or in other words, the unit of M is "the amount of diffusing material which would fill the initial volume of reactant at concentration C_1".

The calculations leading to Figure IV.7 were based on a constant k_T, i.e. constant (D C_1). But it has already been pointed out that there is a transition at $\alpha = 0.62$ involving a decrease in either D or C_1 to a value, from the ratio of slopes in Figure IV.6 (curve A) of 0.431 times its previous value. However, it was found experimentally that the activation energy is the same in both regions. This suggests that the value of D is constant and only C_1 changes. This is quite conceivable that C_1 could change, e.g., by some slight re-arrangement of co-ordination octahedra analogous to those discussed by Wadsley [20] in many oxide systems, which would allow for a slight adjustment in stoichiometry, but would quite possibly leave diffusion paths essentially unaltered.

If it is assumed that the boundary concentration of the mobile species decreases at $\alpha = 0.62$ to a new value $C_1' = 0.431\ C_1$, then all values of M for $\alpha > 0.62$ must be multiplied by 0.431. The recalculated M values are shown in Figure IV.9 and the catalytic activity curve is shown as a dotted line for comparison.

The identification of the diffusing species with an active centre in the catalysis is thus capable of providing an explanation of the existence of two maxima in catalytic activity. The correlation of positions of the two maxima is quite good, but the shapes of the calculated and experimental curve differ appreciably in the region of the second maximum. In this connection, it should

FIG. IV.9

AMOUNT OF DIFFUSING MATERIAL AFTER CORRECTION FOR CONCENTRATION DIFFERENCE

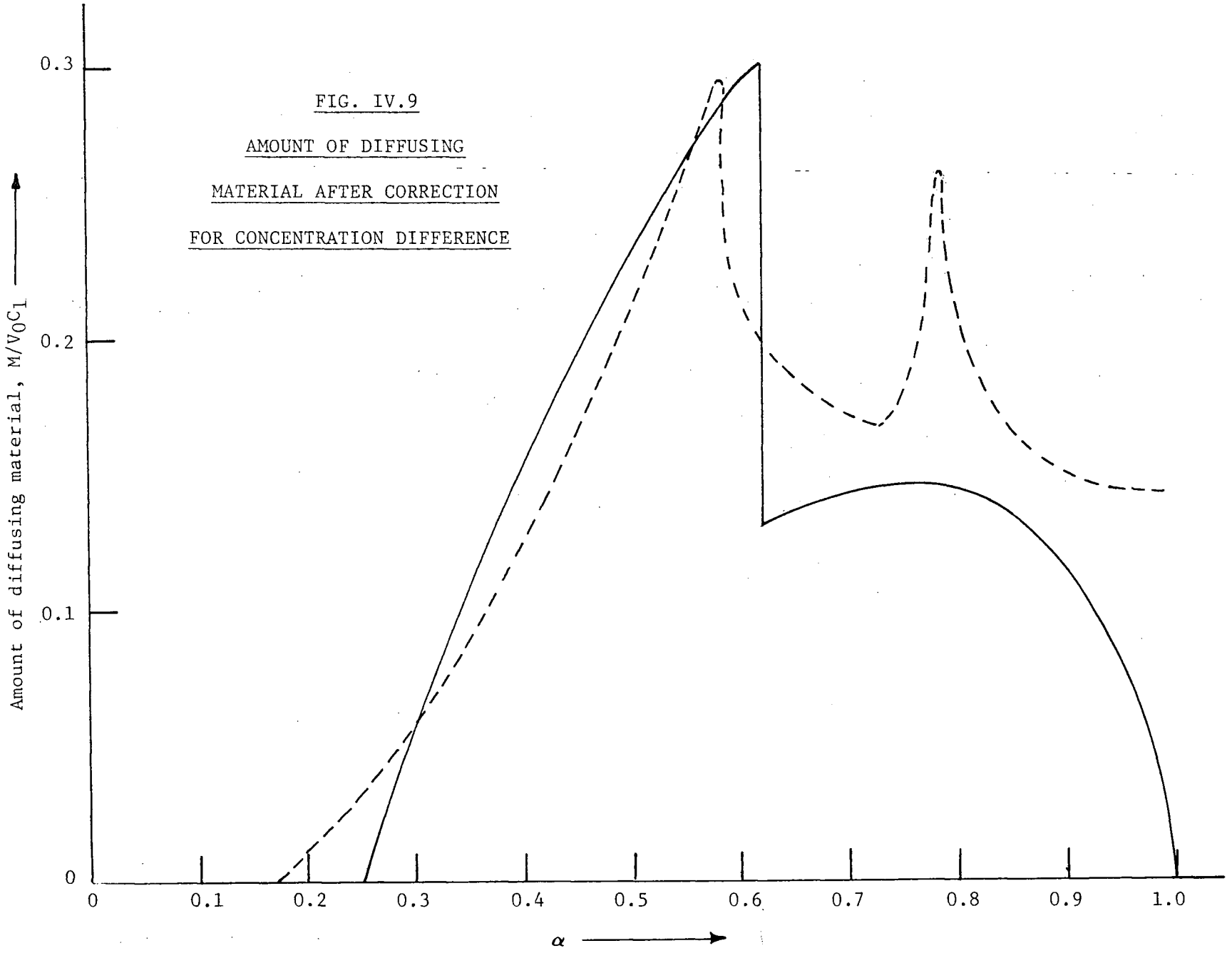

be noted:-

(1) that C_1' has been resumed constant at all $\alpha > 0.63$, whereas the Ginstling-Brounshtein plots are curved beyond $\alpha \sim 0.72$, indicating further gradual decrease in C_1, D, or both; and

(2) that the catalytic activity may depend on other factors besides the concentration of the one active centre. For example, throughout the diffusion process there is a gradual increase in $CuCl_2$ surface area [according to the expression $(0.34 + 0.66 \{\alpha'\}^{2/3})$]. Both of these factors, and possibly others as well, could alter the shape of the second peak.

The kinetics of the $CuCl/Cl_2$ reaction thus provide reasonably strong evidence for a diffusion process in which the mobile species is also an active site in the catalysis of the C_3H_8/Cl_2 reaction. It appears that the mobile species is catalytically active not only when it is at the gas/solid interface, but whenever it happens to be in the $CuCl_2$ layer. The only species likely to be capable of rapid penetration to a depth of the order of μm is a proton. It is therefore postulated that the active centre, which is probably Cu^+, is an aceptor of protons to form CuH^{2+}. This will be discussed fully in the next section.

IV.(2) KINETICS AND MECHANISM OF THE CATALYTIC CHLORINATION OF PROPANE BY COPPER CHLORIDE

CuCl is not catalytically active for the reaction. The catalytically active particles are coated with a $CuCl_2$ layer. Since X-ray powder studies show no new compound in the $CuCl_x$ system, the catalytically active phase is almost certainly a highly defective $CuCl_2$ lattice. This phase has been shown to be significantly different from normal preparations of stoichiometric $CuCl_2$ in respect of rate of the catalysed reaction, and of other physical properties. It was not possible to characterize the difference in catalytic activity in terms of activation energy (which was very low for both $CuCl_x$ and normal $CuCl_2$) or rate law. The latter was determined only for $CuCl_2$, because of experimental difficulties associated with the continuously-changing composition of $CuCl_x$, and showed a Langmuir-Hinshelwood mechanism with weakly-adsorbed Cl_2 and strongly-adsorbed C_3H_8. The evidence on chlorine uptake studies, however, indicates a correlation of catalytic activity with the total amount of a species distributed through the bulk of the defective $CuCl_2$ phase. It was suggested above that this species may be Cu^+, and that it acts in catalysis as a proton acceptor.

Halpern and his associates [4] studied homogeneous catalytic hydrogenation by transition metal ions extensively.

They found that hydrogen can be activated by forming a reaction intermediate which involves either homolytic or heterolytic splitting of the hydrogen molecule.

Thus while in the case of Cu^{2+}, the intermediate is formed according to the reaction

$$Cu^{2+} + H_2 \longrightarrow CuH^+ + H^+ \qquad \text{(heterolytic)}.$$

in the case of Ag^+, the intermediate is formed according to the reaction

$$2\ Ag^+ + H_2 \longrightarrow 2\ Ag\ H^+ \qquad \text{(homolytic)}$$

As pointed out in the last section, the only species which is likely to be able to penetrate rapidly to a depth of the order of μm is a proton, so the active centre is most probably a Cu^+, capable of accepting H in the form of CuH^{2+}. In considering what ionic reaction intermediates may reasonably be postulated in a solid, in relation to those already known in aqueous solution, it should be recognized that the aqueous environment is generally unfavourable to the formation of highly-charged ions (because of entropy of hydration effects) while we are here dealing with a lattice in which there are many sites at which a +2 charge is normal.

A probable mechanism for the catalytic reaction appears to be as follows:

$$2\ Cu_s^{2+} + C_3H_{8(g)} \rightleftharpoons \begin{pmatrix} C_3H_7 \\ | \\ Cu_s \end{pmatrix}^{2+} + \begin{pmatrix} H \\ | \\ Cu_s \end{pmatrix}^{2+} \quad \ldots\ldots\ldots \quad (1)$$

$$\begin{pmatrix} H \\ | \\ Cu \end{pmatrix}^{2+} + \underset{\text{(diffusing material)}}{Cu^+} \longrightarrow Cu^+ + \begin{pmatrix} H \\ | \\ Cu \end{pmatrix}^{2+} \quad \ldots\ldots\ldots \quad (2)$$

$$\begin{pmatrix} C_3H_7 \\ | \\ Cu_s \end{pmatrix}^{2+} + \underbrace{\begin{matrix} Cl \text{ ---- } Cl \\ | \qquad\quad | \\ Cu_s^{2+} \text{----} Cu_s^{2+} \end{matrix}}_{\text{molecular or atomic adsorption}} \xrightarrow{\text{fast}} C_3H_7\,Cl_{(g)} + \begin{pmatrix} Cl \\ | \\ Cu_s \end{pmatrix}^{2+} + 2Cu_s^{2+} \quad \ldots\ldots (3)$$

$$\begin{pmatrix} Cl \\ | \\ Cu_s \end{pmatrix}^{2+} + \begin{pmatrix} H \\ | \\ Cu_s \end{pmatrix}^{2+} \xrightarrow{\text{fast}} HCl_{(g)} + 2\ Cu_s^{2+} \quad \ldots \quad (4)$$

The first step of the reaction is the homolytic splitting of propane through adsorption to two surface Cu^{2+} ions in the $CuCl_2$ lattice. The presence of Cu^+ ions in the lattice serves to reduce the backward rate of reaction (1) by stabilizing the proton released through the second reaction (which occurs in the bulk as well as the surface). In other words, the proton released is removed by Cu^+ ion from the site where the splitting of C_3H_8 occurs to a far away site on the surface or in the bulk. The effectiveness of migration of hydrogen will then be determined by the amount of Cu^+ ions present in the $CuCl_2$ lattice on which, in turn, the reaction rate will depend.

The next step is the reaction between $C_3H_{7(ads)}$ and the adsorbed Cl_2 and would be expected to be fast. The adsorbed chlorine may be either in molecular or in atomic form. For normal stoichiometric $CuCl_2$, the Langmuir-Hinshelwood kinetics indicate weakly-adsorbed molecular Cl_2. The combination of $H_{(ads)}$ and adsorbed chlorine requires the protons to return to positions close to those of adsorbed chlorine. This may take some time, and is in accordance with the observed delay in release of HCl from the catalyst. (The amounts of HCl retained are comparable to the total amounts of diffusing material estimated in the previous section.).

The presence of hydrogen in the lattice should also accelerate the diffusion of Cu^+ ion in the lattice to the surface where it is oxidised by gaseous chlorine because reaction (2) actually amounts to a place exchange of Cu^+ and Cu^{2+} ions. This in fact is confirmed by experimental results as shown clearly in Figure III.10. It is striking indeed that the greatest acceleration effect by propane occurs at almost exactly the same composition which gives the greatest amount of diffusing material. The deceleration of chlorine uptake rate by propane in the low composition region is probably just due to competition for chlorine between copper chloride and propane.

In the postulated mechanism, we have considered that the splitting of C_3H_8 is homolytic. However, one may raise the question that propane could also be split heterolytically as $Cu_s(C_3H_7)^{3+}$ and Cu_sH^+ or $Cu_s(C_3H_7)^+$ and Cu_sH^{3+}. In principle, ESR should be very

useful in furnishing information about the nature of the adsorbed species (heterolytic splitting should give rise to new paramagnetic species whereas homolytic splitting causes pairing of electrons of the surface Cu^{2+} ions and the radicals adsorbed). Unfortunately, the strong antiferromagnetic exchange in the parent $CuCl_2$ lattice introduces uncertainty in the interpretation of ESR results. In other words, the absence of any new structure in the ESR spectrum cannot prove that the splitting must be homolytic.

Without carrying out detailed calculation, one may argue on energy grounds that the heterolytic splitting is unlikely. This is because of the formation of a trivalent complex in the case of heterolytic splitting which should involve a large columbic repulsive force between the adsorbed positive ion and Cu^{2+} ion. Other things being equal, the homolytic splitting should be much more probable.

IV.(3) MECHANISM OF MIGRATION OF Cu^+ THROUGH $CuCl_2$

As indicated by electrical conductivity and magnetic studies, a $CuCl_x$ sample made by chlorination of CuCl is not the same as a mechanical mixture of CuCl and $CuCl_2$ of the same overall composition, and the two preparations remain different after several days at temperatures ranging up to 160°C. A question arises as to which system is in equilibrium in respect of the solubility of Cu^+ in the $CuCl_2$ lattice and what kinetic barrier prevents the other system from reaching equilibrium.

Since we know that Cu^+ ions can move relatively rapidly in the $CuCl_2$ phase of $CuCl_x$, it appears that there is no kinetic barrier in this case, and this consequently represents the equilibrium situation. The question then becomes: Why can Cu^+ not diffuse into normal stoichiometric $CuCl_2$?

In this connection, it is worthwhile to compare the $MgCl_2$ structure (of which the $CuCl_2$ structure is a distorted version) with the spinel structure. In the $MgCl_2$ structure, the octahedral sites are occupied by cations in alternate (111) layers. The vacant layers might be used by a cation as diffusion paths, and the most favourable path of this type involves an alternation of octahedral and tetrahedral positions (so that the migrating cation never has to pass between two neighbouring anions.) In the $MgCl_2$ lattice, however, every vacant tetrahedral

site has a cation very close to it (in one of the adjacent octahedra). In the spinel structure, the Al^{3+} ions occupy positions similar to those of Mg^{2+} in $MgCl_2$, except that one quarter of them are displaced into the otherwise vacant layers. In this way, the layer structure is lost and the lattice regains cubic symmetry. The displacement of the Al^{3+} ions at the same time opens up a complete network of tetrahedral sites, none of which has a cation in any of the neighbouring octahedra. These are the sites occupied by Mg^{2+} in stoichiometric spinel and probably form the diffusion paths in spinel formation.

In the present case, it is suggested that the $CuCl_2$ lattice formed by chlorination of CuCl may initially have some Cu^{2+} displaced in a spinel-like manner, and hence may have some diffusion paths open, involving tetrahedral sites, which are completely blocked in the perfect layer lattice of $CuCl_2$.

Independent evidence that there may be some cations in the normally vacant layers, and that some of these have come from the nromally occupied layers is provided by the X-ray diffraction data, which are discussed in the next section.

IV.(4) EVIDENCE OF DEFECT STRUCTURE IN $CuCl_x$

(A) X-ray Powder Studies

Although the results of X-ray powder studies indicate that there is no structure other than those of CuCl and $CuCl_2$ in the $CuCl_x$ system, they nevertheless suggest that there are small changes in some of the lattice parameters of both the CuCl and $CuCl_2$ lattices over the range of $1 < x < 2$. However, in view of the large limits of error, the results are significant only when averaged over fairly wide ranges of composition.

According to the results, the CuCl lattice undergoes a slight expansion in the range of $1.45 < x < 1.70$ which suggests that there is a significant loss of ions in the CuCl lattice in $CuCl_x$ of this composition range. This is consistent with the findings of kinetic studies which appear to show that some Cu^+ ions in the CuCl lattice have migrated to the $CuCl_2$ layer (which forms a coat on the CuCl particles) during chlorination.

In discussing the data on the $CuCl_2$ lattice parameters, it is useful to bear in mind that the monoclinic $CuCl_2$ structure can be regarded as a severely distorted $MgCl_2$ structure in which a plane containing vacant octahedral sites (cation sites) is present. Thus c_o in $CuCl_2$ traverses this vacant plane; a_o is related to the distance between

adjacent chains; and b_o is the distance between two adjacent Cu^{2+} ions in a chain.

The results show that there is a contraction in c_o and an expansion in b_o over the range of composition of $1.3 < x < 1.7$. For the parameter a_o, a contraction occurs in the range $1.3 < x < 1.45$ and it is not certain whether a_o undergoes contraction as well as expansion in the range $1.45 < x < 1.7$ or whether it remains essentially unchanged (if the averaging procedure is correct. See Table III.12).

Thus, the results are consistent with the displacement of a small number of cations from the chains either to the octahedral sites in layers which are vacant in the perfect $CuCl_2$ lattice (or possibly to tetrahedral sites, some of which are close to the vacant layer, and some of which are close to the occupied layer.) However, the contraction in c_o or a_o may also be due to the presence of Cu^+ ions in the same sites as those just mentioned for Cu^{2+} ions from the chains. The present data do not enable a separation between these two effects.

The present data are not accurate enough to warrant quantitative evaluation of the difference in Jahn-Teller effect (if any) for different composition. In fact, more quantitative information about the behaviour of the various parameters in $CuCl_x$ are obviously desirable from the standpoint of understanding the nature of non-stoichiometry and its relations to other physical and chemical properties of $CuCl_x$. A suggestion for further work is given at the end of this chapter.

(B) Electrical Conductivity Studies

For any pellet sample which is made of a mixture of two substances, the value of observed electrical conductivity will depend on the individual conductivity, the relative amount and the deformability of each substance present. In our case, the CuCl phase has a much higher conductivity than the $CuCl_2$ phase; so the observed conductivity may therefore be expected to be essentially that of CuCl phase until it ceases to be continuous in the pellet sample. $CuCl_2$, however, having a layer lattice, is much softer than CuCl and may be expected to deform easily under the pressure applied in making the pellet so as to form a continuous phase at the lowest possible x value. Thus, it is difficult to assess the critical x value at which one phase ceases to be continuous and therefore extra care must be exercised in the interpretation of conductivity results of a mixture.

From our results (see Figures III.15 - 17), it is quite obvious that the observed conductivity for $CuCl_x$ with x value lying between 1.0 and 1.4 (Type I), and that for $CuCl_x$ with x value lying between 1.75 and 2.0 (Type III) are essentially that of CuCl phase (i.e. x = 1) and $CuCl_2$ phase (i.e. x = 2)respectively. (The results at x = 1 in this work are markedly different from previously reported data[21,22], which refer to CuCl in equilibrium with Cu metal. These data are discussed in more detail later in this section.). The Type II $CuCl_x$ ($1.4 < x < 1.75$), however, exhibits complicated behaviour which requires detailed analysis.

Type I $CuCl_x$ ($1.0 < x < 1.4$)

Since no defective $CuCl_2$ phase is formed for $x < 1.25$, it is likely that the conduction mechanism is due to trace of impurities present. At the beginning of the chlorination process, the CuCl phase is in direct contact with Cl_2 gas. Under this condition, the CuCl lattice can easily take up excess anions. It is reasonable to expect the nature of defective conductivity to be similar to that existing in CuI with iodine excess which was found by Vine & Maurer[23], to be due to the presence of vacant Cu^+ ion lattice sites. Thus, in the case of CuCl, one expects that some Cu^+ ions from the bulk may migrate to the surface to combine with the adsorbed chlorine. The cuprous ion vacancies which are so formed have an effective negative charge and at low temperature trap holes. In other words, the presence of vacant cuprous ion lattice sites introduce acceptor levels into the forbidden gap of the parent CuCl energy levels as illustrated in the following diagram.

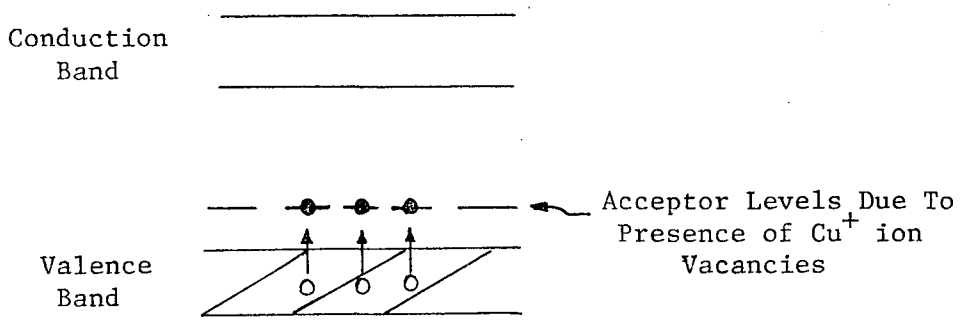

FIGURE IV.10

ENERGY LEVEL DIAGRAM FOR CuCl CONTAINING CUPROUS ION VACANCIES

When the temperature is raised, electrons can be excited to the acceptor levels leaving holes in the valence band and hence giving rise to conductivity. If our model were correct and if the conduction by the holes is the predominant mechanism, then one expects the observed conductivity to be a function of the number of holes created, and the observed activation energy is half the energy difference between the acceptor levels and the valence band, viz. $E_a/2$. It can be readily shown (see e.g. Ref.24) that the number of holes created N_a' follows the relationship

$$N_a' = (2N_a)^{1/2} (2 \pi k T m_e^* / h^2)^{3/4} e^{-E_a/2kT} \quad . . . . \quad (1)$$

where N_a is the number of acceptor levels,

k & h are Boltzmann and Planck constant respectively,

m_e^* is the effective electronic mass, and

T is the temperature in ^oK.

The same equation will apply in the case of donor impurities (then N_a and E_a will be replaced by N_d and E_d respectively).

The conductivity σ is given by

$$\sigma = n \mu e \quad . . . . . \quad (2)$$

where n is the number of charge carriers which is N_a' in this case.

μ is the mobility of the charge carrier (hole in this case).

e is electronic charge.

Therefore, one can estimate the value of N_a from the data of conductivity at 130°C and the activation energy. Such an estimation leads to $N_a = 1.75 \times 10^{15} - 1.75 \times 10^{13}/cm^3$ for hole mobility 10 - 100 cm^2/volt.sec. This is equivalent to a defect concentration of 0.09 to 0.0009 p.p.m. Thus, a trace amount of excess anion could give rise to the observed conductivity.

Therefore, it can be concluded that the results are consistent with the conduction mechanism by holes in the valence band of CuCl due to the presence of cuprous ion vacancies.

Type II $CuCl_x$ $(1.40 < x < 1.75)$

Since we know from kinetic studies of chlorination of copper chloride that there are Cu^+ ions (diffusing material) in the $CuCl_2$ lattice, we shall first of all consider the possible contribution of the Cu^+ ions in the $CuCl_2$ lattice towards the observed conductivity.

The kinetic data provide the values for the diffusion coefficient D and the amount of Cu^+ ion.

By means of the Einstein relationship $\mu = \frac{eD}{kT}$, one can calculate the ionic mobility μ of Cu^+, and hence the conductivity by equation (2). The method of estimation for the concentration of Cu^+ ions in $CuCl_2$ phase from kinetic data is illustrated in Appendix II.(1) whereas the calculation for the conductivity due to Cu^+ ions is exemplified in Appendix II.(2).

Some selected results of such calculations are summarised

in the following table.

T A B L E IV.1

CONDUCTIVITY OF Cu^+ IONS IN $CuCl_2$ PHASE

x in $CuCl_x$	σ ($ohm^{-1}cm^{-1}$) From D, by Einstein Equation	σ ($ohm^{-1}cm^{-1}$) Observed	$\frac{\sigma_{Cu^+}}{\sigma_{Obs.}} \times 100\%$
1.35	1.6×10^{-9}	1.5×10^{-6}	0.1%
1.62	3.35×10^{-9}	5.6×10^{-7}	0.3%
1.72	2.56×10^{-9}	1.58×10^{-8}	16.2%
1.80	2.46×10^{-9}	6.75×10^{-9}	36.4%
2.00	-	2.5×10^{-9}	-

It can be seen from Table IV.1 that the value of σ_{Cu^+} does not vary a great deal (for $x < 1.9$). The contribution towards the observed conductivity is definitely negligible in the range $1.35 < x < 1.62$ (< 0.3% of observed conductivity) and barely significant at $x = 0.72$. Above $x \approx 1.72$, the contribution is quite significant and yet cannot account for the observed conductivity completely, (especially when one bears in mind that the σ value calculated from D is based on the assumption that all $CuCl_2$ particles in the pellet are in the continuous phase). Therefore, one can conclude that the observed conductivity is not due to the Cu^+ ions in $CuCl_2$ phase at least up to $CuCl_{1.7}$ on the ground of the observed

conductivity values. However, beyond x = 1.7, any significant contribution from Cu^+ is still ruled out by the values of activation energy observed (0.65 eV and 0.92 eV) which are not equal to the activation energy for diffusion obtained from kinetic studies (0.50 eV). Therefore, the observed conductivity cannot be directly related to the catalytic activity.

Now, it appears that the observed conductivity in the Type II $CuCl_x$ is likely to be predominantly due to the CuCl phase except for the lower temperature region for $CuCl_{1.68}$ - $CuCl_{1.75}$ which on both the grounds of σ_{sp} and activation energy values could be ascribed to the same conduction mechanism as that of Type III $CuCl_x$.

Since both the values of σ_{sp} and polarization factor appear to suggest that there is a change of mechanism of conduction in the region of $1.6 < x < 1.64$, we shall subdivide the Type II $CuCl_x$ into two groups, viz. Type II.(A) ($1.4 < x < 1.65$) and Type II.(B) ($1.65 < x < 1.75$).

Type II.(A) $CuCl_x$ ($1.4 < x < 1.65$)

In the lower temperature region, the conduction in Type II.(A) $CuCl_x$ can be ascribed to the same mechanism prevalent in Type I $CuCl_x$ viz. hole conduction in the valence band of CuCl. The higher activation energy for $CuCl_{1.63}$ appears to be irregular and probably due to the fact that the transition of mechanism from Type II.(A) to Type II.(B) is ill-defined.

In the higher temperature region, the conduction could be ascribed to lattice vacancies created by migration of Cu^+ ions as evidenced by kinetic and X-ray powder studies (note that an equivalent number of anions also has to leave the lattice according to this mechanism). If that be the case, the σ_{sp} value will depend on the amount of Cu^+ ion migrated, which is probably related to the amount of Cu^+ ion in the $CuCl_2$ phase. It is then understandable that a maximum is observed in the value of σ_{sp} in this narrow region of composition (see Figure IV.9 for comparison of behaviour of amount of Cu^+ ion in the $CuCl_2$ phase). However, the variation in activation energy is difficult to comprehend. It could well be that the activation energy changes in discontinuous jumps with composition rather than according to the amooth curve in Figure III.15, but the scatter of experimental points is too wide to allow a definite decision on this. More data are required in order to clarify this point.

It is very interesting to note that should the postulate for a change of mechanism from Type II.(A) to Type II.(B) be correct, then conductivity studies also correlate with a structural change in the region of $x \sim 1.6$. More interesting still, such a change can be correlated in an indirect way with the change of concentration of Cu^+ ions in the $CuCl_2$ lattice.

Type II.(B) $CuCl_x$ $(1.65 < x < 1.75)$

In the higher temperature region, the observed activation

energy for this type of $CuCl_x$ is of the order of 0.92 eV. This is the closest approach found in the present work to the values reported by Wagner & Wagner[21] and Hsueh & Christy[22] for CuCl (1.06 - 1.1 eV). These authors studied the conductivity of CuCl with copper electrodes to avoid anion excess. The former group found that the electronic conduction of CuCl under this condition is negligible, and the latter group managed to establish by thermoelectric power technique that the conduction is predominantly by cationic Frenkel defects. Furthermore, the conductivity of pure CuCl (sublimed) has also been studied using Pt electrodes by M. Prasad in our laboratory (recent work, unpublished). His results show that CuCl under this condition exhibits two activation energies with the value 0.9 eV in the higher temperature region and a somewhat variable value of the order of 0.45 - 0.6 eV in the lower temperature region; the crossing temperature for the switch of mechanism is $\sim$ 120-150°C. (Values of σ_{sp} in the region of higher activation energy are close to those of W. & W. or H. & C.).

Thus, the conduction mechanism in the higher temperature region for this type of $CuCl_x$ is probably also by cationic Frenkel defects in the CuCl phase.

In the lower temperature region, a comparison with the results of Prasad appears to suggest that the conduction is by some impurities in the CuCl phase. However, as pointed out before, the possibility that the mechanism is the same as that in Type III $CuCl_x$ cannot be ruled out entirely.

Type III $CuCl_x$ ($1.75 < x < 2.0$)

Although the value of σ_{sp} for $CuCl_2$ is a factor of ~ 3 less than the values of other $CuCl_x$ in this region, they are nevertheless of the same order. Thus it appears that one can rule out the possibility of ionic conduction due to Cu^+ ion or the electron conduction in the conduction band due to electron transfer between Cu^{2+} and Cu^+ ions because the amount of Cu^+ ions at $x \sim 2$ is negligible.

The observed activation energy is ~ 0.65 eV which appears too low for intrinsic electronic conduction and too high for extrinsic electronic conduction (other than that due to presence of Cu^+ ions which has just been ruled out). The mechanism is therefore more likely to involve lattice defects.

Without studying the Hall effect or thermoelectric power of the substance, the nature of the dominating charge carrier(s) cannot be definitely established for this type of $CuCl_x$.

Before leaving the discussion of conductivity results, a few words about the observed polarization effect and the behaviour of conductivity for a mechanical mixture are appropriate.

While the observed polarization effect helps establishing the types of conduction mechanism, the actual value of the polarization factor is puzzling. Normally, one expects that ionic conduction will probably give a greater polarization effect than electronic conduction. In our results, the reverse is apparently true. However, a large

polarization effect arising from electronic conduction is not entirely impossible. It is quite well-known that in the electrolysis of NaCl. F centres can form close to the cathode (see e.g. Ref.25). This illustrates that electrons could be quite polarizable if they are in the form of localized electronic defects.

The behaviour of conductivity for a mechanical mixture is the combination of that of CuCl (Type I) and that of $CuCl_2$ (Type III), expected for a simple mixture. This finding not only confirms that $CuCl_x$ prepared by the present method is not a simple mechanical mixture, but also lends support to the interpretation that the conduction in the lower temperature region for the Type II.(B) $CuCl_x$ and that for the Type III $CuCl_x$ cannot be ascribed to the Cu^+ ions nor electronic defects due to its presence in $CuCl_2$ phase.

The findings of conductivity studies can be summarised as follows:

(i) Ionic conductivity due to the diffusion of Cu^+ ions in the $CuCl_2$ phase does not contribute significantly to the observed conductivity over the whole range of composition from CuCl to $CuCl_2$.

(ii) For Type I $CuCl_x$ ($1.0 < x < 1.4$), conduction is by holes in the valence band of CuCl due to the presence of excess anions as a result of the CuCl phase being in contact with gaseous chlorine during chlorination.

(iii) For Type II.(A) $CuCl_x$ ($1.4 < x < 1.65$), two different

mechanisms of conduction are operating in two regions of temperature. The conduction in the lower temperature region probably has the same mechanism as that of Type I $CuCl_x$ while that in the higher temperature region is tentatively ascribed to the diffusion of lattice vacancies introduced by the migration of Cu^+ and Cl^- ions.

(iv) For Type II.(B) $CuCl_x$ ($1.65 < x < 1.75$), two different mechanisms of conduction are also operating in two regions of temperatures. The conduction mechanism in the higher temperature region can be ascribed to cationic Frenkel defects in the CuCl phase. The conduction mechanism in the lower temperature region cannot be established unambiguously. The choice is between impurities in CuCl phase or lattice defects in the $CuCl_2$ phase as prevalent in the Type III $CuCl_x$.

(v) For Type III $CuCl_x$ ($1.75 < x < 2.0$), the conduction mechanism is likely to involve lattice defects in the $CuCl_2$ phase.

(vi) The conductivity results are consistent with the findings of kinetic and X-ray powder studies on the following counts.

(a) As the value α reaches 0.25, the Cl_2 gas is not directly in contact with CuCl phase. Hence the number of defects in $CuCl_{1.0}$ - $CuCl_{1.25}$ is conceivably reduced owing to some structural adjustments when the surface is not in direct contact with the highly electronegative Cl_2. The number of defects becomes insignificant only when $x > 1.6$

($\alpha > 0.6$); and at $x > 1.65$, the CuCl phase approaches the structure of pure CuCl studied by Wagner & Wagner and Hsueh & Christy.

(b) A change in conduction mechanism at $x \sim 1.6$ lends support to the presence of a structural change in this composition range, as evidenced by kinetic studies. Moreover, that the conduction in the higher temperature region in Type II.(A) $CuCl_x$ is by lattice defects other than cationic Frenkel type [as found for Type II.(B)] is consistent with X-ray data.

(C) Magnetic Studies

The unusually high values of various parameters (X_M', μ_{eff} and θ) found in the $CuCl_x$ system are too large to be accounted for by any impurity which has become paramagnetic on Cl_2 oxidation, and therefore appear to arise from Cu^{2+} ions in a defective $CuCl_2$ lattice (CuCl is diamagnetic).

It is convenient to classify the $CuCl_x$ into three types in so far as magnetic properties are concerned. Except for one composition ($CuCl_{1.32}$), these types correspond to the composition ranges for which the numbers II.(A), II.(B) & III were used in discussing conductivity results. The same numbering will be adopted here, and it is convenient to discuss them in reverse order.

Type III $CuCl_x$

The magnetic behaviour for this type of $CuCl_x$ ($x > 1.75$) is very similar to that of $CuCl_2$ suggesting that the structure is also very similar, in agreement with the findings of other studies in this work.

Type II.(B) $CuCl_x$

For this type of $CuCl_x$, the Barraclough plot shows significant departure from linearity. The magnetic properties are field-dependent. $CuCl_x$ in the region of $1.63 < x < 1.75$ (and $CuCl_{1.32}$) exhibits this type of behaviour.

The characteristic of the Barraclough plot (curving upwards in the high temperature region, see Figure III.23) appears to suggest that by introducing a correction for a small amount of temperature independent paramagnetism (T.I.P.), the Barraclough plot may be linearized. Moreover, the $\frac{1}{\chi_M}$ vs. T plot will then be steeper in the highest temperature region and hence the values of μ_{eff} and θ will be reduced. Attempts were therefore made to linearize the Barraclough's plots of $CuCl_{1.321}$, $CuCl_{1.677}$ and $CuCl_{1.740}$.

It was found possible to linearize the plots down to 100°K ($10^3/T = 10$), but the plots which are best linearized down to that temperature show definite departures from linearity at lower temperatures, suggesting that T.I.P. alone cannot completely explain all the effects involved.

One of the modified plots ($CuCl_{1.740}$) is given in Figure IV.11 together with the original plot for comparison. The results due to the introduction of T.I.P. term are summarised in Table IV.2.

T A B L E IV.2

MAGNETIC RESULTS WITH CORRECTION FOR T.I.P.

x in $CuCl_x$	T.I.P. (x 10^6 c.g.s. unit)	μ_{eff} (B.M.)	θ^o
1.321	120	2.00	82
1.677	100	2.06	105
1.740	150	2.04	91
2.000	0	1.99	96

FIG. IV.11

DETERMINATION OF T.I.P.

FOR $CuCl_{1.740}$

(Modified Barraclough Plots)

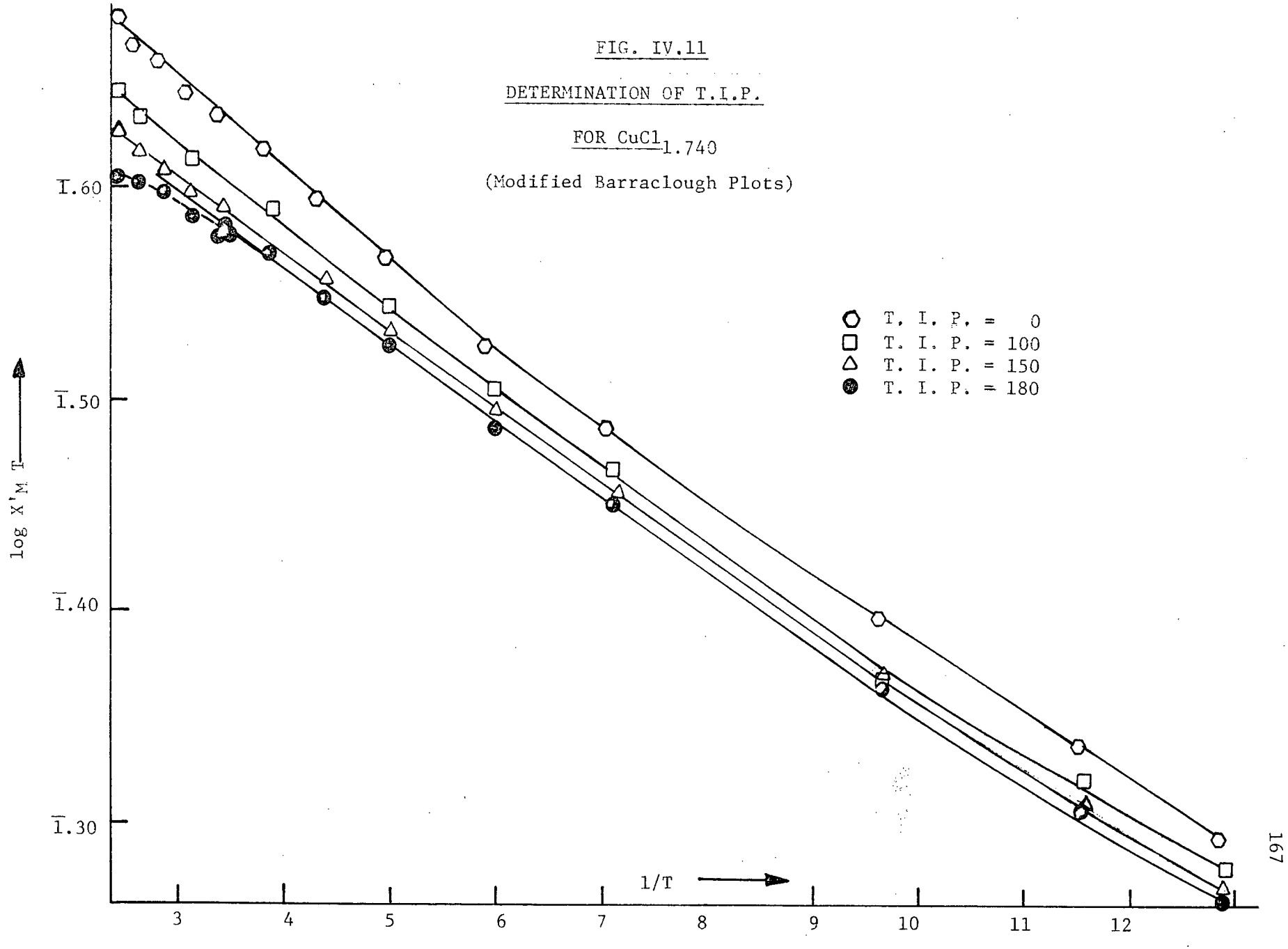

One can see from Table IV.2 that after allowing for T.I.P., the values of μ_{eff} and θ are very close to those of $CuCl_2$ itself.

The T.I.P. term springs from quantum mechanical mixing of the ground state and the low lying excited states through a second order Zeeman effect. It can be shown (see e.g. Ref.26) that the T.I.P. term is proportional to $\sum_{n=1}^{\infty} \frac{\langle n| m^o|n_o\rangle^2}{\langle n|E_n - E_o|n_o\rangle}$ where $\langle n|m^o|n_o\rangle$ is the matrix element of the magnetic moment (the superscript o indicates field free), and $E_n - E_o$ is the difference in energy between the excited state n and ground state n_o. For a transition ion in a ligand field, the value of the denominator in the summation depends on the energy separation between the $d\gamma$ and $d\varepsilon$ levels (usually referred to as 10 Dq by inorganic chemist). Thus, other things being equal, the T.I.P. term will be higher for a lower value of 10 Dq.

Assuming the procedure for estimating the T.I.P. term to be correct, the results appear to suggest that the unusually high apparent values of X_M', μ_{eff} and θ in $CuCl_{1.32}$ and $CuCl_{1.63}$ - $CuCl_{1.74}$ can be ascribed at least partly to some kind of irregularity in the $CuCl_2$ lattice capable of reducing the ligand field strength (such an irregularity would be expected to be the greatest in the region of x where values of X_M', μ_{eff} and θ exhibit a maximum).

Such an effect could arise either from the presence of Cu^+ ions (near to the first octahedral coordination shell of a Cu^{2+}) forming bonds to the chlorine and weakening the Cu^{2+} - Cl bonds, or

from the displacement of some Cu^{2+} into the vacant octahedral sites, which are actually larger than the normally occupied octahedral sites and hence will have lower ligand field.

The slight curvature existing in the lower temperature region in the modified Barraclough plots appears to be a general characteristic for all $CuCl_x$ except those with $x > 1.75$. While this suggests that the structure in the $CuCl_x$ is different from that of $CuCl_2$, no quantitative account can be given for the nature of such deviation at present.

Moreover, the dependence on field strength for this type of $CuCl_x$ is also difficult to comprehend because even allowing for the possibility of the presence of some localized ferromagnetic regions (which is quite possible considering the amount of Cu^+ ions in the $CuCl_2$ lattice which is capable of generating a spinel-like structure — a structure well known for the phenomenon of ferrimagnetism), the working temperature (130^oC) appears too high for ferromagnetic interaction to exist.

Assuming that ferromagnetic interaction really exists at such a high temperature, one possible explanation for the observed field-dependence is that the working field strength is very close to the saturation for magnetisation. The magnetisation curve is normally expected to be of the shape shown in the following diagram

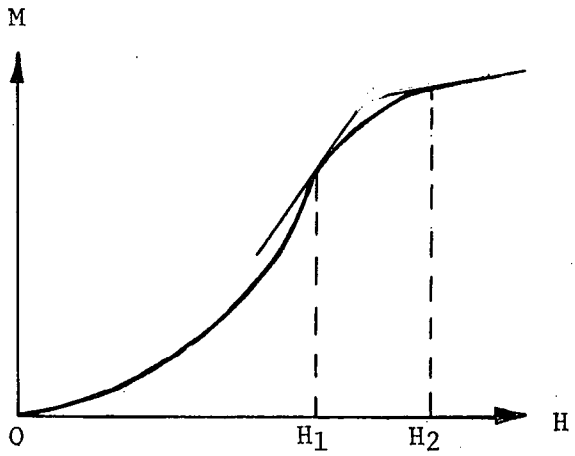

FIGURE IV.12

MAGNETISATION CURVE

It can be seen from the above curve that the slope (i.e. X_M') can be smaller for a higher field strength ($H_2 > H_1$) provided the two field strengths are properly chosen. Such a postulate, however, can be confirmed if magnetic measurements are taken at a greater number of field strengths to establish a proper M-H curve.

Type II.(A) $CuCl_x$

For this type of $CuCl_x$ ($CuCl_{1.5 - 1.63}$) magnetic properties are not field-dependent; the Barraclough plot shows a slight curvature only in low temperature region and consequently no correction for T.I.P. is required.

The results therefore appear to suggest that the mechanism operating in this type of $CuCl_x$ which is responsible for deviation from the $CuCl_2$ behaviour is not entirely the same as that in Type II.(B) $CuCl_x$.

The slight curvature in the lower temperature region of the

Barraclough plot for this type of $CuCl_2$, however, appears to be similar to that of Type II.(B) $CuCl_x$ as mentioned.

In view of the complexity of the problem (the ferromagnetism or antiferromagnetism of a pure compound is already a complicated problem by itself), a detailed theoretical analysis of the results is beyond the scope of this thesis. The results, however, have revealed that the effect of structural defects on magnetic behaviour could be quite significant. They therefore suggest that the magnetic method used by Cini, et al[9] for following the kinetics of the chlorination of CuCl (in their studies, they assumed that the magnetic susceptibility increase during chlorination was simply due to the increase of the amount of a normal $CuCl_2$ phase) was correct only if no defective $CuCl_2$ was formed under their experimental conditions. Moreover, the results provide a fairly convincing evidence for the existence of at least two different defective structures of $CuCl_2$ in $CuCl_x$ in two different ranges of x. While the first range corresponds to the first maximum in the catalytic activity curve, the second range corresponds to the minimum in the catalytic activity curve. Thus, the results are consistent with a structural change at $\sim$ 1.63 found by other studies.

IV.(5) SUGGESTIONS FOR FUTURE WORK

The physics and chemistry of non-stoichiometric (or defective) copper chlorides was virtually unknown until the present work was undertaken. While the present work has revealed some interesting features of this non-stoichiometric system, it has, however, in no way completed the exploration.

The followings are some suggestions for future studies of the $CuCl_x$ system related to the findings of the present work.

(i) Kinetic Studies on Other Reactions

It will be of great interest to test the applicability of the $CuCl_x$ catalyst in other reaction systems such as hydrogenation & dehydrogenation. These types of reaction are suggested since the proposed mechanism for catalytic activity of Cu^+ in $CuCl_2$ in this work indicates that this centre may bring about catalytic activation of hydrogen. Such systems have the advantage that no change of composition of $CuCl_x$ is expected to occur during reaction, and consequently, the interpretation of results should be more straight forward.

(ii) Method of Preparation of $CuCl_x$

Different methods of preparation of $CuCl_x$ should be tried, e.g.

(a) Preparation from more highly purified CuCl, particularly because the CuCl used by Cini, et al apparently reacted more slowly with Cl_2 than that used in this work, and did not show the two-stage reaction, but showed diffusion kinetics from the outset.

(b) Attempted incorporation of CuCl into $CuCl_2$ in a melt or by heating a solid mixture to a higher temperature than the highest used in the work ($160^{\circ}C$).

(iii) X-ray Powder Studies

Although the power of the X-ray powder method is limited for a monoclinic system, one could perhaps adopt a different approach to detect the change in the structure of $CuCl_2$ in $CuCl_x$ in a more quantitative manner. One possible way for doing so appears to be the use of pure $CuCl_2$ as the internal standard. The variation of the line shape (detected by a counter) may then furnish useful information about the structural change of $CuCl_2$ in $CuCl_x$. (lineshape analysis is suggested since the normal & defective $CuCl_2$ lines will probably be incompletely resolved from each other.)

(iv) Studies of Electrical Properties

(a) Conductivity measurements in the presence of Cl_2 as well as reacting mixture (be it C_3H_8/Cl_2 or other systems) should prove valuable. Also, the measurements performed on powder samples (i.e. not in a pellet form) may provide a way to

separate the conductivity due to $CuCl_2$ phase from that of CuCl phase because the latter is coated with a layer of the former according to the present findings.

(b) Thermoelectric power or Hall effect studies should provide useful information about the nature of charge carriers in $CuCl_x$ which were only established indirectly in the present work. Such studies, if carried out in the presence of gas(es) will be even more interesting for then one can actually observe the change in the conduction mechanism during reaction. It would be useful to start some conductivity and Hall effect studies with highly purified CuCl in equilibrium with Cu, and to study carefully the effect of the first small additions of Cl_2.

(v) Magnetic Studies

Unless it is found possible to grow single crystal of the defective $CuCl_2$, the amount of quantitative information which can possibly be derived from magnetic studies will be limited (e.g. one cannot carry out neutron diffraction studies to establish the nature of the spin arrangement in the $CuCl_2$ lattice in the $CuCl_x$ system). However, as suggested in the discussion, one can at least carry out measurements at a greater variety of field strengths so as to establish the mechanism for the observed field-dependence.

(vi) ESR Studies

To the author's knowledge, there is no reported ESR data for

pure $CuCl_2$ not to mention $CuCl_x$. It may be worthwhile to carry out ESR measurements of $CuCl_x$ ($1 < x < 2$) at $20^{\circ}K$ (no signal was observed at $4^{\circ}K$) in the hope of observing an ESR signal with structure, an analysis of which should further our understanding of the behaviour of the electron spin in an antiferromagnetic substance.

APPENDIX I

The following equations were originally derived by Harrison. They are reproduced here in a form directly relevant to the present work.

The Ginstling-Brounshtein Equation: A Modified Form for the Case in Which Volume of Product is not Equal to Volume of Reactant.

Let a spherical particle have initial radius b_o; and at time t, let the unreacted material end at radius a, and the reacted material at radius b. If there is no volume change on reaction, $b = b_o$ = constant. This is the assumption made in the derivation of the Ginstling-Brounshtein equation. If there is a volume change, b will be a function of time, and hence will be functionally related to a. Now the application of the quasi-stationary state approximation to diffusion across a spherical shell leads to the equation

$$D\ C_1\ V_M\ t = \int_{b_o}^{a} [\ a^2/b - a\ ]\ da \quad \ldots\ldots\ldots \quad (1)$$

which remains correct whether or not b is a function of a. Now let the volume of solid product be β times the volume of solid reactant from which it is formed. Then at time t,

volume reacted $= (4\pi/3)\ (b_o^3 - a^3)$

and volume produced $= (4\pi/3)\ \beta\ (b_o^3 - a^3) = (4\pi/3)\ (b^3 - a^3)$

whence $b^3 = \beta\ b_o^3 - (\beta - 1)\ a^3$.

Substituting for b in equation (1) we have:

$$D\ C_1\ V_M\ t = \int_{b_o}^{a} [a^2(\beta b_o^3 - (\beta - 1)\ a^3)^{-1/3} - a]\ da$$

$$= -[\{1/2\ (\beta -1)\}\ \{\beta b_o^3 - (\beta-1)a^3\}^{2/3} + (a^2/2)]_{b_o}^{a}$$

$$= -[1/2\ (\beta-1)]\ [\{\beta b_o^3 -(\beta-1)a^3\}^{2/3} - b_o^2] + (a^2/2)-(b_o^2/2).$$

Dividing through by $b_o^2/2$ and introducing $(1 -\alpha) = a^3/b_o^3$, we have,

$$2\ D\ C_1\ V_M\ t/b_o^2 = -[1/(\beta-1)][\{(\beta-(\beta-1)(1-\alpha)\}^{2/3} -1] - (1-\alpha)^{2/3}+ 1$$

$$= 1 - (1-\alpha)^{2/3} - [1/(\beta-1)][\{1 + (\beta-1)\alpha\}^{2/3} - 1] \quad . \ . \ .(2)$$

This is the modified Ginstling-Brounshtein equation; and for the CuCl chlorination, β = molar volume $CuCl_2$/molar volume CuCl = 39.7/23.9 = 1.660. Hence:

$$2\ D\ C_1\ V_M\ t\ /\ b_o^2 = 1 - (1-\alpha)^{2/3} - 1.516\ [(1 + 0.660\alpha)^{2/3} - 1] \quad . \ . \ .(3)$$

Modification of the Jander Equation to Allow for a Volume Change on Reaction

Let a semi-infinite solid have a plane surface initially at position b_o. At time t, let the unreacted material have receded to a, while the product occupies the space from a to b.

For unit cross section, volume reacted = $(b_o - a)$, and volume produced = $(b - a) = \beta\ (b_o - a)$. In the quasi-stationary state approximation, the concentration change of the diffusing species is linear across the product layer, so that if the concentration is C_1 at a and zero at b, then concentration gradient = $C_1\ /\ (b - a)$ at all intermediate positions.

If the diffusing species has a molar volume V_M in the reactant phase, then

Rate of transport of material = $\frac{1}{V_M} \frac{da}{dt}$

and by Fick's law, this is proportional to the concentration gradient:

$$- \frac{1}{V_M} \frac{da}{dt} = \frac{D\ C_1}{b - a} = \frac{D\ C_1}{\beta(b_o - a)}$$

whence $(D\ C_1\ V_M/\beta) = 1/2\ \frac{d}{dt}\ (b_o - a)^2$

and $(b_o - a)^2 = 2\ D\ C_1\ V_M\ t\ /\ \beta$

The Jander approximation assumes that this equation governs the rate of advance of the reaction interface into a sphere, and thus takes no account of the deviation of the boundaries from planarity, except that $(b_o - a)^2$ is converted into a function of the extent of reaction α by using the equation appropriate to a sphere,

$$1 - \alpha = \frac{a^3}{b_o^3} .$$

Whence $(b_o - a)^2 = [\ 1 - (1 - \alpha)^{1/3}\ ]^2\ b_o^2$

and $\beta\ [\ 1 - (1-\alpha)^{1/3}\ ]^2 = 2\ D\ C_1\ V_M\ t\ /\ b_o^2$

This is the Jander equation modified by introduction of the factor β.

The Total Amount of Diffusing Material in a Spherical Shell

For a spherical shell of inner and outer radii a and b at time t, with fixed concentrations C_1 and 0 at these radii respectively, the quasi-

stationary-state concentration C at radius r is given by

$$C = C_1 \left[1 - \frac{b\,(r - a)}{r\,(b - a)} \right] = C_1 \left(\frac{a}{b-a}\right) \left(\frac{b}{r} - 1\right) \quad \ldots\ldots\ldots\ldots (1)$$

The total amount of diffusing material is

$$M = \int_a^b 4\pi r^2\, C\, dr = 4\pi C_1 \left(\frac{a}{b-a}\right) \int_a^b (br - r^2)\, dr \quad \ldots\ldots\ldots (2)$$

$$M = 4\pi C_1 \left(\frac{a}{b - a}\right) \left(\frac{a^3}{3} - \frac{a^2 b}{2} + \frac{b^3}{6} \right) \quad \ldots\ldots\ldots\ldots (3)$$

Now if the initial radius of the sphere is b_o, then the extent of reaction α at time t is given by

$$(1 - \alpha)^{1/3} = \frac{a}{b_o} \quad \ldots\ldots\ldots\ldots\ldots\ldots\ldots (4)$$

If the reaction involves a volume expansion by a factor β, then (from P.176)

$$b^3 = \beta\, b_o^3 - (\beta - 1)\, a^3 \quad \ldots\ldots\ldots\ldots\ldots\ldots\ldots (5)$$

Eliminating a from equations (4) and (5),

$$b = b_o \left[1 + \alpha\, (\beta - 1) \right]^{1/3} \quad \ldots\ldots\ldots\ldots\ldots\ldots (6)$$

so that $$\frac{a}{b} = \frac{(1 - \alpha)^{1/3}}{1+\alpha\, (\beta-1)^{1/3}} = \gamma \quad \ldots\ldots\ldots\ldots\ldots (7)$$

In order to correct the expression for M into a function of α, it must first be written as a function of b and $\frac{a}{b}$. This may be done as follows. From equation (3),

$$\frac{M}{4\pi C_1} = \left(\frac{a}{b-a}\right)\left[\left(\frac{a^3}{3} - \frac{b^3}{3}\right) + \left(\frac{b^3}{2} - \frac{a^2 b}{2}\right)\right]$$

$$= \frac{a}{b-a}\left[\frac{(a-b)}{3}(a^2 + ab + b^2) + \frac{b}{2}(b+a)(b-a)\right]$$

$$= a\left[-\frac{(a^2 + ab + b^2)}{3} + \frac{b}{2}(b+a)\right]$$

$$= a\left[-\frac{a^2}{3} + \frac{ab}{6} + \frac{b^2}{6}\right]$$

$$= b^3\left[-\frac{a^3}{3b^3} + \frac{a^2}{6b^2} + \frac{a}{6b}\right]$$

Then, substituting for b and a/b from equations (6) and (7),

$$M = \frac{1}{2}\left(\frac{4}{3}\pi b_o^3\right) C_1 \left[1 + \alpha(\beta-1)\right]\left[\gamma + \gamma^2 - 2\gamma^3\right]$$

$$M = \frac{1}{2} V_o C_1 \left[1 + \alpha(\beta-1)\right]\left[\gamma + \gamma^2 - 2\gamma^3\right] \quad \ldots\ldots\ldots \quad (8)$$

This is the required equation for computation of M.

APPENDIX II

(1) ESTIMATION OF DEFECT CONCENTRATION

In IV.(1), it is estimated that for $1.25 < x < 1.63$, C_1, the highest concentration of Cu^+ ions in the $CuCl_2$ layer which occurs near the interface of CuCl and $CuCl_2$ (see Figure IV.8) is 2.4×10^{-5} mole/(cm^3 of $CuCl_2$ formed). The average concentration of Cu^+ ions in the $CuCl_2$ lattice will be somewhat smaller than this value. For conductivity estimation, it is the average concentration, or rather the total amount of Cu^+ ions in the $CuCl_2$ lattice which is relevant because the concentration gradient will be smoothed out when the catalyst is not in contact with Cl_2.

As shown in Figure IV.9, the amount of diffusing material is a function of α. The volume of $CuCl_2$ formed is also a function of α. Moreover, one should bear in mind that only when $\alpha > 0.25$, does the $CuCl_2$ formed contain Cu^+ ions.

A sample calculation for the estimation of defect concentration is given as follows for the case of $\alpha = 0.62$ for 1 mole of starting material.

(i) At $\alpha = 0.62$, $M/V_o C_1 = 0.30$ moles/(cm^3 of reactant at $\alpha = 0.25$)(C_1)

with $C_1 = 2.4 \times 10^{-5}$ moles/(cm^3 of product)

$\therefore \frac{M}{V_o} = 0.30 \times 2.4 \times 10^{-5}$ moles of Cu^+ ion/(cm^3 of reactant)

$= 7.2 \times 10^{-6}$ moles of Cu^+ ion/(cm^3 of reactant)

(ii) Since the $CuCl_2$ layer starts to cover the CuCl particle only after $\alpha = 0.25$, the volume of $CuCl_2$ formed V from unit volume of CuCl at $\alpha = 0.25$ is given as

$$V = 1.66 \left(\frac{\alpha - 0.25}{0.75} \right)(V_o)$$

$$\therefore \quad \frac{M}{V} = \frac{M}{V_o} \times \frac{V_o}{V} = 7.2 \times 10^{-6} \times \frac{0.75}{1.66\ (\alpha - 0.25)}$$

$$= 8.8 \times 10^{-6} \text{ moles/(cm}^3 \text{ of product)}$$

Compared with the concentration of Cu^{2+} ion in the lattice, the average concentration of Cu^{+} ions in $CuCl_2$ lattice is then

$$8.8 \times 10^{-6} / 2.5 \times 10^{-2} = 3.52 \times 10^{-2} \text{ mole \%}$$

(2) ESTIMATION OF IONIC CONDUCTIVITY OF Cu^+ IN DEFECTIVE $CuCl_2$ PHASE

From kinetic data, it was found that the value of diffusion coefficient D for Cu^+ ion is $\sim 3.2 \times 10^{-9}$ $cm^2/sec.$ throughout the range of $1.3 < x < 1.76$. Thus the mobility μ of the species can be calculated by means of the Einstein equation.

$$\mu = \frac{eD}{kT}$$

where e is electronic charge

k is Boltzmann constant

T is absolute temperature, $403^{o}K$ in this case.

$$\therefore \quad \mu = \frac{1.6 \times 10^{-19} \text{ (Coulumb)} \times 3.2 \times 10^{-9} \text{ (cm}^2\text{/sec.)}}{1.38 \times 10^{-23} \text{ (joule)} \times 403 \text{ (}^{o}\text{K)}}$$

$$= 9.2 \times 10^{-8} \text{ cm}^2\text{/volt sec.}$$

The conductivity σ can then be simply calculated by the equation

$$\sigma = N \mu e$$

N is the number of Cu^+ ions in the $CuCl_2$ phase per cm^3 of pellet sample, given as

$$N = \left[\frac{\text{Concentration of } Cu^+ \text{ ions in } CuCl_2 \text{ phase}}{}\right] \left[\frac{\text{Volume of } CuCl_2 \text{ in the sample}}{\text{Volume of sample}}\right]$$

The volume of sample = The vol. of unreacted CuCl

+ The vol. of $CuCl_2$ formed after $\alpha=0.25$

+ The vol. of $CuCl_2$ formed before $\alpha=0.25$.

If we denote the original volume of CuCl as V_A, then

$$\text{the total volume of sample} = (1-\alpha)\ V_A + 1.66\ \left(\frac{\alpha-0.25}{0.75}\right)(1-0.25)\ V_A + 1.66 \times 0.25\ V_A$$

$$= (1 + 0.66\alpha)\ V_A$$

$$\text{then}\quad N = [\text{Conc.of } Cu^+ \text{ ions in } CuCl_2 \text{ phase}]\left[\frac{1.66\ (\alpha - 0.25)\ V_A}{(1 + 0.66\alpha)\ V_A}\right]$$

$$\frac{\text{Moles of } Cu^+ \text{ ion in } CuCl_2 \text{ phase}}{cm^3 \text{ of sample}}$$

for $\alpha = 0.62$,

$$N = (8.8 \times 10^{-6})(0.435) = 3.82 \times 10^{-7} \text{ moles/cm}^2$$

$$= 3.82 \times 10^{-7} \times 6.023 \times 10^{23}/cm^3$$

$$= 2.3 \times 10^{17}/cm^3$$

so, the conductivity is given as

$$\sigma = 2.3 \times 10^{17} \times 9.2 \times 10^{-8} \times 1.6 \times 10^{-19}$$

$$= 3.35 \times 10^{-9}\ \Omega^{-1}\ cm^{-1}$$

The observed conductivity is $5.6 \times 10^{-7}\ \Omega^{-1}\ cm^{-1}$.

So, the ionic conductivity of Cu^+ ion in $CuCl_2$ phase only amounts to 0.6% of the observed conductivity.

REFERENCES

1. L. G. Harrison, M. D. Baijal,and D. J. Bird, Trans. Far. Soc., 60 1099 (1964)

2. L. G. Harrison, R. J. Adams, and R. C. Catton, J. Chem. Phys., 45 4023 (1966)

3. L. G. Harrison, R. C. Catton, and A. K. Rantamaa, Proc. Intern. Symp. Reactivity Solids, 6th Schenectady, 1968, 65 (1969)

4. J. Halpern, "Advances in Catalysis", Vol. 11, 301 (1959)

5. L. H. Reyerson and Y. S. Yuster, J. Phys. Chem., 39 1111 (1935)

6. L. G. Harrison, "Comprehensive Chemical Kinetics", Vol.2, Ed. Bamford and Tipper, Elsevier (1969)

7. K. J. Gallagher, Proc. Intern. Symp. Reactivity Solids, 5th Munich, 1964, 192 (1965)

8. Cini el al, Annali di Chimica (Rome), 51 1129 (1961)

9. Cini et al, ibid, 51 1113 (1961)

10. A. F. Wells, J. Chem. Soc., 1670 (1947)

11. C. G. Barraclough and C. F. Ng, Trans. Far. Soc., 60 836 (1964)

12. R. Wyckoff, "Crystal Structures", Vol. 1, 2nd Ed., Interscience (1963)

13. S. Whitlow, Ph. D. Thesis, University of B. C. (1969)

14. B. N. Figgis and R. Nyholm, J. Chem. Soc., 4190 (1958)

15. A. I. Vogel, "Quantitative Inorganic Analysis", Longmans (1948)

16. Y. S. Yuster and L. H. Reyerson, J. Phys. Chem., 39 859 (1935)

17. K. J. Laidler, "Chemical Kinetics", 2nd Ed., McGraw-Hill (1965)

18. R. S. Burington and D. C. May, "Handbook of Probability and Statistics with Tables", Handbook Publishers (1958)

19. DeHaas and Gorter, Comm. Leiden, 215a, 4 (1931)

20. A. D. Wadsley, Proc. Intern. Symp. Reactivity Solids, 6th Schenectady, 1968, 1 (1969)

21. J. B. Wagner and C. Wagner, J. Chem. Phys., 26 1597 (1957)

22. Y. W. Hsueh and R. W. Christy, J. Chem. Phys., 39 3519 (1963)

23. B. H. Vine and R. J. Maurer, Z. physik. Chem., 198 147 (1951)

24. C. Kittel, "Introduction to Solid State Physics", 2nd Ed., John-Wiley (1956)

25. J. H. Schulman and N. O. Compton, "Color Centers in Solids" Pergamon (1963)

26. J. H. Van Vleck, "Theory of Electrical and Magnetic Susceptibility", Oxford-Clarendon (1932)